FACULTY OF SCIENCE AND TECHNOLOGY

MASTER'S THESIS

Study programme / specialization: Masters in Biological Chemistry/Molecular Biology	Spring Semester 2023 Open / Confidential
Author: Nora Elizabeth Anise	
Supervisor at UiS: Associate Professor, Hanne R. Hagland	
Thesis title: Metformin's Influence on Pancreatic Ductal Adenocarcinoma Metabolism and Chemotherapy Response	
Credits (ECTS): 60 ECTs	
Keywords: PDAC Metabolism, Metformin Pre-treatment, Chemoresistance, OXPHOS, glycolysis, Metabolic Biomarkers, 3D spheroids	Pages:114 + appendix: 16 Stavanger, *June 2023*

"Pursue some path, however narrow and crooked, in which you can walk with love and reverence"

-Henry David Thoreau

Abstract

Pancreatic cancer is a highly lethal disease with a 5-year survival rate of approximately 10%. One of the primary reasons for its lethality is the prevalence of chemoresistance. Several studies have found Oxidative Phosphorylation to be a major contributor of Pancreatic Ductal Adenocarcinoma (PDAC) chemoresistance. It has therefore been postulated that inhibiting mitochondrial respiration can mitigate chemoresistance. It is of the upmost importance to investigate this claim to prolong survival outcomes among suffering patients. The commonly prescribed biguanide anti-diabetic drug, metformin, has been found to hinder Oxidative Phosphorylation by inhibiting complex I of the Electron Transport Chain. Metformin may therefore prevent or reverse PDAC chemoresistance when used as an adjuvant treatment with common chemotherapies. Not much research has analyzed the impact of a metformin-chemotherapy adjuvant treatment with clinically relevant conditions. Furthermore, a thorough examination of the molecular impact on PDAC metabolisms in relation to metformin must be conducted. The overall aim of this study is to assess how metformin affects the metabolic profiles of treated PDAC cell lines, and to analyze how a combination of metformin and various chemotherapies impact the growth and viability of PDAC cells grown in 3D. The overarching results show that the effectiveness of metformin strongly depends on the cell line. For example, metformin successfully altered the metabolism and proliferation rates of AsPC-1 cells, but not Panc-1 cells. Furthermore, not all chemotherapies were made to be more effective by a metformin pretreatment. Several chemotherapies did not hinder the growth of PDAC spheroids even when preincubated with metformin. Therefore, the effectiveness of metformin depends on the cell line and the chemotherapy used.

Acknowledgements

I would like to start by expressing my appreciation for my supervisor, Dr. Hanne R. Hagland. I started off the project overwhelmed and unconfident, but through Hanne's immense support and guidance, I successfully adjusted to independent research. At times, I flooded her with questions which were always answered and then some. Her insight and passion for the topic of cancer metabolism inspired me to get excited about experimental results and to always question why. I would also like to express my gratitude towards Julie Nikolaisen who always made time to train me in the cell lab. I started off the project with no prior knowledge of mammalian cell culture, but through Julie's guidance, I quickly became familiarized with the techniques. Whatever question I had, whether theoretical or practical, she always had an answer.

A big thank you to all my fellow master's students, Gillian Tawse, Ine Holand, and Trine Markvardsen, who were always there to offer encouraging advice and to mitigate some of the pressure through well-needed comic-relief. A special thanks to Marina Alexeeva who always made time to answer all my questions both lab-related and personal. Her advice and guidance helped me immensely throughout the year, and her cheerful and happy-go-lucky attitude really lit up my day during stressful periods. I would also like to thank Marwin Jafari, Marcus Roalsø, Sheida Naderi, and all other PhD candidates for their help in the lab.

A sincere thank you to my friends and family who always supported me in my endeavors even if it meant leaving them and moving to Norway. I would like to specifically thank my dad for always being there for me and providing me with the unconditional love I needed to accomplish moving to a different country and completing a master's degree. Finally, thank you to my partner Philip, who has been my rock the past two years. Adjusting to life in Norway, feeling homesick, and balancing the workload of a master's has been strenuous, but with your endless love and encouragement, I made it through. You are my best cheerleader.

Table of Contents

List Of Figures

Chapter 1

Chapter 3

Chapter 4

Chapter 8

List of Tables

Chapter 3

Chapter 4

Chapter 8

List of Equations

Chapter 3

List of Abbreviations

Tumor Suppressor Genes TSGs

Adenosine Triphosphate/Diphosphate ATP, ADP

Citric Acid Cycle TCA cycle

Oxidative Phosphorylation OXPHOS

Nicotinamide Adenine Dinucleotide NAD^+

Hexokinase HK

Phosphate Isomerase PGI

Phosphofructokinase1/2 PFK1/2

Pyruvate Kinase PK

Pentose Phosphate Pathway PPP

Hexosamine Biosynthesis Pathway HSP

Succinate Dehydrogenase SDH

Electron Transport Chain ETC

Lactate Dehydrogenase/A LDH/LDHA

Glucose Transporters 1/3 GLUTS1/3

Monocarboxylate Transporters1/4 MCT1/4

ATP Citrate Lyase ACLY

Tumor Microenvironment TME

Pancreatic Ductal Adenocarcinoma PDAC

Pancreatic Intraepithelial Neoplasia PanINs

Reactive Oxygen Species ROS

Glutaminases GLS

Pancreatic Cancer Stem Cells PaCSCs **Epithelial-to-mesenchymal transition** EMT

Insulin-like Growth Factor 1 Receptor IGF1R

Cell Surface Adhesion Receptor CD44 **Dihydropyrimidine Dehydrogenase** DPD

Thymidylate Synthase TS **5-Fluorouracil** 5-FU

Mitochondrial DNA mtDNA **Type II Diabetes** T2D

Adenosine Monophosphate Kinase AMPK

Organic Cation Transporters 1-3 OCTs1-3

Rapamycin Complex I mTORC1 **Oxygen Consumption Rate** OCR

Extracellular Acidification Rate ECAR **Carbonyl Cyanide-4 (trifluoromethoxy)**

Phenylhydrazone FCCP **Uncoupling Protein 2** UCP2

2-Deoxy-glucose 2-DG **ADP-forming subunit beta** A-SCs

American Type Culture Collection ATCC

Dulbecco's Modified Eagle's Medium DMEM

Propidium Iodide PI

Chapter 1 Literature Review

1.1 Cancer Overview

Cancer is a relentless disease that afflicts millions globally every year. The scientific community continues to grapple with cancer's immense complexity and individual uniqueness. Although our understanding of the disease has improved drastically over the past couple of decades, its complexity has many unascertained characteristics. Despite commendable efforts to mitigate the prevalence of the disease through the introduction of vaccines and improved treatments, the number of cancer cases and deaths is expected to more than double in future decades (1). Nearly half of all cancers are caused by preventable exposures to physical, chemical, and biological carcinogens. Contrastingly, there are types of cancer that are inherited and can occur in individuals that are seemingly young and healthy. Whether the cancer is caused by unhealthy choices, or inherited genes, all cancers are instigated by certain genetic and epigenetic changes (2,3).

1.2 Cancer Molecular Biology

Cancer is defined as the formation of aberrant cells that evade normal cellular processes and grow uncontrollably. These cells can form in any part of the body and can metastasize to other organs. The disease is caused by the accumulation of genetic and epigenetic changes in two types of genes: tumor suppressor genes (TSGs) and oncogenes (2,3). Normally, cells grow and divide by progressing through a tightly controlled cell cycle. Oncogenes code for proteins that help drive the cell cycle forward, while TSGs code for proteins that restrict the cell cycle (4). Altered or mutated oncogenes form abnormal protein products that force cells to progress through all stages of the cell cycle, which leads to unchecked cell division (4). In contrast to oncogenes, mutated TSGs code for proteins that fail to stop cellular growth and division, repair damaged DNA, and promote apoptosis at the various checkpoints throughout the cell cycle (2,4). These genetic changes confer the ability to avoid cell-cell contact inhibition and disregard growth factors (5). The complex phenotypes and genotypes that cancer cells demonstrate as they transition from normalcy to neoplastic growth states to malignant tumors have been organized into unifying parameters called the Hallmarks of Cancer (6). Initially proposed in the year 2000, there are currently 10 hallmarks and 4 emerging hallmarks that are outlined in Figure 1. 1.

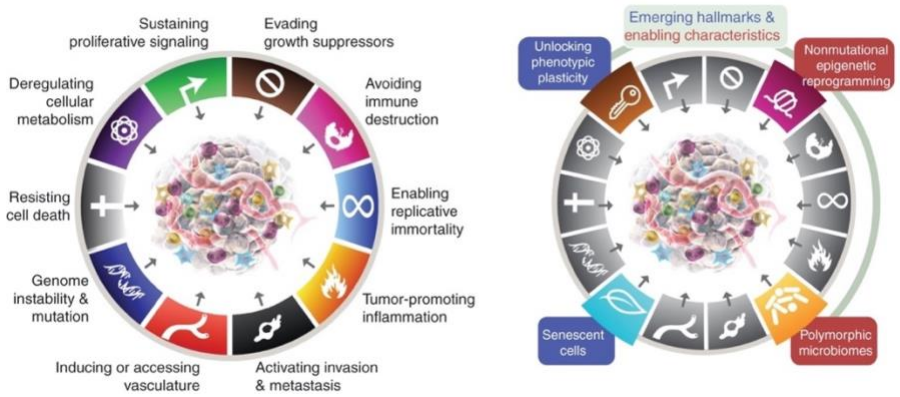

Figure 1. 1 The Hallmarks of Cancer.
According to Hanahan, the hallmarks of cancer help articulate the immense complexity of cancer phenotypes and genotypes into a set of underlying principles (6). *Cancer development occurs in a multistep process where numerous hallmarks may be acquired through molecular instability (TSG and oncogene mutations) to establish tumorigenesis. The hallmark of interest in this study is 'Deregulating cellular metabolism'.*

The authors of the Hallmarks of Cancer, Hanahan and Weinberg, articulated that genome instability, inflammation, and the recruitment of normal cells to act as tumorigenesis-aiding stroma, are the culprits of hallmark acquirement (7). The hallmark of interest in this research project is cancer's ability to reprogram its cellular metabolism to promote tumorigenesis.

1.3 Cell Metabolism

To understand how cancer cells adapt their metabolisms, comprehension of normal cell metabolism is critical. In normal cells, metabolism retains a balance between anabolism and catabolism (8). Consumed food is catabolized to produce energy in the form of adenosine triphosphate (ATP) which can be dephosphorylated to adenosine diphosphate (ADP) to release the energy needed to fuel cellular processes. Glucose is the fundamental nutrient catabolized by normal cells (9). The nutrient is transformed into ATP via the process of cellular respiration, which is performed in the presence (aerobic) or absence (anaerobic) of oxygen. Aerobic respiration consists of three vital metabolic pathways: aerobic glycolysis, the citric acid cycle (TCA cycle), and oxidative phosphorylation.

1.3.1 Aerobic Glycolysis

To start, glucose is converted to two molecules of pyruvate via glycolysis in the cell's cytosol (8,10). The glycolytic pathway consists of ten oxidation reactions that are catalyzed by ATP and

nicotinamide adenine dinucleotide (NAD^+) (8). Glycolysis is split into an energy investment phase, and an energy-generation phase (11). In the energy investment phase, there are two important rate-limiting steps worth mentioning. First, glucose is phosphorylated to glucose 6-phosphate by hexokinase (HK) in a rate-limiting, irreversible step that is dependent on ATP. Next, glucose 6-phosphate is rearranged into fructose 6-phosphate catalyzed by the enzyme, glucose phosphate isomerase (PGI). Lastly, phosphofructokinase (PFK) catalyzes the phosphorylation of fructose 6-phosphate into fructose-1,6-bis-P by consuming a molecule of ATP in another rate limiting irreversible step (12). In total, the energy investment phase consumes two ATP molecules. During the energy-generation phase, 4 ATP molecules, as well as 2 NADH coenzymes are produced to create a net total of 2 ATPs. The last step of the energy-generation phase, the conversion of phosphoenolpyruvate to pyruvate by the enzyme pyruvate kinase (PK), is the final rate limiting irreversible step of glycolysis (12). Notably, there are several anabolic metabolic pathways that branch from glycolysis that are crucial in delivering the necessary building blocks needed to form new cells including nucleotides, fatty acids, and amino acids. Among these pathways are the pentose phosphate pathway (PPP), hexosamine biosynthesis pathway (HSP), and serine biosynthesis (5,13). The enzymes that catalyze the steps of glycolysis, as well as which constituents are diverted to the other metabolic pathways are outlined in Figure 1. 2.

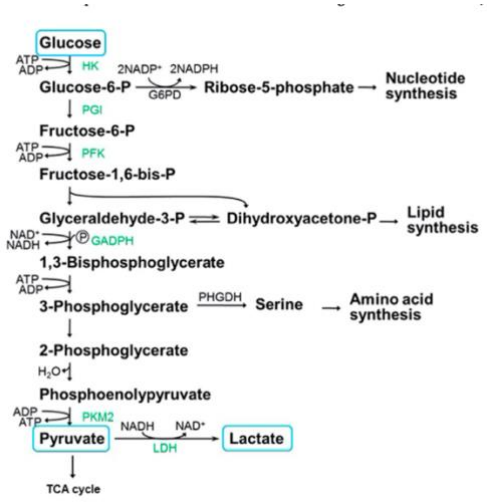

Figure 1. 2 The Glycolytic Pathway and its Associated Anabolic Pathways(8).
Glycolysis is the initial catabolic pathway of glucose metabolism that splits glucose into two molecules of pyruvate. Numerous anabolic pathways that are crucial for cell growth and division diverge from glycolysis.

1.3.2 TCA Cycle

In the presence of oxygen, each pyruvate molecule produced in glycolysis is oxidized into acetyl CoA in the mitochondria, where they are then metabolized into a series of intermediates during the TCA cycle. This process releases ATP, and the reducing coenzymes, $FADH_2$ and NADH (14). The various metabolites generated in the TCA cycle can be transported into the cytosol where they can be used as building blocks for macromolecular synthesis (14). These metabolites, as well as the steps that generate the coenzymes, $FADH_2$ and NADH, are shown in Figure 1. 3. Succinate dehydrogenase (SDH) is the only enzyme of the TCA cycle that also participates in the electron transport chain (ETC).

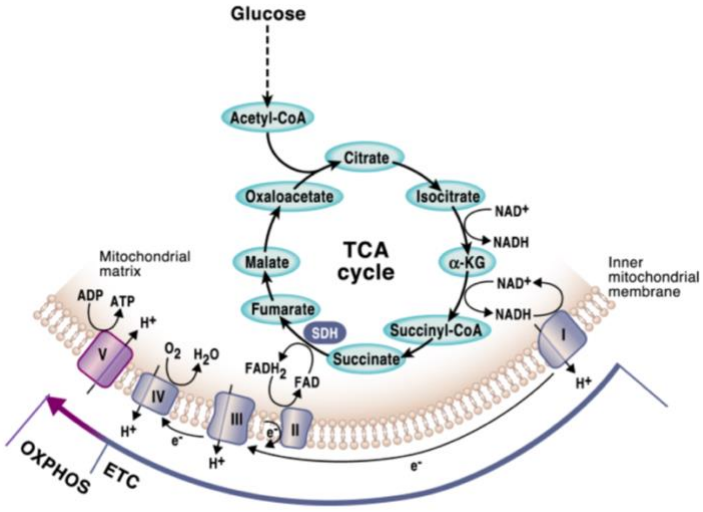

Figure 1. 3 The TCA Cycle and the Electron Transport Chain(14).
It is important to note Succinate dehydrogenase as the only enzyme of the TCA cycle to also take part in the Electron Transport Chain. It is highlighted in purple in the figure. SDH two roles is to catalyze the oxidation of succinate to fumarate in the TCA cycle and transfer electrons from succinate to complex II in the ETC(15).

1.3.3 Oxidative Phosphorylation/ETC

The $FADH_2$ and NADH, produced in the TCA cycle are then shuttled to the ETC where they act as coenzymes in the process of oxidative phosphorylation (OXPHOS) (8,10). The ETC encompasses a variety of proteins complexes bound to the inner mitochondrial membrane including Complex I, II, III, IV, and V. Locations of these complexes are illustrated in Figure 1. 3. Electrons provided by $FADH_2$ and NADH, pass through the protein complexes through a series of redox reactions that release energy used to create an electrochemical gradient across the inner mitochondrial membrane (16). The energy potential fostered in the protein gradient is used

in the process of chemiosmosis to produce a large amount of ATP via the protein, ATP synthase (complex V) (10).

1.3.4 Anaerobic Glycolysis

Contrary to oxidative phosphorylation, under hypoxic conditions (poor availability of oxygen), the pyruvate generated in glycolysis is converted to lactate by lactate-dehydrogenase (LDH) in a process known as anaerobic glycolysis. The process regenerates NAD^+ from the NADH produced in glycolysis to maintain anaerobic glycolysis (5).

1.4 Cancer Metabolism

To fuel the unhinged cell proliferation that characterizes tumorigenesis, cancer cells alter their metabolisms. One function of the oncogenic pathway is to facilitate cellular nutrient uptake and proliferative metabolism, whereas a function of tumor suppressor pathways is to thwart the cell's ability to use nutrients for anabolic purposes (17). Cancer cells acquire certain mutations that alter those functions to support rapid proliferation. The idea that cancer fashions a unique metabolism was first promulgated by Otto Warburg nearly 100 years ago. He observed that cancer cells rely on aerobic glycolysis as opposed to mitochondrial oxidative phosphorylation in a process known as the Warburg effect (5,8,11,17–19). That is, even in the presence of oxygen, cancer cells promote tumorigenesis by fermenting glucose into lactate. Warburg originally hypothesized that cancer cells develop defective mitochondria that are unable to sustain aerobic respiration (17). However, recent studies have revealed that inhibiting the mitochondria leads to a decrease in tumorigenesis suggesting that the mitochondria has a robust role in cancer metabolism (8). Many tumor types rely on glycolysis to supply the energy needed despite glycolysis affording an ATP production that is ~18 fold lower in efficiency than OXPHOS (7). The most prominent explanation for this phenomenon is that glycolytic intermediates can be funneled into anabolic pathways that promote the de novo synthesis of nucleotides, lipids, and amino acids which are needed to build new cells (20). Interestingly, certain products of these anabolic pathways promote redox homeostasis which is needed for unrestrained cell proliferation (5,20). Additionally, cancer cells make up for the loss in ATP production by increasing glucose uptake. Cancer metabolism is heterogenous by nature due to distinct tumor microenvironments,

as well as genetic mutations that arise in certain cancers, but not in others (5). The following overview of cancer metabolism is simplified and general to elucidate key facets.

1.4.1 Glucose Metabolism

Upregulated glycolysis is driven by TSG and oncogenic mutations such as cMyc, KRAS, and p53, as well as signal molecules and transcription factors, HIF-1α, cMyc, Akt, and mTOR, that activate glycolytic enzymes (21). Glucose is shuttled into the cell via glucose transporter (GLUT) proteins, and once in the cytoplasm, is phosphorylated by HK during the first step of glycolysis. To sustain their highly glycolytic attribute, cancer cells must increase their uptake of glucose (8). Oncogenes such as cMyc and KRAS upregulate GLUT1 expression in cancer cells to allow for a greater influx of glucose into the cells (5). Similarly, the loss of function of the TSG, p53, increases GLUT3 expression. High expression of GLUT1 and GLUT3 proteins are associated with dismal survival rates in most types of cancer (22). An increased consumption of glucose promotes increased rates of glycolysis, and thus glycolytic enzymes are upregulated. The PI3K/AKT pathway, a signaling pathway that induces cell cycle progression, is hyperactivated in cancer cells, and upregulates HK2, an isoform of HK (5,17). However, multiple other oncogenes and TSGs along with HIF-1 α promote HK2 upregulation (21). Each glycolytic enzyme is therefore upregulated by multiple factors. Phosphofructokinase-1 (PFK1) serves as an imperative driver of glycolytic flux and is thus upregulated in cancer (21). Additionally, the expression of PFK2, the second isoform of Phosphofructokinase, is upregulated to promote the production of fructose-2,6-bisphosphate, which acts as an allosteric activator of PFK1 to overcome the negative feedback inhibition PFK1 is subjected to by ATP (21). Thus, no matter how much ATP is produced, glycolysis will proceed to sustain unchecked proliferation. Because cancer cells rely on aerobic glycolysis, the conversion of pyruvate to lactate by LDH is overexpressed. LDHA is the most prevalent LDH isoform in cancer due to its preference for pyruvate to lactate transitions (20). The lactate produced via LDHA is then transported out of the cell via monocarboxylate transporters (MCT1-4). MCTs, especially, MCT1 and MCT4, are therefore, also upregulated in cancer.

1.4.2 TCA Cycle/ Glutamine Metabolism

Although it has been largely stipulated that the anabolic pathways that diverge off glycolysis provide cancer cells with necessary nucleotides, lipids, and amino acids, recent evidence has shown that the TCA cycle serves as an anabolic hub for tumor growth (20). In addition to its catabolic role, the TCA cycle supplies the precursors for fatty acid and steroid biosynthesis in the cytoplasm, as well as gluconeogenesis, amino acid biosynthesis, and hemes (8,23). Glutamine, the most abundant amino acid in plasma, is heavily consumed by cancer cells (24). A major function of increased glutamine metabolism in cancer cells is to provide the TCA cycle with its required intermediates. In the glutamine-TCA cycle axis, glutamine is catalyzed first to glutamate, then to α-KG, which can then enter the anabolic phase of the TCA cycle to produce citrate (5,8). The citrate can then migrate from the mitochondria to the cytoplasm where it is catalyzed into acetyl-CoA by the ATP citrate lyase (ACLY) enzyme. That acetyl-CoA is then used in the Fatty Acid Synthesis Pathway (5,25). Glutamine metabolism in cancer is not only involved in supplying the TCA cycle with its necessary constituents, but it also serves as a nitrogen donor for amino acid and nucleotide biosynthesis (24).

1.4.3 Nutrient Scavenging/TME Interactions

A tumor is not simply a cluster of cancer cells, but rather a conglomeration of cancer cells, non-cancerous host cells, secreted factors, blood vessels, and extracellular matrix that is collectively known as the tumor microenvironment (TME) (26). As tumors grow, accessibility to nutrients may become compromised due to their proximity to vasculature or their dense surroundings. Unlike normal blood vessels, tumor vasculature often branches irregularly leading to the poor delivery of nutrients and the nutrient heterogeneity that defines the TME (20). To cope with depleted supplies of essential nutrients, certain cancers have acquired mutations that activate nutrient scavenging pathways (27). Micropinocytosis, a process by which protein rich extracellular fluid is taken up by cells, is upregulated in certain cancers. Once in the cell's interior, the engulfed macropinosomes fuse with lysosomes to release amino acids for the cell's use. Another nutrient-scavenging pathway that promotes tumorigenesis under nutrient-poor conditions is autophagy. Unlike micropinocytosis, autophagy is a form of self-cannibalism, in which intracellular substrates such as proteins, protein complexes, lipids, ions, and even whole organelles are engulfed and degraded to recycle the nutrient components for proliferative uses

(28). There has also been growing evidence that the metabolism's of non-cancerous cells of the TME, including endothelial cells, stromal cells such as fibroblasts, and immune cells, promote tumor progression (20). Through metabolic crosstalk between the different cell types in the TME, cancer cells are able exploit the metabolic products of stromal cells. For example, in pancreatic tumors, stroma-associated pancreatic stellate cells and fibroblasts can provide carbon sources such as alanine and glutamine to support TCA cycle in cancer cells (20). This adds another level of complexity to cancer metabolism.

1.4.4 OXPHOS in Cancer

Otto Warburg's proposition that cancer cells have defective mitochondria, and are therefore incapable of mitochondrial respiration, has since been confounded. Mitochondria play an integral role in tumorigenesis. They supply energy, provide building blocks for proliferation, control redox homeostasis, oncogenic signaling, innate immunity, and apoptosis (25). Moreover, there are some tumors that exhibit high levels of oxidative phosphorylation (25). Recently, the prevalence of "metabolic symbiosis" between hypoxic and aerobic regions of cancer cells was established (8). The highly glycolytic cells in hypoxic regions secrete lactate, which is taken up by surrounding aerobic cells through the lactate transporter monocarboxylate transporter 1 (MCT1). The lactate is then converted to pyruvate which can then undergo OXPHOS to generate a large amount of ATP (8). A consequence of OXOPHS is the generation of reactive oxygen species (ROS) by the electron transport chain. Although excess ROS triggers apoptosis, it is also necessary for tumor proliferation. Previous studies elucidate that the ROS generated by OXPHOS has been linked to anchorage independent growth (29). This reiterates the crucial role mitochondrial ROS generation plays in cancer cell proliferation and tumorigenesis. Furthermore, cancer cells that lack the mitochondrial DNA needed to encode several subunits of the respiratory chain have been generated in vitro. When implanted into mice, the manipulated cancer cells did not survive (30). This further supports the proposition that OXPHOS is necessary for tumor growth.

1.5 Pancreatic Cancer Overview

Pancreatic cancer is a notoriously deadly disease with a 5-year survival rate of approximately 10% in the USA (31). It is the seventh leading cause of cancer death in both men and women

globally, and it is anticipated that pancreatic cancer will surpass breast cancer as the third leading cause of cancer deaths in the European Union (31). Popular risk factors include smoking, alcohol consumption, chronic pancreatitis, obesity, and type 2 diabetes (31,32). Diabetes is linked to the development of pancreatic cancer with a relative risk ratio of 2.1 (31). Patients with the cancer are often divided into four categories based on the respectability of tumor growth: resectable, borderline resectable, locally advanced, and metastatic (31). A mere 15% to 20 % of patients are surgically treated upon diagnosis (33). Most are diagnosed at a later stage due to the lack of symptoms caused by early tumor progression. Additionally, the poor survival outcomes are in part due to the lack of effective targeted treatments. Currently, surgical resection followed by rounds of chemotherapy is the only way to cure the disease (31,34). Later stages are uncurable, and short life expectancies are extended through rounds of chemotherapy and radiation. Common chemotherapy combinations include FLORFIRNINOX (folinic acid, irinotecan, 5-fluorouracil, and oxaliplatin), gemcitabine plus nab-paclitaxel (35). However, these therapeutics fail to extend patient survival more than an additional several months (36). Chemoresistance as well as poor drug penetration of the dense stroma that surrounds PDAC tumors, make the disease difficult to treat (37). Over the past decade, only modest improvements in diagnostic approaches and therapies have been made. This is mainly attributed to the genetic complexity of the disease and the lack of prognostic markers (35).

1.6 Disease Development

The pancreas has both endocrine and exocrine functions (36). The overall purpose of the glandular organ is to retain metabolic homeostasis by generating hormones that modulate blood glucose levels as well as digestive enzymes (36). The most common tumor type is Pancreatic Ductal Adenocarcinoma (PDAC), a malignancy of the exocrine pancreas that constitutes 90 % of all pancreatic cancers (31). PDACs originate from epithelial cells that line the pancreatic duct. The development of PDAC begins with a pre-cancerous lesion, pancreatic intraepithelial neoplasia (PanINs) (38). The progression of PanINs to malignant PDAC is characterized by various oncogene activation and tumor suppressor inactivation. KRAS oncogene mutations are defined early in the PanIN stage and occur in 95% of all PDAC cases (38). Mutations in KRAS lead to the activation of the RAS-RAF and PI3K-AKT pathways, which are involved in cell cycle regulation and angiogenesis stimulation (31). The activation of these pathways induces cell

cycle progression and increases cell proliferation and motility. The tumor suppressor genes p16/CDKN2A are also inactivated in over 90% of cases to promote the transition of the cell cycle from the G1 to S phase (31). The inactivation of these tumor suppressors characterizes the transition from PanIN1 to PanIN2 as seen in Figure 1. 4. TP53 and SMAD4 mutations are observed in the late stages of disease development as the tumor transitions from PanIN3 to PDAC (34). TP53 inactivation supports tumorigenesis through heightened proliferation, increased survival, and inhibition of apoptosis (31).

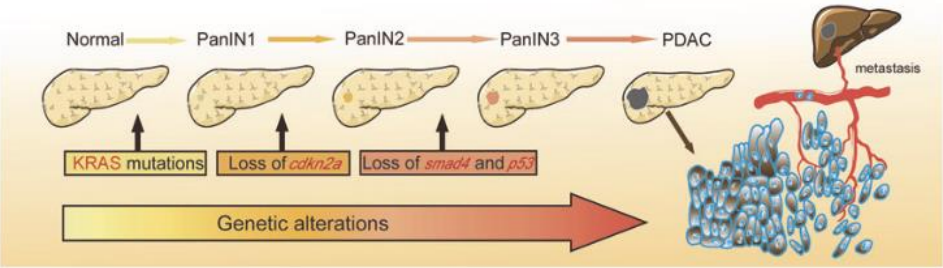

Figure 1. 4 The Stages of PDAC Development(34).
The Development of PDAC is characterized by various oncogene and TSG mutations.

Altogether, the various mutations culminate to drive pancreatic tumorigenesis. As the cancer develops, changes in the surrounding tissue stroma arise (39). PDAC hijacks the immune, vascular, and connective tissue components of the surrounding stroma to create a proliferative favoring TME (39). Myofibroblasts-like cells in the pancreas (pancreatic stellate cells) are activated to produce a fibrosis known as the desmoplasia surrounding the tumor (39). The dense desmoplasia forms a mechanical barrier around the tumor cells, which results in a hypoxic and nutrient-poor environment, especially in the tumor core (40). The TME is also under immense physical and oxidative stress which causes interstitial pressure induced vascular collapse (41). This results in tumor hypoperfusion, limited oxygen, nutrients, and drug delivery to the cancer cells (41). The limited availably of nutrients and oxygen prompts PDAC metabolic rewiring to support continued proliferation.

1.7 PDAC Metabolism

Pancreatic cancer cells rewire their glucose, amino acid, and lipid metabolism to sustain cell growth and division (40). Beyond upregulated metabolic pathways, PDAC cells activate the nutrient salvage pathways, autophagy, and micropinocytosis (13). Furthermore, extensive

metabolic crosstalk occurs between tumor cells and cells of the TME. It is important to emphasize the sheer complexity and heterogeneity that characterizes PDAC metabolism. Patients of PDAC exhibit different metabolic phenotypes. Even the same patient can have tumor subtypes that exhibit different metabolic preferences. Metabolic heterogeneity is driven by genetic mutations, the TME, and the availability of nutrients (40). For example, the availability of nutrients and oxygen heavily influences the metabolic phenotype exhibited by PDAC cells.

1.7.1 Glucose Metabolism

Altered glycolysis is viewed as the major metabolic alteration of PDAC (13). KRAS mutations in PDAC enhances aerobic glycolysis by upregulating the expression of glucose transporters and the rate-limiting enzymes of glycolysis as discussed in section 1.4.1, including GLUTs, HK2, PFK1, LDHA, and MCT 1/4 (13). Increased glycolytic activity promotes PDAC tumorigenesis by providing energy (glycolytic flux and TCA cycle), new building blocks (PPP and serine biosynthesis pathway), ROS regulation (glutamine metabolism and TCA cycle), signal modulation (HBP), and DNA methylation (serine biosynthesis pathway) (13). The diagram that outlines the upregulation of glycolytic enzymes in PDAC in Figure 1. 5, shows that many of the same factors that upregulate glycolysis in other cancers, namely cMyc, KRAS, and HIF-lα, are involved in the upregulation of PDAC glycolysis (13).

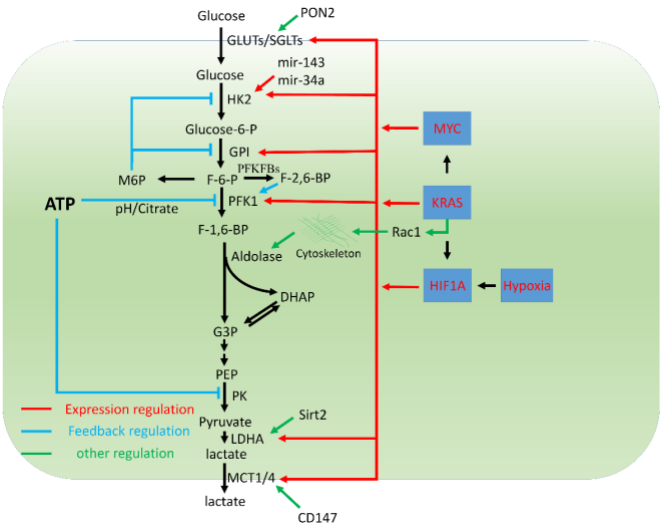

Figure 1. 5 Glycolysis Upregulation in PDAC and its Feedback and Expression Regulation(13). *The oncogenes, cMyc and KRAS, as well as the transcription factor HIF-1α induced by hypoxia, are key regulators of the upregulation of key glycolytic enzymes such as GLUTs, HK2, PFK1, LDHA, and MCT1/4.*

Among the GLUTs isoforms, GLUT-1 is linked to PDAC progression (13). Once glucose accumulates in the cells, several rate-limiting enzymes control the glycolytic process. Among them, PFK1, serves as the gatekeeper for glycolysis and is allosterically inhibited by ATP and low pH in a negative feedback regulation. To support a high glycolytic rate, intracellular pH must be regulated by exporting lactate into the extracellular space. As a result, monocarboxylate transporter 1 and 4 (MCT1 and MCT4) are overexpressed in PDAC (13,42). The buildup of cellular and extracellular lactic acid promotes tumorigenesis by instilling PDAC genetic changes, impairing the anti-tumor immune response, and reducing the adherent junctions on cell membranes (42).

1.7.2 Glutamine Metabolism and the TCA Cycle

Like most other cancers, PDAC cells use the amino acid glutamine to fuel anabolic processes. Glutamine provides a carbon source to fuel the TCA cycle, and a nitrogen source for nucleotide, nonessential amino acids, and hexosamine biosynthesis (43). Glutamine metabolism in PDAC is also crucial in maintaining redox balance (38). Initially, glutaminases (GLS) convert glutamine that enters the mitochondria into glutamate in a process known as glutaminolysis (44). PDAC cells rely on a distinct pathway to fuel the TCA cycle that is mediated by oncogenic KRAS. In a non-canonical pathway, glutamine-derived carbon is converted to aspartate through a series of reactions in the mitochondria (38,43). The glutamine-derived aspartate is then released into the cytoplasm where it is converted to oxaloacetic acid and malate, which eventually produce NADPH, an important modulator of ROS homeostasis and fatty acid synthesis (38).

1.7.3 OXPHOS in PDAC

New studies have revealed that certain PDAC cells heavily rely on mitochondrial OXPHOS to satisfy their metabolic needs (42,45). Pancreatic cancer cells depend on OXPHOS in nutrient poor conditions, or more specifically glucose poor conditions (42). In poorly perfused PDAC, glucose is even more limiting than oxygen. An siRNA screen of metabolic genes performed under low glucose conditions revealed that the mitochondrial genes encoding the ETC components were the most crucial genes in cancer cell survival (42). Therefore, in nutrient rich conditions, pancreatic cancer cells are proliferative in nature and engage in heightened glycolysis to provide building blocks for growth, while in nutrient poor conditions, the cells are put into

survival mode where ATP generation is prioritized over proliferation (42). This is highlighted in Figure 1. 6. Furthermore, a study conducted by Shiratori *et al*. demonstrated that the suppression of glycolysis in Panc-1 pancreatic cancer cells induced a metabolic switch towards an OXPHOS phenotype (45). This reiterates the metabolic heterogeneity, as well as the metabolic flexibility of PDAC cells. Different pancreatic cancer subpopulations also exist, one of which, the pancreatic cancer stem cells (PaCSCs), rely on OXPHOS and are drivers of tumorigenesis and metastasis (46). Pancreatic cancer cells can therefore be metabolically classified into a glycolytic, OXPHOS, or a hybrid glycolytic/OXPHOS phenotype (45). Therefore, Glycolysis and mitochondrial respiration through OXPHOS coexist in PDAC, although one pathway usually dominates (45,47).

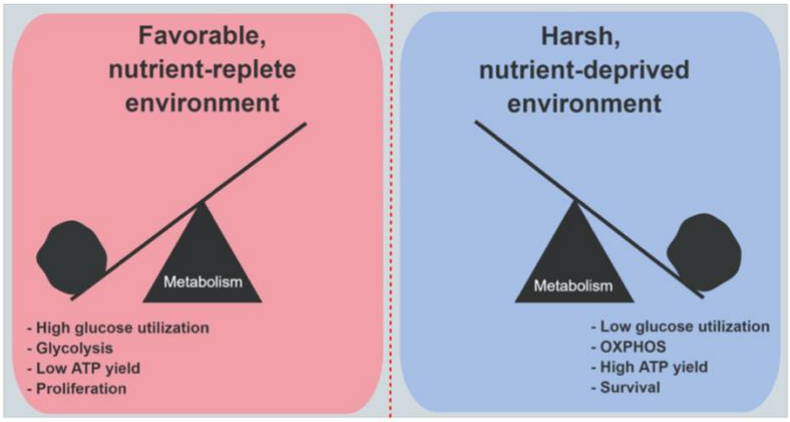

Figure 1. 6 PDAC Metabolic Phenotypes Depend on Glucose Availability (42).
Under nutrient favorable conditions, PDAC exhibits glycolysis, while under nutrient depleted conditions PDAC favors OXPHOS.

1.8 Chemoresistance in PDAC

Because of the lack of symptoms attributed to PDAC, the disease is often diagnosed at a late stage. Consequently, chemotherapies tend to be largely ineffective due to the cancers having acquired cytoprotective mechanisms that render them drug resistant (36). Compared with other chemotherapy regimens, the resistance of PDAC to gemcitabine is well documented. Gemcitabine enters pancreatic cancer cells and engages in a series of phosphorylation steps. The derivatives can then interfere with DNA synthesis and block cancer cell proliferation (40). PDAC resistance results from multiple molecular and cellular changes that affect nucleotide metabolism enzymes, apoptosis pathways, drug efflux pumps, cancer stem cells or epithelial-to-mesenchymal transition (EMT) pathway, and up-or-down regulated expression of specific

microRNA (miRNA) (48). One study conferred that gemcitabine resistance in PDAC is caused by the transcription factor, insulin-like growth factor 1 receptor (IGF1R), induced upregulation of cell surface adhesion receptor (CD44) expression and isoform switching (49). CD44 acts as a regulator of EMT and epithelial plasticity, and PDAC cells with high levels of CD44s are more invasive and gemcitabine resistant (49). Another study found that the aberrant expression of genes related to cell survival and apoptosis are key drivers of gemcitabine resistance (50). Other players in chemoresistance include the upregulation of drug metabolism enzymes. For example, PDAC patients with high levels of 5-FU catabolism enzymes, dihydropyrimidine dehydrogenase (DPD) and thymidylate synthase (TS), were more resistant to 5-FU (48). Chemoresistance in PDAC is therefore, highly multifactorial. Emerging studies have revealed PDAC metabolism may in part be a result of its altered metabolism.

1.8.1 OXPHOS and Chemoresistance

As elucidated previously, PDAC cells are metabolically heterogenous and flexible, exhibiting either a glycolytic phenotype, an OXPHOS phenotype, or a hybrid depending on the availability of nutrients and oxygen in the TME, as well as key oncogenes and tumor suppressor genes (45). Recent studies have revealed that reprogrammed metabolism is a primary promoter of chemoresistance, radioresistance, and immunosuppression (40). Specifically, OXPHOS drives cancer drug resistance and influences the response of chemotherapy treatments (51). mtDNA mutations or reductions in the number of mtDNA, alter OXPHOS physiology and are common in most cancers including PDAC (45). In fact, cancer cells that lack mtDNA or possess a low number of copies show higher apoptosis rates under chemotherapy, supporting the mounting evidence that OXPHOS play a dynamic role in PDAC chemoresistance (45). This is further supported by the existence of the highly OXPHOS dependent subset of PDAC cells, PaCSCs, that are known to be responsible for chemoresistance and cancer recurrence (32,52) The mechanisms for OXPHOS induced chemoresistance is complex and unclear, but it is believed that cytotoxic chemotherapy drugs target cells that proliferate rapidly, thus targeting glycolytic as opposed to OXPHOS performing cells (53). The mitochondria may therefore serve as a crucial target for novel therapeutics to reverse chemoresistance in PDAC. In recent years, much attention has been given to complex I (NADH dehydrogenase) of the ETC. One study revealed that high OXPHOS tumors are enriched in mitochondrial respiratory complex I at protein and

mRNA levels (47). Targeting complex I of the ETC by various therapeutics, such as metformin and phenformin, to promote chemoresistance reversal has been a hot research topic in recent years. Both drugs are used to treat patients with type II diabetes (T2D) and are classified as biguanides, however, for the purposes of this study, metformin's role in OXPHOS inhibition will be discussed.

1.9 Metformin

Metformin, a biguanide derivative, works by controlling blood-glucose levels in patients with T2D. It restores the body's response to insulin and decreases the amount of blood sugar that the liver produces due to a reduction in the rate of gluconeogenesis (47). Metformin does this by activating adenosine monophosphate kinase (AMPK) resulting in the inhibition of the enzymes involved in in gluconeogenesis and glycogen synthesis in the liver, while prompting insulin signaling and glucose transport in muscles (47). In recent years, metformin has also been found to have a dual effect on PDAC.

1.9.1 Metformin and PDAC

Metformin is associated with a reduced risk of pancreatic cancer in patients with type 2 diabetes (T2D) (54). However, the effect of metformin on those with established pancreatic cancer is unconfirmed. A meta-analysis performed to analyze the effect of metformin on the survival of pancreatic cancer patients at various stages revealed that there was significant improvement in survival in metformin users compared with the control group (55). Contrastingly, other studies have revealed no association between metformin usage and survival in patients with pancreatic cancer (56). Moreover, preclinical trials have produced promising results, however these investigations have applied higher concentrations of metformin than what is achieved in vivo (57). When metformin is prescribed to diabetic patients, doses typically start at 500-850 mg administers orally every 12 hours, increasing to maximum dose of 2550 mg/day (57). The maximum blood plasma concentration of metformin achieved is usually below 1.5 μg/mL (58). Current in vitro results are therefore inaccurate, and further experiments are necessary.

1.9.2 Mechanism of Action

Once in the body, the hydrophilic drug can only cross the lipid membranes of cells with the help of Organic Cation Transporters (OCTs1-3)(59). There have been multiple proposed theories as to how metformin treats PDAC. Some studies describe the metformin anti-PDAC effect through the activation of AMPK, which in turn inhibits mammalian target of rapamycin complex I (mTORC1) and reduces protein synthesis and cell proliferation (45,60,61). On study found that PDAC cells treated with metformin had a higher proportion of cells were in the G_0/G_1 phases of growth than those in the S-phase due to metformin's activation of AMPK and inhibition of mTOR (60,61). In addition, metformin AMPK activation has shown to disrupts the crosstalk between the insulin/IGF-1 receptor and GPCR signaling in PDAC, which mitigates the growth of treated cells in xenograft models (62). Most importantly, metformin is then speculated to inhibit complex I of the ETC in the mitochondria, NADH dehydrogenase (45). This leads to a decrease in mitochondrial respiration and a promotion of glycolysis to compensate for inefficient mitochondrial metabolism (45). Several studies have shown that the highly OXPHOS dependent PaCSCs can be eliminated by a metformin treatment. One found that a pretreatment of 3 and 10 mM of metformin on in vitro PaCSCs spheres led to the inhibition of the CSCs' self-renewal capacity as well as reduced their migratory and invasive capacity(32). This conclusion was drawn based on the observation that the metformin pretreatment decreased the size and number of spheres formed. Additionally, the formation of spheres in the second and third passages were drastically hindered (32). Due to the reduced metabolic plasticity of PaCSCs, another study found they have a limited ability to switch to glycolysis upon metformin mitochondrial inhibition and are effectively eliminated as a result (63). The mechanism of action divulged in both studies was that metformin treatment reduced ATP levels and decreased the mitochondrial transmembrane potential due to complex I inhibition. Metformin's ability to hinder OXPHOS has major implications for chemoresistance reversal. The use of metformin as an adjuvant therapy to chemotherapy can potentially reverse chemoresistance and cancer reoccurrence (64). The success of this combined treatment was highlighted in a study that analyzed mice xenograft models of a triple-negative breast cancer cell line (65). The combination of metformin and the chemotherapy, doxorubicin, led to the elimination of both CSCs and non-CSCs, which reduced tumor mass and prolonged remission more effectively than either drug alone in the xenograft models (65). A combination therapy of metformin and chemotherapy could produce promising

results in PDAC. However, it is crucial to use clinically relevant concentrations in vitro to best predict in vivo results.

1.10 Modelling Cancer In Vitro

To test whether certain drugs have an anticancer activity, they are first tested in vitro with 2D monolayer cell cultures. Unfortunately, 2D cell cultures do not accurately represent in vivo environments, and successful results produced in vitro do not always translate to success in the human trials (66). In 2D monolayer cultures, cells grow side-by-side to each other, adhered to a plastic surface. This eliminates any ability to engage in cell-cell and cell-ECM interactions, which are both essential cell proliferation, vitality, responsiveness to stimuli, drug metabolism, and expression of genes (67). Additionally, cells grown in 2D have unlimited access to nutrients in the provided medium since each cell is directly exposed to the culture medium (67). However, cancer cells have varying availability to nutrients due to the TME and other cancer cells that surround tumors. It is crucial to implement in vitro cultures that better mimic in vivo tumor environments.

1.10.1 3D Spheroids in Drug Testing

3-dimensional culture models may bridge the gap between monolayer cell culture and in vivo studies (68). Instead of simply growing side-by-side, cells can be grown on top of one another, which introduces a 3D element. The 3D culture is often referred to as spheroids. Compared to 2D culture models, 3D spheroids mimic the microenvironment often seen in tumor tissues (69). They therefore better replicate cell-cell interactions, cell-matrix interaction, nutrient and oxygen gradients, and cell polarity (68). In solid tumors, oxygen, and nutrient delivery to cells in the inner areas of the tumor becomes compromised due to increased diffusion distances and abnormal vascular architectures, this is especially true in PDAC. This leads to nutrient and oxygen gradients and metabolic reprogramming. During the growth of spheroids, a nutrient and oxygen gradient is also established, where cells in the center of the spheroid are deprived of oxygen and nutrients, and are therefore hypoxic, while cells in the outer spheroid are aerobic and nutrient rich (70). This discrepancy also influences the metabolism of the spheroid, where cells in different regions exhibit different metabolic phenotypes, much like what occurs in vivo (70). This is highlighted in Figure 1. 7.

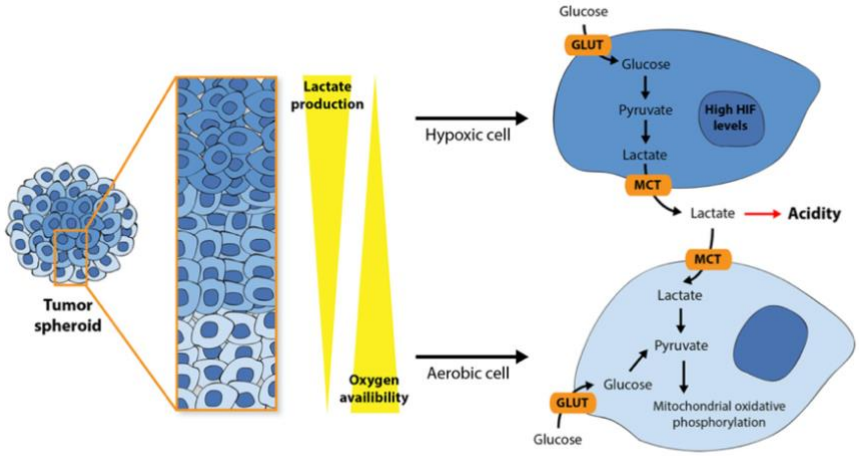

Figure 1. 7 Oxygen Availability in Tumor Spheroids(70).
Cells located in the center of the spheroid have poor oxygen perfusion and are therefore, hypoxic. Whereas cells away from the center have better oxygen availability.

Spheroids can therefore mimic the chemoresistance that occurs due to rewired metabolism and would serve as better in vitro models for the analysis of the effects of metformin and chemotherapy in PDAC.

1.11 In Vitro Metabolic Analysis

Because the alteration of cellular metabolism plays a critical role in PDAC progression and complexity, the ability to measure metabolic rates in-vitro is crucial to oncology research. Agilent Technologies has developed machines called, Seahorse XF Analyzers, that are capable of automatically measuring energy metabolisms in real time. They do this by measuring oxygen consumption rates (OCR) and extracellular acidification rates (ECAR) of live cells. Mitochondrial respiration is aerobic in nature where the ETC encompasses a series of exergonic reactions that ultimately reduce molecular oxygen to water (71,72). OCR is therefore an excellent indicator of mitochondrial respiration. Contrastingly, in the absence of oxygen, anerobic glycolysis converts pyruvate to lactate, which is then secreted into the extracellular matrix (73). ECAR values are, therefore, indicators of glycolysis rates. To measure the OCR of cells on the Seahorse XFp analyzers, an Agilent Seahorse XFp Cell Mito Stress Test is performed. The assay works by adding modulators of respiration into the cell wells during the assay to determine the parameters of mitochondrial function(74). The modulators used in the kit are Oligomycin, Carbonyl cyanide-4 (trifluoromethoxy) phenylhydrazone (FCCP), Rotenone,

and Antimycin (74). The injection sequence, as well as the mitochondrial parameters each modulator reveals is outlined in Figure 1. 8.

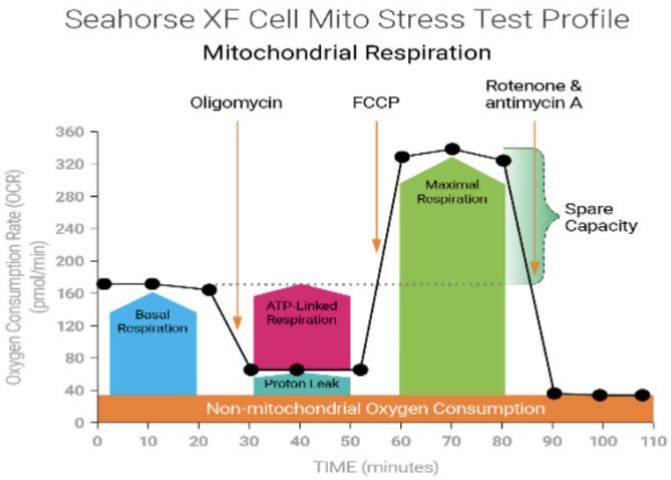

Figure 1. 8 The Injection of Mito Stress Test Modulators to Assess Mitochondrial Respiration Parameters (74).

The first modulator to be injected, Oligomycin, inhibits ATP synthase (complex V) of the ETC (74). A nonfunctional ATP synthase impedes the flow of electrons through the ETC, resulting in a reduction of mitochondrial respiration or OCR (72,75). Basal respiration measures respiration before the addition of modulators, which includes ATP-linked respiration and proton leak pathways (72). The injection of oligomycin allows for the determination of ATP production (ATP-linked respiration), which is the OCR value that is used to drive ATP production. The mitochondrial OCR remaining after oligomycin injection is a measure of proton leak. This occurs when OXPHOS is incompletely coupled, allowing protons to leak across the inner membrane independent of ATP synthase. The electrons leak through the membrane through uncoupling proteins (UCPs) (76). The next modulator injection is FCCP, which is an uncoupling agent that collapses the proton gradient and obstructs the mitochondrial membrane potential(74). This results in an unhinged flow of electrons through the ETC, and oxygen consumption by complex V reaches a maximum, which determined maximal respiration. The FCCP injection also determined spare capacity or spare respiratory capacity, which is defined as the difference between basal respiration and maximal respiration; or the ability of the cell to meet an increased demand in energy (72). The final injection is a mixture of Rotenone, a complex I inhibitor, and Antimycin, a complex III inhibitor. This allows for the complete shutdown of mitochondrial

respiration and determined nonmitochondrial respiration, or OCR values that are attributed to processes outside the mitochondria (74).

To measure the ECAR of cells on the Seahorse XFp analyzers, an Agilent Seahorse XFp Glyco Stress Test is performed. Like the Mito Stress Test, different modulators are injected sequentially to reveal key parameters of glycolytic flux: Glycolysis, Glycolytic Capacity, and Glycolytic Reserve (77). The modulators as well as the parameters are highlighted in Figure 1. 9.

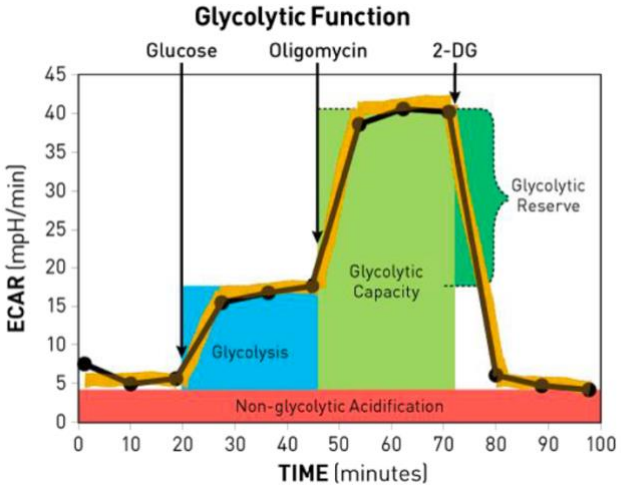

Figure 1. 9 The Injection of Glyco Stress Test Modulators to Assess Glycolysis (77).

The first injection is a saturating concentration of glucose (10 mM) (77). The cells catabolize this glucose through glycolysis resulting in a spike of ECAR. This glucose-induced response is characterized as the rate of glycolysis under basal conditions(77). The second injection is Oligomycin, which was already described as a complex V inhibitor. The inhibition of complex V shifts the entire energy production of the cell to glycolysis, thus revealing the glycolytic capacity of the cell. The final injection is 2-deoxy-glucose (2-DG), a glucose analog, competes with glucose for binding to glucose hexokinase (77). This process inhibits glycolysis and causes a dramatic decrease in ECAR, which confirms that the ECAR produced throughout the experiment was due to glycolysis (77). Any ECAR that remains is causes by processes other than glycolysis and is termed non-glycolytic acidification. Lastly, the difference between glycolytic capacity and glycolysis is the glycolytic reserve.

1.12 Biomarkers of Interest in PDAC Metabolic Interpretation and Treatment

The response and effectiveness of metformin depends on the metabolic phenotype of the PDAC cells, glycolytic, OXPHOS, or hybrid (45). Because metformin hinders OXPHOS, it is largely effective against phenotypically OXPHOS cells. Therefore, the effectiveness of a metformin-chemotherapy combination in vivo will largely depend on the metabolic profile of the individual patient. Depending on the metabolic phenotype expressed by the PDAC cells, certain metabolic genes will be upregulated or downregulated. For example, genes that express glycolytic enzymes will be upregulated in phenotypically glycolytic cells, whereas genes that express OXPHOS enzymes will be upregulated in phenotypically OXPHOS cells. A genetic analysis of common metabolic genes may therefore serve as an indication of metformin effectiveness both in vitro and in vivo. The common metabolic genes of interest in this project include UCP2, LDHA, SUCLA2, SLC22A1, SLC16A1, PFKM, NDUFS1, ATP5F1A, and HK2. The first, UCP2 encodes the protein uncoupling protein 2 (UCP2), which has already been elucidated to facilitate the transportation of electrons in protein leak pathways (76). It has been found that UCP2 is upregulated in highly glycolytic cancer cells as a cryoprotective measure against increased ROS exposure (78). The mitochondrial uncoupling of the protein leak pathways has been identified as an important regulator of the excessive ROS produced among highly glycolytic cells (78). LDHA expresses the enzyme Lactate Dehydrogenase A (LDHA) and has already been recognized to be upregulated in highly glycolytic PDAC (13). The gene, SUCLA2, encodes the protein succinate-CoA ligase ADP-forming subunit beta (A-SCS), which is an essential component of the TCA cycle, and would thus be upregulated in OXPHOS cells. SLC22A1 encodes OCT1, the transporter protein that facilitates the transport of metformin into the cell (59). SLC16A1 encodes MCT1, which exports lactate out of the cell and is upregulated in highly glycolytic PDAC (13). PFKM expresses PFK1, which catalyzes a crucial rate-limiting step of glycolysis and is upregulated in highly glycolytic PDAC (12,13). NDUFS1 encodes NADH dehydrogenase or complex I of the ETC. It has been found that highly OXPHOS cancer cells are enriched in complex I proteins (47). ATP5F1A encodes ATP synthase or complex IV of the ETC and is upregulated in highly OXPHOS PDAC. Lastly, HK2 expresses HK2, which is highly upregulated in phenotypically glycolytic PDAC (13).

Chapter 2 Research Aims and Hypothesis

2.1 Rationale

Pancreatic cancer cells, like many other cancers, upregulate glycolysis to sustain rapid proliferation. However, metabolic flexibility allows the PDAC cells to switch to OXPHOS when nutrient availability, specifically glucose, is scarce (42). Furthermore, a subset of PDAC cells, PaCSCs, are largely OXPHOS dependent, and are major contributors of chemoresistance. Mitochondrial respiration may, therefore, have a major role in PDAC chemoresistance (46). Preventing mitochondrial respiration may mitigate or even reverse chemoresistance. The Type 2 Diabetic drug, metformin, has been found to inhibit complex I of the ETC, and therefore hinder the cell's ability to undergo OXPHOS. As a result, cells are put under metabolic stress and switch to glycolysis to meet the energy demands of the cell. Metformin may therefore be used as an adjuvant treatment in addition to chemotherapy. However, previous studies that have investigated the impact of metformin, have used unrealistically high concentrations of the drug in vitro with very short exposure times. The use of clinically relevant concentrations and exposure times of metformin is critical to replicate in vivo conditions. Furthermore, the effectiveness of metformin in its ability to treat patients with pancreatic cancer remains inconclusive. This may be due to pancreatic cancer's metabolic heterogeneity, and the exhibition of different metabolic phenotypes among different patients. Not much research has been generated in analyzing the effect of metformin on the metabolic profiles of cancer cells. This research will therefore analyze metformin's impact on metabolic rates of homogenous pancreatic cancer cell lines. The goal is to assess how metformin alters the metabolic phenotypes and performances of homogenous cells to predict how it would perform among heterogenous cells in vivo. Additionally, this research will analyze the impact metformin has on the performance of different chemotherapy drugs by performing in vitro experiments using clinically relevant concentrations of all drugs involved.

2.2 Specific Aims

The overall aim of this project is to assess how metformin affects the metabolic profiles of treated PDAC cell lines, and to analyze how a combination of metformin and various chemotherapies impact the growth and viability of PDAC cells grown in 3D. To accomplish this the following objectives will be implemented:

- To test if AsPC-1 and Panc-1 pancreatic cancer cell lines exposed to a pre-treatment of 11.6 μM metformin become sensitized to various chemotherapies (5-FU, Oxaliplatin, SN-38, and Gemcitabine) by assessing 3D spheroid growth and viability
- To analyze the metabolic changes of the same cell lines after the metformin pretreatment by performing seahorse assays
- To assess any metabolic gene expression changes that may occur due to the metformin pretreatment by performing a SYBR green RT-qPCR to identify any novel metabolic biomarkers

Chapter 3 Materials and Methods

3.1 Materials

All materials used in this thesis are listed in Appendix A.

3.2 Methods

3.2.1 Aseptic Technique

Most of the methods described in this thesis were performed in adherence to aseptic technique. Upon entry to the cell lab, donning of the appropriate PPE was conducted. Gloves were always worn and sprayed with 70% ethanol while handling laboratory equipment and cells. Before using the biosafety cabinets, they were thoroughly disinfected with 70 % ethanol. Any equipment to be used in the biosafety cabinet, were sprayed with 70 % ethanol prior to their placement in the cabinet. After biosafety cabinet use, its surfaces were disinfected with 70 % ethanol. The sash was closed, and the UV light was switched on to eliminate any remaining contaminants.

3.2.2 Cell Lines

Two different pancreatic cancer cell lines were used in this study: AsPC-1 and Panc-1. The American Type Culture Collection (ATCC) numbers, as well as a description of the primary source are listed in Table 3. 1 (79,80).

Table 3. 1 Information Provided by ATCC of the Cell Lines, AsPC-1 and Panc-1

Cell Line	ATCC #	Primary Source	Disease
AsPC-1	CRL-1682	Derived from nude mouse xenografts established with cells from a 62-year-old, White, female patient	Adenocarcinoma
Panc-1	CRL-1469	Derived from the pancreatic duct of a 56-year-old, White, male	Epithelioid Carcinoma

Both cell lines are commonly used to study PDAC in-vitro. In this study, AsPC-1 was found to be largely quiescent, while Panc-1 cells largely OXPHOS phenotypically.

3.2.3 Resuscitation of Frozen Cell Lines

Cryotubes containing AsPC-1 and Panc-1 cell lines were removed from liquid nitrogen storage and thawed at room temperature. The contents of the each cryotube were then transferred to a 75 cm^2 or 25 cm^2 culture flask filled with 10 mL or 5 mL of prewarmed complete growth media, respectively. The culture flasks were labelled with the name of the cell line, passage number, and date before incubating at 37 ℃ 5% CO_2.

3.2.4 Complete Cell Medium

Cell medium was composed of all the components and volumes listed in Table 3. 2. The Fetal Bovine Serum, Pen/Strep solution, L-glutamine, and glucose solution were all added to the Dulbecco's Modified Eagle's Media (DMEM). The 1 M glucose was prepared from 45% glucose solution. To replicate in vivo conditions, the cell lines were grown in a physiological relevant concentration of glucose, 1 M, which is defined as a *low glucose* level (hypoglycemia). According to the World Health Organization, typical blood-glucose levels range from 4-11 mM, 1 M would, therefore, be considered a hypoglycemic level (81).

Table 3. 2 DMEM Complete Media Recipe

Components	Volume (mL)
DMEM (Dulbecco's Modified Eagle's Media) without glucose, L-glutamine and sodium pyruvate	500
Fetal Bovine Serum, heat inactivated, South America	50
PenStrep solution 100 X	5
L-glutamine, 200 mM	5
Glucose solution, 1M	2.75

3.2.5 Adherent Cell Culture and Cell Passaging

The cell lines grew to the surface of a 75 cm^2 or 25 cm^2 culture flask. Every other day, the culture medium was aspirated out of the culture flask and replaced with 10 mL (75 cm^2) or 5 mL (25 cm^2) of prewarmed fresh complete medium. Cell growth was analyzed everyday using the Olympus CKX41 Light Microscope to assess the confluency of the cells and check for the presence of contamination. The confluency percentage that prompted a cell passage depended on which assay was to be performed. Generally, cells were passaged at 70-90 % confluency. To

passage the cells, the media in the culture flask was aspirated out. The flask was then rinsed with ~ 5 mL of pre-warmed 1xPBS (PBS) to ensure that any serum in the monolayer was properly removed before the addition of 1X Trypsin-EDTA (Trypsin). After gyrating the PBS in the flask, it was aspirated out and 1 mL of prewarmed trypsin was added. Immediately after the addition of trypsin, the flask was placed in the 37 ℃ 5 % CO_2 incubator for ~1 min. The flask was then assessed under the microscope. If most cells were still adhered to the bottom of the flask, the flask was placed back into the incubator. Once 90 % of cells were in suspension, trypsinization was stopped by adding ~4 mL of prewarmed complete media. The added medium was dispersed by pipetting over the cell layer surface at least 3 times. The cell suspension was then added to a 15 mL falcon tube and either used for splitting or for assays. In the case of splitting, the cells were usually split in a 1:2 or 1:5 ratio. A new culture flask was used every 10 days.

3.2.6 Cell Counting using the Muse Count and Viability Assay

To harvest a certain density of cells for experiments and assays, the correct cell count was determined using the Muse™ Cell Count and Viability Assay. Approximately 0.5 mL of cell suspension was transferred from the 15 mL falcon tube as described in section 3.2.5 to a 1.5 mL Eppendorf tube. A microcentrifuge tube was obtained and filled with the appropriate amount of Muse™ Count and Viability Reagent. The amount of reagent added was based on the concentration of original cell suspension (cells/mL), which was usually 1x 10^5 to 1x 10^6. The amount of both Muse™ Count and Viability Reagent and cell suspension to be added to the microcentrifuge tube is described in Table 3. 3.

Table 3. 3 Muse™ Cell Suspension Dilutions

Concentration of original cell suspension (cells/mL)	Dilution factor	Cell suspension Volume (μL)	Count & Viability Reagent Volume (μL)
1x10^5 to 1x 10^6	10	50	450
1x 10^6 to 1x 10^7	20	20	380
1x 10^7 to 2x 10^7	40	20	780

Once the appropriate amounts of Count and Viability Reagent and cell suspension were added, the microcentrifuge tube was vortexed and incubated for 5 min in a drawer. After the incubation, the "run assay" option was selected, and the microcentrifuge tube of cell suspension and reagent

was vortexed and loaded into the instrument. A viability plot produced by the Muse™ Cell analyzer is equipped with adjustable markers that allow for the elimination of debris and nucleated dead cells. The viability values were obtained: the number of viable cells/mL and viability %. Typically, viability percentages were no less than ~97 %. A visual representation of the viability plots provided by the Muse™ Cell analyzer is provided in Figure 3. 1.

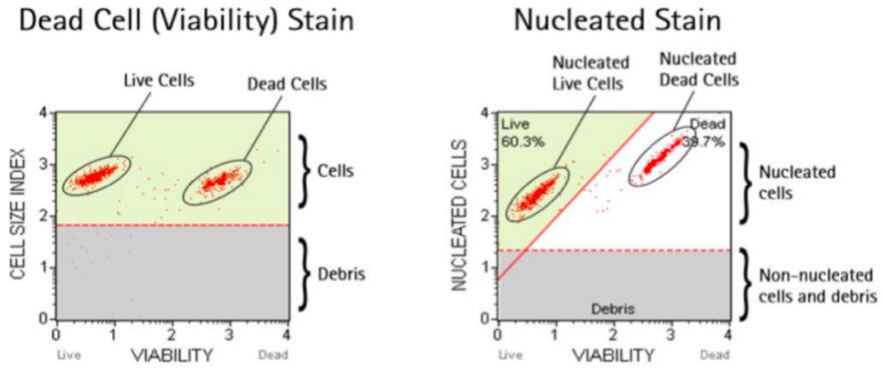

Figure 3. 1 Muse Viability Plots that allow for the Elimination of Debris and Dead Cells
The plot titled "Dead Cell (Viability) Stain" allows for the elimination of debris, while the plot labelled "Nucleated Stain" allows for the elimination of dead cells. This process ensures that an accurate cell count and viability percentage is determined.

3.2.7 Metformin Aliquots

The cell lines, AsPC-1 and Panc-1 were subjected to a pretreatment of metformin. As already explained, previous studies examining the effect of metformin on cancer cells have used unrealistically high concentrations of the drug. To mimic in vivo, the pancreatic cancer cells in this study were subjected to a clinically relevant concentration for an extended period, 11.6 µM of metformin. The chosen value is within the range of the mean maximum plasma concentration of metformin, between 0.4 and 5 µg/mL (82). To begin the process, 3 mM metformin aliquots were prepared from a 1 M prefiltered stock concentration that had been previously aliquoted by a former PhD candidate and were kept frozen at -25 ℃. All dilutions were performed in dH_2O in 1.5 mL Eppendorf tubes. The aliquots were correctly labelled and frozen at -25 ℃ until use.

3.2.8 Culturing Cell Lines in the Presence and Absence of Metformin

To address the impact that a metformin pretreatment has on pancreatic cancer cells, several outcomes were examined: the impact on gene expression, cell growth, chemotherapy performance, and metabolic profile. The experiments analyzing these traits were compiled into a workflow described in Figure 3. 2.

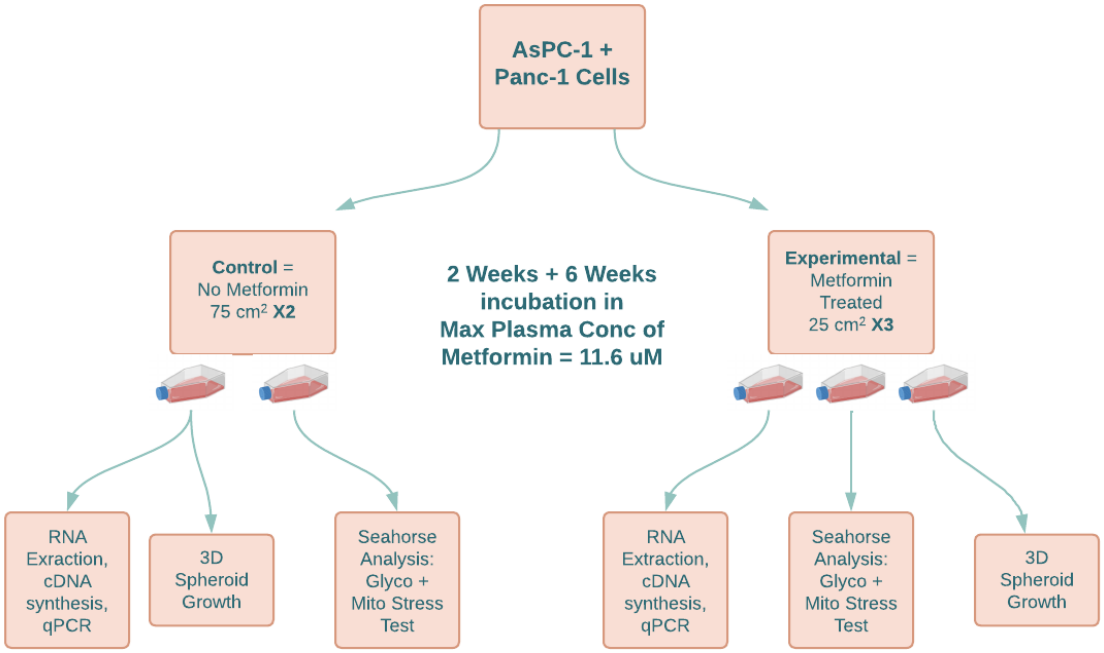

Figure 3. 2 A Flowchart Outlining the Experiments Performed to Analyze the Impact of the Metformin Pretreatment on AsPC-1 and Panc-1 Pancreatic Cancer Cells.
Cells were cultured in 11.6 µM of metformin for a total of 6 weeks. Three 25 cm^2 culture flasks were designated as the experimental group, which were subjected to the metformin treament. Additionally, two 75 cm^2 culture flasks served as the contorl group, which were cultured in the absence of metformin. Each flask was used in an experiment at the end of 2 weeks, and 6 weeks of incubation.

To inoculate cell culture with metformin, prewarmed complete DMEM was spiked with metformin. The treated DMEM was made fresh for every use. For each cell line, three 25 cm^2 flasks were prepared with 5 mL of the metformin-treated media. Additionally, two 75 cm^2 control flasks were prepared with 10 mL of DMEM without metformin. When passaging the treated cells, cell trypsinization was stopped with the metformin-treated media. Cells were incubated in the 37 ℃ 5% CO_2 incubator for a total of 6 weeks to mimic the prolonged clinical administration of the drug, which is usually taken for extended periods of time. After 2 weeks of incubation, the metformin-treated and control cells were subjected to three different assays, an

RNA extraction, a seahorse analysis (Glyco and Mito Stress Test), and 3D Spheroid seeding. All experiments were repeated after 6 weeks of incubation. It's important to note that each metformin-treated flask was assigned to a specific experiment to allow the same cells to undergo its designated experiment at 6 weeks of treatment. To ensure that enough time was allotted to each experiment, the AsPC-1 cell culture was instigated one week before the Panc-1 cell culture.

3.2.9 RNA Extraction

To analyze metformin-treatment induced gene expression changes, an RT-qPCR was performed. To prepare for this procedure, RNA was first extracted from the cell lines after 2 weeks and 6 weeks of incubation. The Quick-RNA Miniprep kit from Zymo Research was used to extract RNA according to the manufacturer's protocol. Both the metformin-treated cells and the control cells were trypsinized, and 1 mL of each cell suspension was transferred to a 1.5 mL Eppendorf tube. Duplicates of the cell suspensions were made to create a total of two metformin samples and two control samples for each cell line. The cell suspensions were centrifuged at 2,000 rpm for 5 min to pellet the cells. The supernatants were then discarded, and the RNA extraction proceeded. After extraction, the RNA was quantified by the NanoDrop One UV-Vis spectrophotometer. The A_{260}:A_{280} ratio of each sample was determined (>1.9). All data, including the A_{260}:A_{280} ratios and the total concentration of each RNA sample in ng/µl, was recorded. An additional RNA quality control was conducted using the Bioanalyzer RNA 6000 Nano Assay. Results of the assay revealed the quality and characterization of total RNA. The values from both the Nanodrop and RNA kit can be found in Appendix B and Appendix C. The extracted RNA samples were then labelled and stored at -80℃ for future use.

3.2.10 cDNA synthesis

The extracted RNA from each sample was reversed transcribed into cDNA using the QuantiTect Reverse Transcription Kit according to the manufacturer's protocol. The concentrations of RNA in ng/µl were used to calculate the volumes of the RNA samples needed to achieve a total of 1 µg of RNA. All cDNA synthesis reactions were performed with 1 µg of RNA. The synthesized cDNA samples were dissolved in RNAse free water and stored at -80℃ to await RT-qPCR execution.

3.2.11 Designing Primers for RT-qPCR

To design primers for the following genes, UCP2, LDHA, SUCLA2, SLC22A1, SLC16A1, PFKM, NDUFS1, ATP5F1A, and HK2. The primer designing program, Primer3 was used. First, each gene was located on the NCBI Gene database, and the NCBI Reference Sequences (RefSeq) option was selected, which revealed the exon sequences of the gene. The FAFSTA sequence was copied and pasted into Primer3, and any necessary exclusions were made. All primers were designed in the exon region. To ensure that no contaminating gDNA was amplified, primers were also designed to flank between two exons. The primers are listed in Table 3. 4. The last two primers were ready to use QuantiTect Primer Assays by Qiagen, and they served as the reference genes.

Table 3. 4 SYBR Green Gene Expression Primers

Gene Symbol	Gene Name	Supplier	Sequence	Primer Length	Amplicon Length
UCP2	Uncoupling Protein 2	Invitrogen	L: GAG ACC TTA CAA AGC CGG CT R: ATT CCT GAC CTT GAG CTG GG	20	78
LDHA	Lactate Dehydrogenase A	Invitrogen	L: ACG TGC ATT CCC GAT TCC TT R: AAC AGC ACC AAC CCC AAC AA	20	130
SUCLA2	Succinate-CoA Ligase ADP-forming subunit beta	Invitrogen	L: GCT GGT GGT AGA GGA AAA GGA R: TCT GCC CTT TTC TCC CGT TC	21, 20	144
SLC16A1	Solute carrier family 22 member 1	Invitrogen	L: TTG ACC AGC ACA GTT CCC AG R: TTG TTG GTG GCT GCT TGT CA	20	106
PFKM	Phosphofructokinase	Invitrogen	L: GCT GAC ACC TTC CGT TCT GA R: TGG ACT TCG TAG CCT CCT CA	20	88
NDUFS1	NADH: ubiquinone oxidoreductase core subunit S1	Invitrogen	L: GAA CGA CCG TCC TCC AAG TT R: CAT CAC ACC TTC CCT GGC TT	20	145
ATP5F1A	ATP synthase F1 subunit alpha	Invitrogen	L: TCA GTC TAC GCC GCA CTT AC R: AGA CAC GCC CAG TTT CTT CA	20	142
HK2	Hexokinase 2	Invitrogen	L: TGG GAC AGA ACA CGG AGA GT R: TTT CAC CCA AAG CAC AAG GA	20	70
ACTB	Actin, beta	Qiagen	-	-	-
RRN18S	18S Ribosomal RNA	Qiagen	-	-	-

3.2.12 SYBR Green Relative RT-qPCR Analysis

A SYBR Green primer assay was used to assess cell gene expression. The SsoAdvanced Universal SYBR Green Supermix by BioRad was used to run the RT-qPCR for all cDNA samples. The reaction master mix was prepared according to Table 3. 5 with 10% overage of each component. Reactions were performed with a total of 20 µl. To begin, 100 µM stock concentration of each primer, both forward and reverse, was diluted to 50 uL of 6 µM in

nuclease-free water. The assay master mix was mixed thoroughly and 18 µl was dispensed into the appropriate wells of a 96-well PCR plate.

Table 3. 5 Master Mix Components and Volumes for RT-qPCR with SYBR Green

Component	Volume per 20 µl Reation	Final Concentration
SsoAdvanced universal SYBR Green supermix (2x)	10 µl	1 X
Forward primer	1 µl	400 nM
Reverse primer	1 µl	400 nM
Nuclease-free H_2O	6 µl	-
Total	18 µl	-

3.2.13 Amplification Efficiency

To determine the cDNA concentration that yields Cq values within 20-30 cycles for each gene tested, amplification efficiencies were performed for each primer against each cDNA sample: Panc-1 metformin-treated, Panc-1 control, AsPC-1 metformin-treated, and AsPC-1 control. A series of 10-fold dilutions were made for each cDNA sample (1:10, 1:100, 1:1000, 1:10000). The cDNA samples were run in triplicate. To the master mix in each well, 2 µl of cDNA sample was added to create a reaction total of 20 µl. The 96-well plates were then sealed with an optically transparent film and centrifuged for 1 min at 2500 rpm. The BioRad CFX OPUS qPCR was programed to the protocol outlined in Table 3. 6.

Table 3. 6 RT-qPCR Protocol for SYBR Green

Polymerase Activation and DNA Denaturation		**95 ℃ for 30 sec**
Denaturation	Amplification	95 ℃ for 10 sec
Annealing/Extension + Plate Read		60 ℃ for 20 sec
Cycles		39 cycles
Melt-Curve Analysis		65 to 95 ℃ Inc. 0.5 ℃ for 5 sec each

The CFX OPUS qPCR displayed the amplification plot and the Cq values for each sample, as well as the melting peaks and melting temperatures for each sample. The cDNA dilution that yielded the most optimal Cq value, 20-30 cycles was used in gene expression analysis. The amplification efficiencies for all primers were determined by plotting the standard curves for each primer, the Cq values plotted against the log concentration of cDNA. Once the standard curves were produced, the slopes of each were used to calculate the amplification efficiencies with Equation 3. 1 and Equation 3. 2.

Equation 3. 1

$$E = 10^{-1/slope}$$

Equation 3. 2

$$\%E = \left(10^{-\frac{1}{slope}} - 1\right) * 100$$

To determine gene expression, Rt-qPCR experiments were run with the cDNA dilution that yielded the optimal Cq values for each primer. The same master mix components as in Table 3. 5 and protocol as in Table 3. 6 were used.

3.2.14 Seeding 3D Spheroids

After the AsPC-1 and Panc-1 cells were incubated for 2 weeks and 6 weeks, the metformin-treated and control cells were seeded in 3D in preparation for chemotherapy exposure. The growth of 3D spheroids served to track the growth of the cancer cells in respect to a metformin-chemotherapy combined treatment. The cells were trypsinized and transferred to a 15-mL falcon tube, as well as 1.5-mL Eppendorf tube for a Muse Count and Viability Assay. The cell count was then used to calculate the volume of cells needed to seed 5,000 cells per 50 µl sphere in a low-attachment 96-Well, PS, U-Bottom CELLSTAR® microplate. Dilutions were prepared in prewarmed growth media for the control, or metformin-treated complete media for the experimental group. Once the dilutions were made, the control cells were seeded on one half of the plate and the metformin-treated cells were seeded on the other. To create a uniform and solid sphere, 50 µl of cell suspension was pipetted into each well and a total of 20 control spheres and 20 Metformin-treated spheres were plated. To prevent the cells from drying out, 200 µl of PBS was added to the wells bereft of cells. The microplate was then labelled and put into the 37 ℃ 5% CO_2 for 4 days to allow for the formation of spheroids.

3.2.15 Preparing Stock Concentrations of Chemotherapy from Powder

Three of the chemotherapies used in this study were ordered in as concentrated powders, Gemcitabine, Oxaliplatin, and SN-38. Stock concentrations were prepared under the fume hood according to the manufacturers protocol. Stock concentrations were either made with dH_2O or DMSO.

3.2.16 Spheroid Chemotherapy Exposure

To understand how metformin impacts the efficacy of chemotherapies on pancreatic cancer cells, the Panc-1 and AsPC-1 spheroids were exposed to a series of clinical concentrations of various chemotherapy drugs. An analysis of spheroid size upon chemotherapy exposure revealed how pairing metformin with chemotherapies alters pancreatic cancer growth. Once spheroids formed, they were ready for chemotherapy exposure. Initially, 5-fluorouracil (5-FU) was used since it had been previously diluted by a former PhD candidate and was ready experimental use. There were 10 mL, 1 mg/mL prefiltered aliquots of 5-FU stored at -25 ℃. The stock concentration was diluted to a series of concentrations that are typical for clinical use: 0.25 µg/mL, 8 µg/mL, and 16 µg/mL (83). All dilutions were prepared using prewarmed complete media in 15-mL falcon tubes. Because chemotherapy is a toxin, all dilutions were performed with caution under a biosafety cabinet equipped with the appropriate filter. After all necessary preparations, 100 µl of chemotherapy was pipetted to the assigned wells. The plate map in Figure 3. 3 was used as a template for the addition of chemotherapy. A total of 5 spheroid replicates was achieved for each treatment. The spheroids that did not receive chemotherapy treatment served as the control. Once the chemotherapy was added, the microplate was placed in the 37 ℃ 5% CO_2 for a total of 4 days. The media was exchanged on day 4 and every other day thereafter. To exchange the media without disrupting the spheroids, 75 µl of media was carefully removed from each well and replaced with 75 µl of fresh prewarmed media.

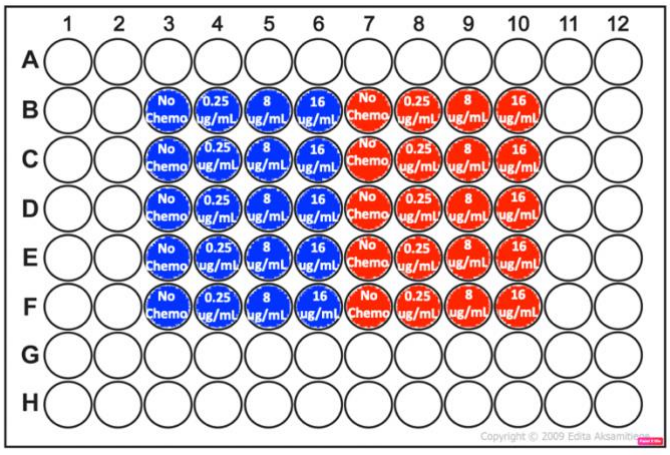

Figure. 3 The Plate Map Designed in Preparation for Spheroid Chemotherapy Exposure
After 4 days of growth, spheroids were exposed to chemotherapy treatments. The blue wells represent spheroids that did not receive a pretreatment of metformin, while the red wells represent spheroids that received either a 2-week or 6-week pretreatment of metformin. Column 3 and column 7 did not receive any chemotherapy; they served as the control. The spheroids were treated with increasing doses of chemotherapy. The example in the plate map, is of 5-FU. Each treatment had five replicates.

Initially, spheroids were exposed to 5-FU for 4 days, and day 5 (the day after the first media exchange) marked the end of the experiment. However, to better mimic the clinical

administration of chemotherapy treatment, subsequent chemotherapies were applied to spheroids on day 14 of incubation for a second-round of treatment. The end of the experiment was therefore, extended to day 18. A timeline of treatment and imaging analysis is outlined in Figure 3. 4. The chemotherapies tested in the 18-day experiments were Gemcitabine, SN-38, and Oxaliplatin. Again, clinically relevant concentrations of the chemotherapies were used, which were as follows: 1 µM, 2.5 µM, 5 µM for Oxaliplatin, 25 µM, 100 µM, and 500 µM for Gemcitabine, and 3 ng/mL, 10 ng/mL, and 20 ng/mL for SN-38 (83–85).

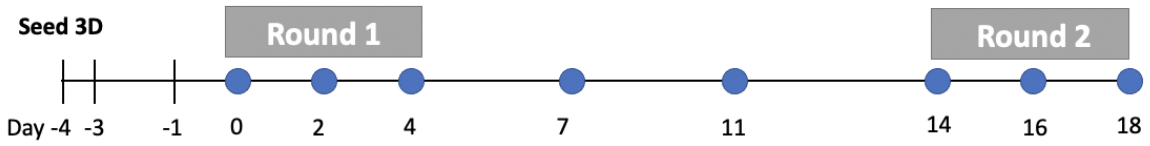

Figure 3. 4 A Timeline of Chemotherapy Treatment and Imaging Analysis for AsPC-1 and Panc-1 Spheroids.
Day 0 marked the start of chemotherapy exposure. The spheroids were treated with chemotherapy for a total of 4 days before a media exchange. Media was exchanged on day 4 and every other day thereafter until day 14, on which the spheroids were inoculated with a new round of chemotherapy. The blue circles denote the days on which an image analysis of spheroids was conducted. On day 18, a confocal image to assess spheroid viability was also conducted.

3.2.17 Imaging and Image Analysis

Different imaging and image analysis techniques were used for the 5-day 5-FU experiment compared to the 18-day experiments. To measure the growth of the 5-day experiment spheroids, brightfield images were taken using the Olympus CKX41 Light Microscope or the Leica TCS SP8 CSU Confocal Microscope in brightfield mode. An image of each spheroid was taken before the addition of chemotherapy on day 0, on day 4 of chemotherapy exposure, and on day 5. To image the spheroids on the Olympus light microscope, the 4X dry objective was used, while the 5X objective was used for the Leica microscope. To monitor the changes in spheroid size in relation to 5-FU treatment, diameters were measured. Each microscope required a different process for the determination of diameter in microns (µM). The Leica microscope is equipped with a measuring tool to measure the dimensions of the captured image in microns under the designated objective lens. Unlike, the Leica microscope, the light microscope required the diameter of each spheroid to be estimated by measuring the length of the field of view at the 4X magnification in mm with a metric ruler, which was 4.5 mm (4500 microns). Unlike the 5-day

experiment, the 18-day experiments were imaged using the Leica TCS SP8 CSU Confocal in brightfield mode at the 5X objective. The spheroids were imaged on the days indicated in Figure 3. 4. Spheroid images were then saved as TIFF files and inputted into a high-throughput image analysis software application in MATLAB called SpheroidSizer (86). The program measures the major and minor axial length of the imaged spheroids to calculate the volume of the spheroids accurately and automatically in μM^3, using Equation 3. 3 (86).

Equation 3. 3

$$V = 0.5 * Length * Width^2$$

Once the diameters and volumes of all spheroids were determined, they were inputted into an excel worksheet and the average spheroid size of each treatment group was calculated. Results were analyzed further in the form of bar charts.

3.2.18 Viability Staining

To measure the viability of the spheroids on day 18 of growth, the spheroids were stained with Propidium Iodide (PI) to stain dead cells and Calcein AM to stain living cells. The first row of spheroids was selected for staining, so that a viability profile for each type of spheroid, metformin-treated, non-metformin treated, metformin-chemotherapy-treated, non-metformin-chemotherapy-treated, was acquired. The stains were added on day 17 and incubated with the spheroids overnight for imaging the next day. Calcein AM was added with a final well concentration of 4 µg/mL, while PI was added with a final well concentration of 7.5 µg/mL. Z-stacks of fluorescent images were captured using the Leica confocal microscope at a 5X objective. *Hyd* were the lasers used in the imaging process (CAM, Ex: 488 nm, Em: 493-529 nm; PI, Ex: 552 nm, Em: 630-643 nm). The images were processed and analyzed using ImageJ/FIJI macros. Viability charts of each stain was generated and represented the area in microns each stain encompassed within the spheroid. These charts are listed in Appendix H. The areas were then used to plot viability profiles for both AsPC-1 and Panc-1 spheroids.

3.2.19 Mito and Glyco Stress Test

To analyze the change in mitochondrial respiration and glycolytic function of the AsPC-1 and Panc-1 cells in relation to Metformin treatment, a Mito and Glyco Stress Test was conducted, respectively. The Cell Mito Stress Test measures crucial parameters of mitochondrial function by

recording the OCR of cells in real time on the Seahorse XFp Extracellular Flux Analyzer. As described in section 1.11, the assay employs built-in ports of the XFp sensor cartridges to deliver a specific dose of respiration modulators into cell wells during the assay to measure the principal parameters of mitochondrial function. The volumes and concentrations at which these modulators were added are listed in Table 3. 9. Similarly, the Glyco Stress Test assesses the parameters of glycolytic flux by measuring the ECAR in real time on the Seahorse XFp Extracellular Flux Analyzer. Like the Mito Stress Test, modulators are injected into the assay wells during the experiment to reveal the key parameters of glycolytic function. The added volumes and concentration of these modulators are described in Table 3. 10. Before the Mito and Glyco Stress Tests were performed, a series of preparatory steps were carried out the day before the assay. Both assays were performed on the same day.

3.2.19.1 Day Before the Assay

Once the Panc-1 or AsPC-1 cells achieved confluency at 2 weeks and 6 weeks of incubation, the cells were trypsinized and the cell suspensions were transferred to a 15-mL falcon tube, as well as 1.5-mL Eppendorf tube for a Muse Count and Viability Assay. The seahorse assay microplate was seeded with the optimal cell seeding density of each cell line, which was empirically established as 20,000 cells per well. The cell count from the Muse Assay was used to calculate the volume of cells needed to seed 20,000 cells per 180 µl volume. The seahorse assay plate was seeded according to the plate map in Figure 3. 5. The 180 µl volumes were pipetted into each well. To prevent the evaporation of the culture medium, 400 µl of 1xPBS was added to the moat chambers of the assay plate. The assay plate was then covered and labelled with its appropriate cell line and placed in the 37 ℃ 5% CO_2 to be read the next day. Finally, two XFp sensor cartridges, one for the Mito and one for the Glyco Stress Test, were retrieved and hydrated with the following volumes of XF Calibrant: 200 µl in all 8 wells, and 400 µl in the moat chambers. The sensor cartridges were then incubated in the 37 ℃ non-CO_2 incubator overnight.

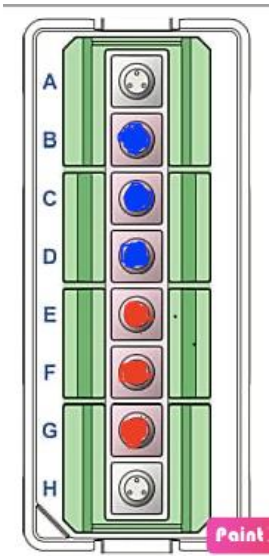

Figure 3. 5 The Plate Map of the Seahorse XFp Assay Plate Designed in Preparation for the Mito and Glyco Stress Test.
This plate map was used to seed both the AsPC-1 and Panc-1 cells in preparation for the Mito and Glyco stress tests after 2 weeks and 6 weeks of incubation. There are a total of 8 wells (A-H) and 8 surrounding moat chambers. The wells that are not shaded served as the blank, the wells shaded in blue served as the control group (the cells bereft of Metformin treatment), while the wells shaded in red served as the experimental group (the cells treated with 11.6 µM of Metformin). Each well apart from the blank wells, received 180 µl of cell suspension with a density of 20,000 cells. The blank well received 180 µl of prewarmed complete media.

3.2.19.2 Day of the Assay

Seahorse assay media was prepared in a 15-mL falcon tube with the components listed in Table 3. 7 for the Mito Stress Test, and Table 3. 8 for the Glyco Stress Test.

Table 3. 7 Seahorse Assay Media for Mito Stress Test

Components	Volume
L-glutamine 200 mM	100 µl
Glucose 1 mM	50 µl
Seahorse Base Media	9.837 mL
NaOH 1M	~10 µl

Table 3. 8 Seahorse Assay Media for Glyco Stress Test

Components	Volume
L-glutamine 200 mM	100 µl
Seahorse Base Media	9.887 mL
NaOH 1 M	~ 10 µl

A seahorse microplate that had been prepared the day before was retrieved from the incubator and analyzed under the Olympus microscope to ensure the presence of cells at equal densities in each well. Next, the media in each microplate well was carefully removed without disturbing the cells at the bottom of the wells. The media was replaced with 180 µl of prepared seahorse assay media. The microplate was inspected under the microscope once more to confirm that no cells had been mistakenly removed in the media exchange process. It was then placed in the 37 ℃ non-CO_2 incubator for at least 1 hour. The modulators for the associated assay were then

prepared. All modulators were retrieved from the XFp Cell Mito and Glyco Stress Test Kits. First, stock solutions of the modulators were prepared by carefully resuspending each modulator with the specified volume of seahorse assay medium. The specific volumes and concentrations are specified in Table 3. 9 and Table 3. 10.

Table 3. 9 Stock Solution for Mito Stress Test

Modulator	Volume of seahorse assay medium	Final Stock Concentration
Oligomycin	280 µl	45 µM
FCCP	288 µl	50 µM
Rot/AA	216 µl	25 µM

Table 3. 10 Stock Solutions for Glyco Stress Test

Modulator	Volume of seahorse assay medium	Final Stock Concentration
Glucose	300 µl	100 mM
Oligomycin	288 µl	50 µM
2-DG	300 µl	500 mM

Once the stock concentrations of the modulators were prepared, they were diluted down to their specified final injection concentrations in 1.5 mL Eppendorf tubes. This is described in Table 3. 11 and

Table 3. 12. To ensure accurate OCR measurements during the Mito Stress Test, the optimal final concentration of FCCP had to be determined for each cell line due to the modulator's sensitive impact. This was previously accomplished via FCCP titrations by a former PhD candidate. The determined concentrations for Panc-1 and AsPC-1 were 0.5 µM and 1 µM, respectively.

Table 3. 11 Final Concentrations of Each Modulator for Mito Stress Test

Modulator	Final well concentration	Stock volume added	Seahorse assay media volume added
Oligomycin	1.5 µM	100 µl	200 µl
FCCP	0.5 µM (Panc-1) and 1 µM (AsPC-1)	30 µl, 60 µl	270 µl, 240 µl
Rot/AA	0.5 µM	60 µl	240 µl

Table 3. 12 Final Concentrations of Each Modulator for Glyco Stress Test

Modulator	Final well concentration	Stock volume added	Seahorse assay media volume added
Glucose	10 mM	300 µl	75 µl
Oligomycin	1 µM	54 µl	246 µl
2-DG	50 mM	300 µl	0 µl

Once the final concentrations of the modulators were created, the hydrated sensor cartridges were retrieved from the 37 ℃ non-CO_2 incubator and loaded with the modulators. Each modulator was loaded into different ports of the sensor cartridges at different volumes. The location of modulator loading, as well as the methodology is described in Figure 3. 6. Each volume of modulator was added with a p100 micropipette.

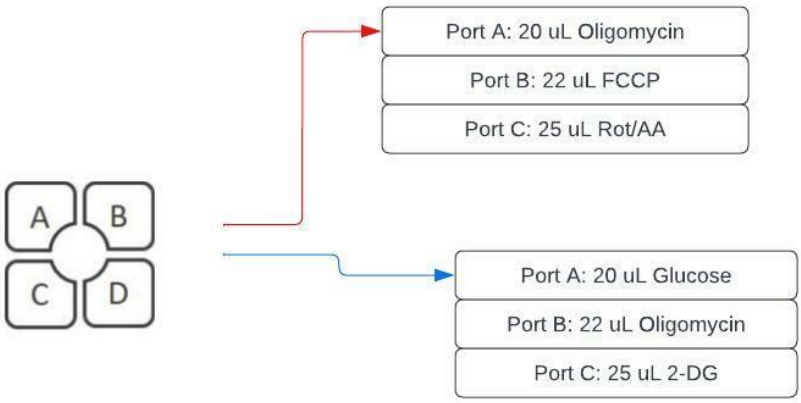

Figure 3. 6 The Location of Injection Ports on Sensor Cartridges and Associated Modulator Volumes
The ports on the sensor cartridges are labelled A, B, C, and D. The red line indicates the modulator volumes for the Mito Stress Test, while the blue line indicates the modulators for the Glyco Stress Test. Nothing was pipetted into port D.

After loading the sensor cartridge, it was placed into the Seahorse XFp Extracellular Flux Analyzer for a calibration. Once the calibration was completed, the sensor cartridge was replaced with the associated seahorse microplate and the experiment was run. Upon completing the assays, the media in each seahorse microplate well was removed and the microplates were labelled and frozen at -25 ℃.

3.2.20 Normalization of Seahorse Results with BCA Assay

Differing cell density and cell proliferation rates between the wells causes variation in OCR and ECAR measurements. To mitigate those variations and ensure an accurate interpretation of results, the Mito and Glyco Stress Tests were normalized to the concentration of protein in each well, μg/mL by performing a Pierce™ BCA Protein Assay (ThermoFisher Scientific). The Panc-1 or AsPC-1 frozen seahorse microplate was retrieved from the freezer, and each well was resuspended with 200 μl of cold PBS to lyse the cells. The lysed cells were then transferred to 1.5-mL Eppendorf tubes labelled with their corresponding well. The tubes were then centrifuged at 16,000 x g for 10 min to separate the proteins from other contaminants The supernatants in each tube were then transferred to a newly labelled tube. All tubes were then kept on ice and the microplate procedure from the Pierce™ BCA Protein Assay procedure from Thermoscientific was followed. The protein solutions along with the standard solutions were pipetted onto the BCA microplate in duplicate. After its incubation period, the absorbances of the microplate's wells were read at 595 nm with the SpectraMax Paradigm Multi-Mode Microplate Reader. The results were saved and analyzed on an excel spreadsheet to calculate protein concentration in μg/mL for each seahorse assay microplate well. The BCA results are listed in Appendix F.

3.2.21 Mito and Glyco Stress Test Data Analysis

The calculations for all parameters were automatically computed for each experiment using report generators. An Agilent Seahorse XF Cell Mito Stress Test Report Generator, along with a Seahorse XF Glyco Stress Test Report Generator were downloaded from the Agilent website. The Wave Desktop was used generate the reports. The parameters for the Mito and Glyco Stress Test were calculated according to Table 3. 13 and Table 3. 14, respectively.

Table 3. 13 Calculations of Mitochondrial Respiration Parameters from Mito Stress Test Results

Parameter Value	Equation
Non-mitochondrial Oxygen Consumption	Minimum rate measurement after Rotenone/antimycin A injection
Basal Respiration	(Last rate measurement before first injection)- (Non-Mitochondrial Respiration Rate)
Maximal Respiration	(Maximum rate measurement after FCCP injection)- (Non-Mitochondrial Respiration)
H^+ (Proton) Leak	(Minimum rate measurement after Oligomycin injection)- (Non-mitochondrial Respiration)

ATP Production	(Last rate measurement before Oligomycin injection)- (Minimum rate measurement after Oligomycin injection)
Spare Respiratory Capacity	(Maximal Respiration)- (Basal Respiration)
Spare Respiratory Capacity %	(Maximal Respiration)/ (Basal Respiration) *100
Acute Response	(Last rate measurement before oligomycin injection)- (Last rate measurement before acute injection)
Coupling Efficiency	(ATP Production Rate)/ (Basal Respiration Rate) *100

Table 3. 14 Calculations of Glycolytic Function Parameters from Glyco Stress Test Results

Parameter Value	Equation
Glycolysis	(Maximum rate measurement before Oligomycin injection)- (Last rate measurement before Glucose injection)
Glycolytic Capacity	(Maximum rate measurement after Oligomycin injection)- (Last rate measurement before Glucose injection)
Glycolytic Reserve	(Glycolytic Capacity)- (Glycolysis)
Glycolytic Reserve as a %	(Glycolytic Capacity Rate) /(Glycolysis)*100
Non-Glycolytic Acidification	Last rate measurement prior to glucose injection
Acute Response	(Last measurement rate before glucose injection- Last rate measurement before acute injection)

3.2.22 Metabolic Phenotype Determination

The change in metabolic phenotype as a result of metformin-treatment was determined automatically from a report generator downloaded from the Agilent website called the "Seahorse XF Cell Energy Phenotype Test Report Generator". The Mito Stress test results were then exported as a Seahorse XF Cell Energy report from the Wave Desktop. The system determined the metabolic phenotype of each cell line at both baseline and stressed conditions using the associated OCR and ECAR measurements. The 4 different phenotypes were, aerobic, energetic, quiescent, glycolytic. The change in metabolic phenotype from baseline to stressed conditions is defined as the metabolic potential and was calculated by the report using Equation 3. 4.

Equation 3. 4

$$\text{Stressed OCR (\%)} = \frac{\text{Stressed OCR}}{\text{Baseline OCR}} \text{ x } 100$$

$$\text{Stressed ECAR (\%)} = \frac{\text{Stressed ECAR}}{\text{Baseline ECAR}} \text{ x } 100$$

3.2.23 Proliferation Assay to Calculate the Doubling Times

To determine the doubling times of both the metformin-treated and control cells, a Click-iT™ EdU Proliferation Assay by ThermoFisher for Microplates was used. This revealed whether a metformin pretreatment effects the proliferation rate of AsPC-1 and Panc-1 cells. The Click-iT™ technology uses the nucleoside analog EdU (5-ehtynyl-2'-deoxyuridine), which is added to live cells and incorporated into DNA during active DNA synthesis. The EdU contains an alykne group, which covalently attaches to an azide group in HRP (horseradish peroxidase). Amplex™ UltraRed reagent is then added to provide fluorescent signal. The fluorescent signal, therefore, indicates the number of cells. To begin the assay, AsPC-1 cells and Panc-1 cells were plated at 5,000 cells per well in a 96-well plate, with 5 replicates of both the control and experimental cells. Because the assay had never been performed, two different concentrations of EdU were tested, 10 µM and 20 µM, to determine the optimal concentration for each cell line. The experiment was followed according to the manufacturer's protocol, with an EdU incubation time of 2 hours. The plates were read with the SpectraMax plate reader with an excitation of 568 nm and an emission of 590 nm. The results were then analyzed in excel. The growth rates and doubling times were calculated using Equation 3. 5 and Equation 3. 6, respectively.

Equation 3. 5

$$r = \ln\left(\frac{N(t)}{N_0}\right)/t$$

Equation 3. 6

$$Doubling\ Time = \ln(2)\ /r$$

3.2.24 Statistical Analysis

Statistical analyses were carried out to compare the means among the various groups tested. A T-Test was performed for the Mito and Glyco Stress Tests OCR and ECAR results. The two groups

tested in that case were the OCRs and ECARs without metformin and with metformin. An ANOVA test was carried out for the spheroids size estimations, where the 3 groups tested were the effect the different doses of chemotherapy had on spheroid size, the effect the metformin-chemotherapy combination had on spheroid size, and the interaction between the metformin-chemotherapy treated spheroids and just the chemotherapy treated spheroids. The results of each statistical analysis can be found in Appendix E and Appendix G.

Chapter 4 Results

4.1 The Effect of a Metformin Pretreatment on the Doubling Times of AsPC-1 and Panc-1 Cells

To determine whether an 11.6 µM metformin pretreatment effects proliferation, the doubling times of both the control and metformin pretreated AsPC-1 and Panc-1 cells were calculated according to Equation 3. 6. The fluorescent signals of both Panc-1 and AsPC-1 cells at 24, 48, and 72 hours of growth are listed in Figure 4. 1 and Figure 4. 2, respectively. The strength of the fluorescent signal equates to the number of EdU molecules incorporated into the cells' DNA. Because the fluorescent signals increase linearly for both cell lines, they were used to estimate the number of cells at each time point. The Panc-1 fluorescent signals of the control and metformin-treated cells overlap, demonstrating the same slope for both groups. Both groups have larger slopes, 2E+08, compared to the AsPC-1 cells. The AsPC-1 fluorescent signals of the metformin-treated are larger than that of the control group. The calculated growth rates and doubling times in hours for each cell line are listed in Table 4. 1. The Panc-1 cells, both treated and control have the same growth rates and nearly the same doubling times. The doubling times of the Panc-1 cells are larger than the AsPC-1 cells. The growth rate of the AsPC-1 control group is larger than the rate of the experimental group. Furthermore, the doubling time of the experimental group is larger than the doubling time of the control.

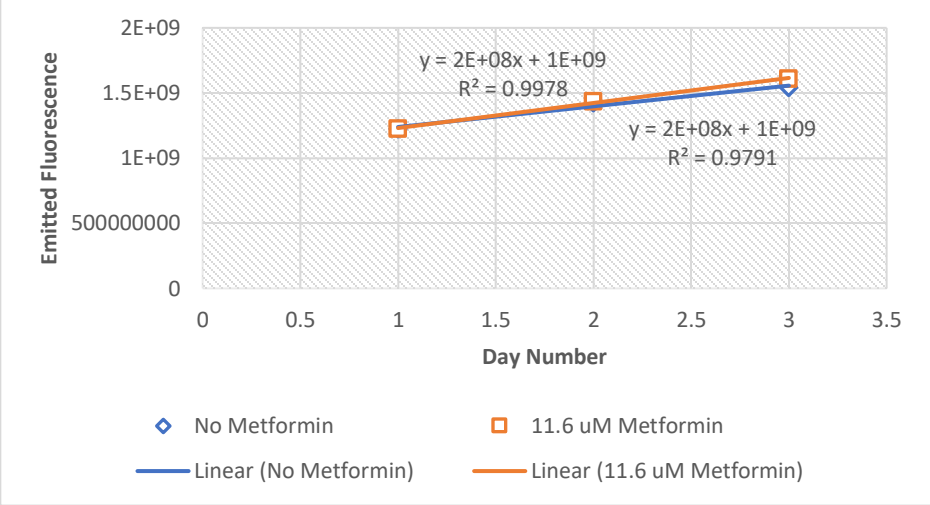

Figure 4. 1 The Fluorescent Signal Emitted from Panc-1 cells Pulsed with 10 µM of EdU.
To determine the doubling times of the Panc-1 cells pretreated with metformin compared to the non-treated (control), a Click-iT EdU Proliferation Assay was performed. Initially, the control

and experimental cells were seeded at 5,000 cells. After, 24, 48, and 72 hours of growth, an assay was performed. All Panc-1 cells were pulsed with 10 µM of EdU for 2 hours before the start of the assay.

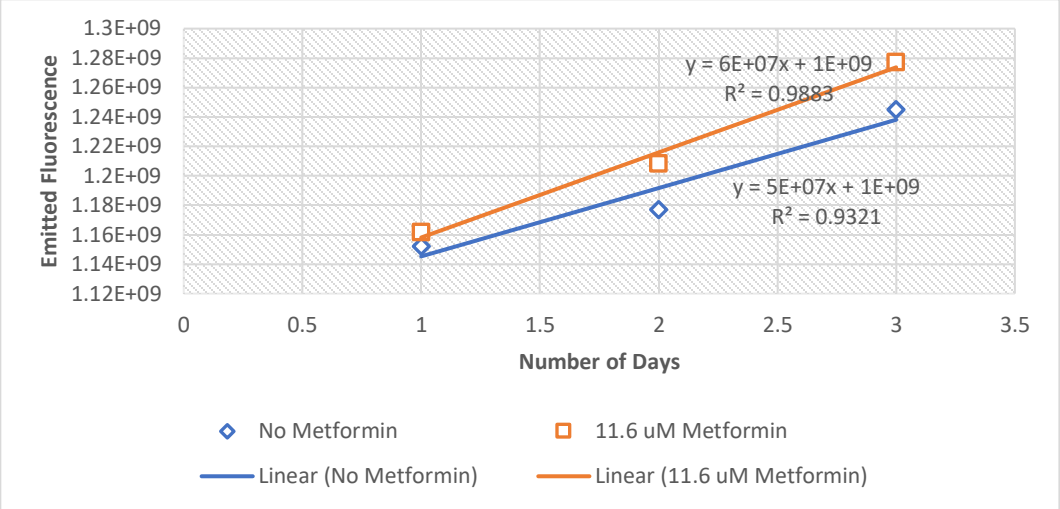

Figure 4. 2 The Fluorescent Signal Emitted from AsPC-1 cells Pulsed with 20 **µ**M of EdU. *To determine the doubling time of the AsPC-1 cells pretreated with metformin compared to the non-treated (control), a Click-iT EdU Proliferation Assay was performed. Initially, the control and experimental cells were seeded at 5,000 cells. After, 24, 48, and 72 hours of growth, an assay was performed. All Panc-1 cells were pulsed with 20 µM of EdU for 2 hours before the start of the assay.*

Table 4. 1 Growth Rates and Doubling Times (in hours) of the AsPC-1 and Panc-1 Cell Lines

Cell Line	Treatment	**Growth Rate**	Doubling Time (hours)
AsPC-1	No Metformin	.027	25.34
Panc-1	No Metformin	.005	153.7
AsPC-1	11.6 µM Metformin	.009	77.41
Panc-1	11.6 µM Metformin	.005	155.82

4.2 A Pretreatment of Metformin Alters the Metabolic Phenotype of Both Panc-1 and AsPC-1 Pancreatic Cancer Cell Lines

To understand how the cells' metabolisms are altered due to prolonged metformin treatment, the metabolic phenotypes of each cell lines were determined at both 2 weeks and 6 weeks of metformin treatment. The changes in metabolic phenotypes are highlighted in Figure 4. 3. AsPC-

1 control cells at both 2 weeks and 6 weeks of incubation as seen in Figure 4.3A and Figure 4.3C, are slightly quiescent phenotype under baseline conditions and energetic phenotype under stressed conditions. Furthermore, the metabolic potentials of the experimental groups are both quiescent, however, the cells become more quiescent at 6 weeks of treatment in metformin compared to 2 weeks. Unlike AsPC-1, the Panc-1 control cells remain in the aerobic phenotype during the baseline to stressed transition as seen in Figure 4.3B. The experimental cells at 2 weeks of treatment show a metabolic transition from slightly quiescent to aerobic with a higher ECAR value. In Figure 4.3D, both the control and experimental cells move from a slightly aerobic phenotype to a slightly quiescent phenotype that borders a glycolytic phenotype.

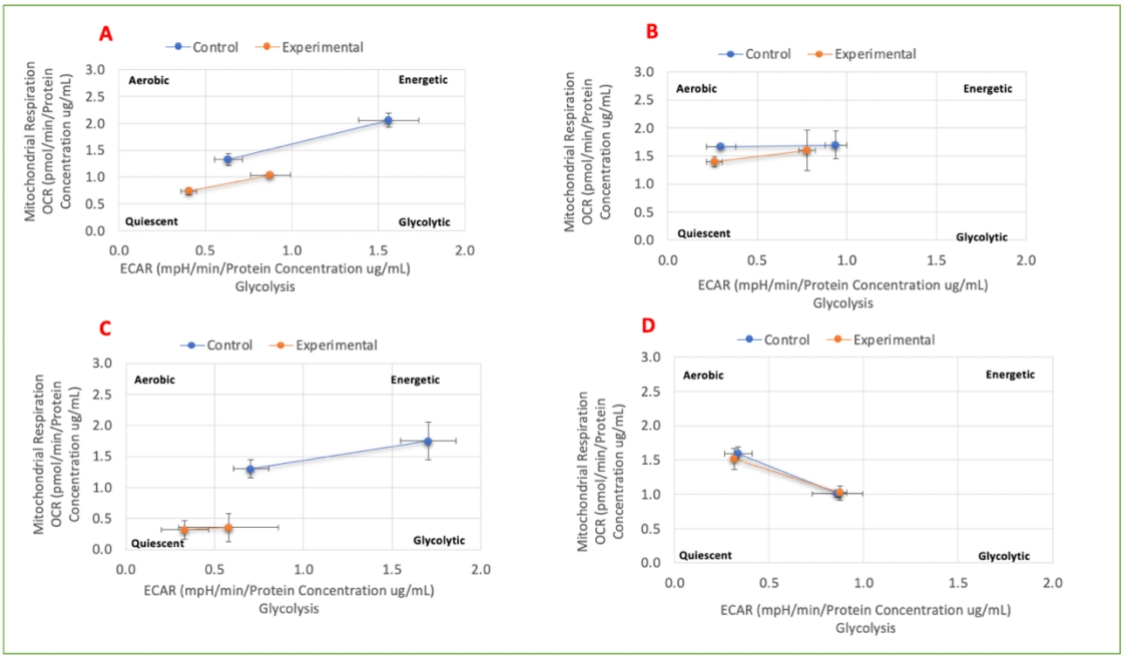

Figure 4. 3 The Cell Metabolic Phenotype of Panc-1 and AsPC-1 Pancreatic Cancer Cell Lines After 2-Weeks and 6-Weeks of Metformin Treatment.
To determine the metabolic phenotypes of each cell line, the results of the Mito Stress Tests were put into a Seahorse XF Cell Energy Phenotype Report Generator. The control group are the cells that did not receive a metformin pretreatment, whereas the experimental group are the cells that were pretreated with metformin. Each panel of the figure illustrates the metabolic phenotype of the following: (A) AsPC-1 cell line after 2 weeks of metformin treatment, (B) Panc-1 cell line after 2 weeks of metformin treatment, (C) AsPC-1 cell line after 6 weeks of metformin treatment, and (D) Panc-1 cell line after 6 weeks of metformin treatment. All panels highlight the metabolic phenotypes of the cell lines at baseline and stressed conditions. The error bars indicate the standard deviation of the ECAR and OCR measurements at both baseline and stressed conditions. Each quadrant of the graphs is labelled with a corresponding metabolic type: aerobic, energetic, quiescent, and glycolytic. The data is normalized to the concentration of protein in µg/mL.

The metabolic flexibilities, or metabolic potentials, are examined in Figure 4. 4. The more drastic the change in metabolic potential, the greater the metabolic flexibility of the cell. Overall, the ECAR metabolic potentials are larger than the OCR potentials. Apart from Figure 4.4D, the control groups have larger potentials than the experimental groups. The metabolic potentials of the AsPC-1 cells decrease from 2 weeks to 6 weeks of incubation as seen in Figure 4.4A and Figure 4.4C. The same is true of the Panc-1 cells, as seen in Figure 4.4B and Figure 4.4D. However, at 6 weeks of incubation, the experimental Panc-1 cells show a slightly larger metabolic potential than the control cells for both ECAR and OCR.

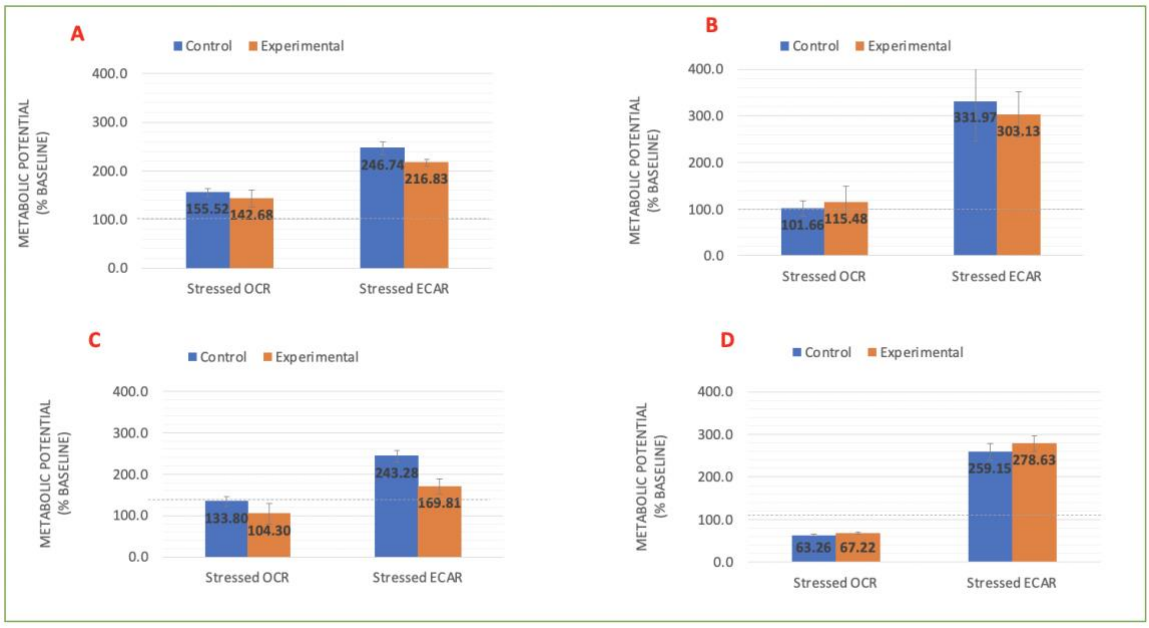

Figure 4. 4 The Percentage Metabolic Potential of Panc-1 and AsPC-1 Pancreatic Cancer Cell Lines After 2-Weeks and 6-Weeks of Metformin Treatment.
The metabolic potential is defined as metabolic flexibility or the extent to which a cell may change its metabolic phenotype in response to stress. Each panel of the figure illustrates the metabolic potential of the following: (A) AsPC-1 cell line after 2-weeks of metformin treatment, (B) Panc-1 cell line after 2-weeks of metformin treatment, (C) AsPC-1 cell line after 6-weeks of metformin treatment, and (D) Panc-1 cell line after 6-weeks of metformin treatment. The error bars represent the standard deviation of all metabolic potential calculations computed from each well's stressed OCR/ECAR and baseline OCR/ECAR.

4.3 A Pretreatment of Metformin Alters the Mitochondrial Metabolisms of Both Panc-1 and AsPC-1 Pancreatic Cancer Cell Lines

4.3.1 Shift in OCR Values

To analyze alterations in mitochondrial metabolism in response to a pretreatment of 11.6 µM metformin, a Mito Stress Test was performed using a Seahorse XFp Analyzer for each cell line after both 2-weeks and 6-weeks of metformin incubation. Real-time shifts in mitochondrial respiration are represented in Figure 4. 5. The collected OCR values were used to calculate relevant metabolic parameters to further elucidate each cell line's metabolic phenotype. In Figures 4.5A and 4.5C, the results denote larger OCR values in the AsPC-1 cell's that did not receive a metformin treatment (control), compared to those that did (experimental). The Panc-1 cells are an exception. In Figures 4.5B and 4.5D, the OCR values of the control and experimental groups overlap. In Figure 4.5A, it is evident that the experimental group has smaller OCR measurements at all modulator injections compared to the control. Furthermore, Figure 4.5C, reveals that the gap between the OCR values of the control and experimental widens after 6 weeks of treatment in metformin. The control group's OCR values remain largely stagnant with minor shifts at 6 weeks of incubation compared to 2 weeks. Unlike the AsPC-1 cell line, Figure 4.5B, illustrates that the difference in OCR values between the control and experimental group of Panc-1 at 2 weeks of incubation is minimal. The measurements in the graph appear to nearly overlap. In Figure 4.5D, the overlap between the control and experimental is augmented, and the OCR values after the FCCP injection are smaller at the 6 weeks of incubation compared to 2 weeks.

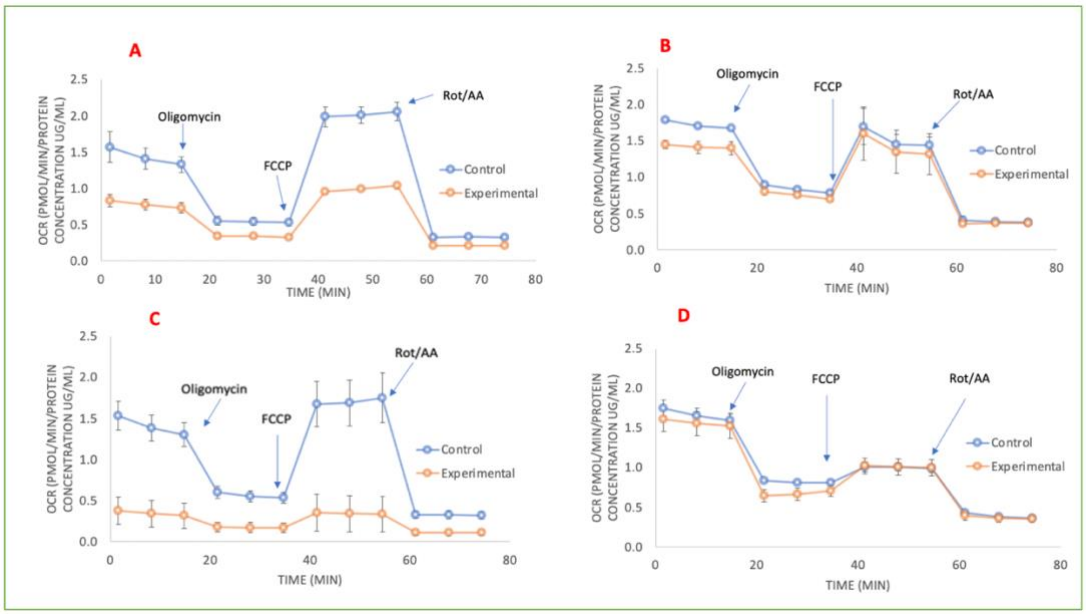

Figure 4. 5 The Mitochondrial Respiration of Panc-1 and AsPC-1 Pancreatic Cancer Cell Lines After 2-Weeks and 6-Weeks of Metformin Treatment.
A Seahorse XFp Analyzer was used to run a Mito Stress Test to measure the change in oxygen consumption (OCR) in pmol/min vs. time in minutes for each cell line. Each panel of the figure illustrates the mitochondrial respiration of the following: (A) AsPC-1 cell line after 2-weeks of Metformin treatment, (B) Panc-1 cell line after 2-weeks of Metformin treatment, (C) AsPC-1 cell line after 6-weeks of Metformin treatment, and (D) Panc-1 cell line after 6-weeks of Metformin treatment. The error bars represent the standard deviation of the OCR pmol/min measurements taken from each seahorse assay well. The points where each modulator, Oligomycin, FCCP, and Rot/AA, were injected are labelled on the graphs. The data is normalized to the concentration of protein in µg/mL.

4.3.2 Change in Basal Respiration, Spare Respiratory Capacity, Proton Leak, and ATP Production Averages

The results in Figure 4. 6 illustrate the basal respiration, spare respiratory capacity, proton leak, and ATP production averages of the cell lines. These parameters were calculated using the equations described in Table 3. 13. Basal respiration is determined from the OCR values before modulator injections, while spare respiratory capacity is determined from the injection of rotenone and antimycin A. Apart from Figure 4.6B, the basal respiration and spare respiratory capacity averages are larger in the control group compared to the experimental. The most prominent difference between the control and experimental groups is among the AsPC-1 cell line in Figure 4.6A, the difference between the control and experimental groups at 2 weeks of incubation is about 0.5 pmol/min for both parameters. At 6 weeks of incubation, Figure 4.6C illustrates that the difference between the control and the experimental increases for both parameters. Notably, the spare respiratory capacity of the experimental group decreases to a mere 0.04 pmol/min, while the parameter values of the control groups experienced a minimal decrease in value despite the extra 4 weeks of incubation. Unlike the AsPC-1 cells, the Panc-1 in Figure 4.6B, observes a nominal difference between the experimental and control group for both parameter averages. Interestingly, the spare respiratory capacity average of the control is only 0.03 pmol/min, while experimental is 0.20 pmol/min, which demonstrates that despite previous observed patterns, the spare respiratory capacity of the experimental group is larger than the control. Additionally, the basal respiration averages of Panc-1 are larger than AsPC-1, but the opposite is observed when analyzing spare respiratory capacity. In Figure 4.6D, the experimental group's basal respiration increases, but the control's slightly decreases. Furthermore, unlike at 2 weeks of incubation, there is no spare respiratory capacity at 6 weeks of incubation in either group.

The proton leak parameter was calculated from the OCR results after the injection of Oligomycin and FCCP during the Mito Stress Test, while the ATP production parameter was determined from the injection of Oligomycin. In all panels, the control cells have larger values of both proton leak and ATP production compared to the experimental. The only exception is Figure 4.6D, where the experimental group has a larger ATP production than the control. In general, the proton leak averages are small, and the observed differences between the control and the experimental are nominal. The differences in ATP production between the control and experimental groups are more prominent. The largest deviations are observed among the AsPC-1 cells. In Figure 4.6A, the difference in ATP production at 2 weeks of incubation is 0.39 pmol/min, while at 6 weeks of incubation that difference increases to 0.62 pmol/min, as seen in Figure 4.6C. Additionally, the control averages of both parameters remain the same at 6 weeks of incubation compared to 2 weeks. The averages of proton leak are small, the smallest being the AsPC-1 experimental group at 6 weeks of incubation at 0.06 pmol/min. Furthermore, the averages of both parameters are larger among the Panc-1 cells compared to AsPC-1. At 6 weeks of incubation, Figure 4.6D, proton leak of the control increases, while it slightly decreases for the experimental group (only .05 pmol/min) from their values at 2 weeks of incubation. Interestingly, the ATP production of the experimental is larger than the control at 6 weeks of incubation.

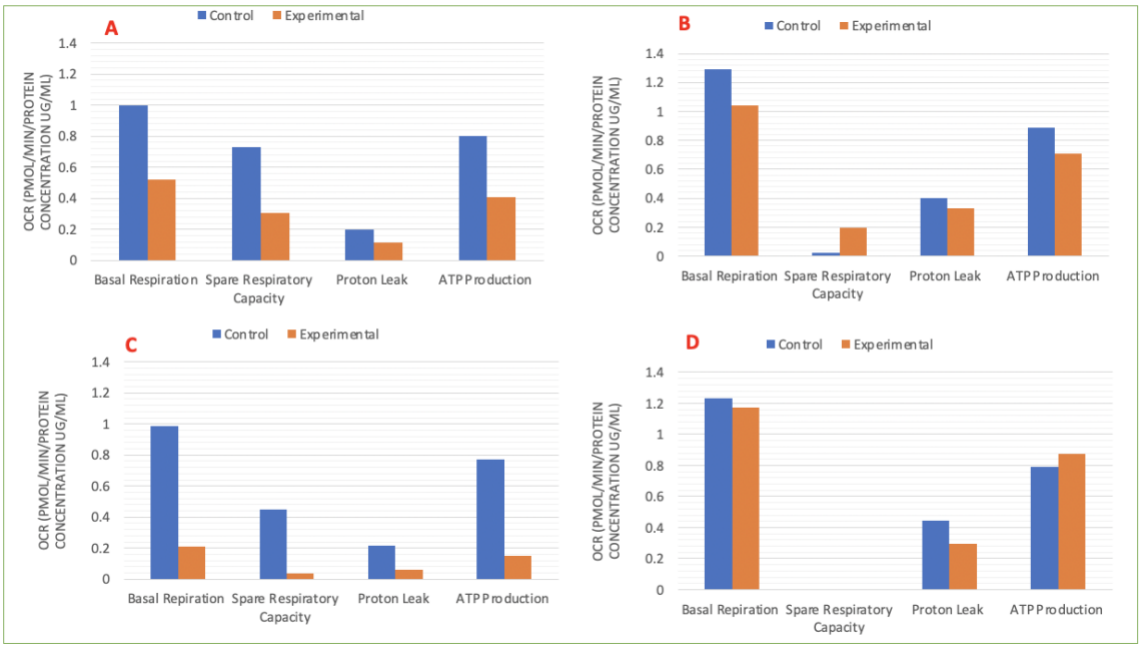

Figure 4. 6 The Average Basal Respiration, Spare Respiratory Capacity, Proton Leak, and ATP Production of Panc-1 and AsPC-1 Pancreatic Cancer Cell Lines After 2-Weeks and 6-Weeks of Metformin Treatment.
Basal respiration, spare respiratory capacity, Proton Leak, and ATP Production are parameters calculated from OCR values measured during the Mito Stress Test. Each panel of the figure illustrates the average basal and spare respiratory capacity of the following: (A) AsPC-1 cell line after 2-weeks of metformin treatment, (B) Panc-1 cell line after 2-weeks of metformin treatment, (C) AsPC-1 cell line after 6-weeks of metformin treatment, and (D) Panc-1 cell line after 6-weeks of metformin treatment. The error bars represent the standard deviations of the parameter values calculated from each seahorse assay well. The data is normalized to the concentration of protein in µg/mL.

4.3.3 Change in Coupling Efficiency Percentages

In Figure 4. 7, the impact of metformin treatment on the coupling efficiency of AsPC-1 and Panc-1 cells is investigated. The calculation of coupling efficiency is described in Table 3. 13. Apart from Figure 4.7C and Figure 4.7D, all panels show a very similar coupling efficiencies between the control and experimental groups. The AsPC-1 cells incubated for 2 weeks have the largest coupling efficiencies, at 79.7 % for the control group, and 78.05 % for the experimental group. The coupling efficiency of the experimental group then decreases to 69.19 % after 6 weeks of treatment as seen in Figure 4.7C. The control values of the parameter remain the same. Additionally, the Panc-1 cells at 2 weeks in Figure 4.7B observe slightly smaller coupling efficiencies compared to the AsPC-1 cells. The percentages between the control and experimental almost overlap. In Figure 4.7D, however, the coupling efficiency of the control decreases, while the efficiency of the experimental group increases from 2 weeks of incubation. The experimental group, therefore, has a larger coupling efficiency than the control, with a percentage of 74.77 %, while the control is 63.72 %.

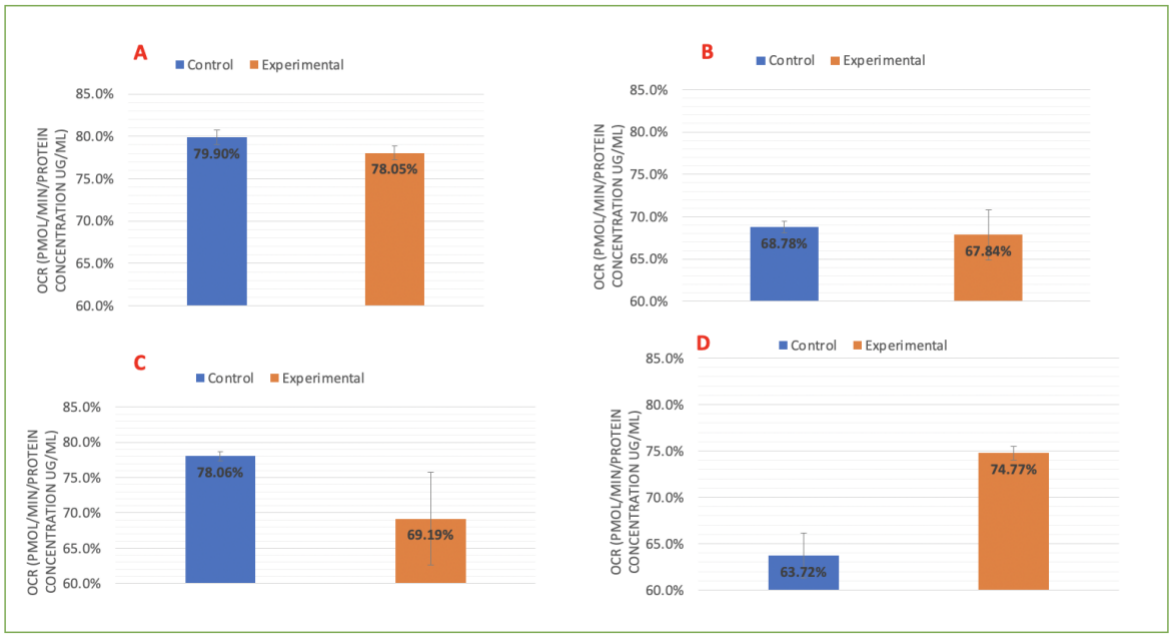

Figure 4. 7 The Coupling Efficiency as a Percentage of Panc-1 and AsPC-1 Pancreatic Cancer Cell Lines After 2-Weeks and 6-Weeks of Metformin Treatment.
Coupling efficiency is the percentage of basal respiration that is coupled to ATP production and presented as an OCR measurement in pmol/min. Each panel of the figure illustrates the coupling efficiency of the following: (A) AsPC-1 cell line after 2-weeks of metformin treatment, (B) Panc-1 cell line after 2-weeks of metformin treatment, (C) AsPC-1 cell line after 6-weeks of metformin treatment, and (D) Panc-1 cell line after 6-weeks of metformin treatment. The error bars in each panel represent the standard deviations of the coupling efficiency percentages calculated from each well of both the control and experimental groups. The data is normalized to the concentration of protein in µg/mL.

4.4 A Pretreatment of Metformin Alters the Glycolytic Metabolisms of Both Panc-1 and AsPC-1 Pancreatic Cancer Cell Lines

4.4.1 Shift in ECAR Values

To analyze shifts in glycolytic function in response to a pretreatment of 11.6 µM metformin, a Glyco Stress Test was performed using a Seahorse XFp Analyzer for each cell line after both 2 weeks and 6 weeks of metformin incubation. The change in ECAR (mpH/min) represents the glycolytic function of the cells, or the rate of glycolysis. This change is illustrated in Figure 4. 8. Apart from Figure 4.8D, the control cells display slightly larger ECAR values compared to the treated experimental cells. However, unlike the OCR values in Figure 4. 5, the differences in ECAR between the control and experimental groups are minimal. Interestingly, the control AsPC-1 cells that were incubated for 6 weeks as seen in Figure 4.8C, show an overall increase in

ECAR compared to the cells incubated for 2 weeks. Comparatively, the ECAR values of the experimental group remain largely the same despite the increase in incubation time. The Panc-1 cells that were incubated for 2 weeks as seen Figure 4.5B, reveal that the control cells have slightly larger ECAR values than the experimental group. However, when the cells were incubated for an additional 4 weeks as seen in Figure 4.5D, both the control and experimental cells showed a decrease in ECAR. Additionally, the ECAR values of the two groups appear to overlap. The ECAR levels of the Panc-1 cells at 2 weeks of incubation are slightly larger than their AsPC-1 counterpart. However, the Panc-1 cells at 6 weeks of incubation are smaller than the AsPC-1 cells incubated for 6 weeks.

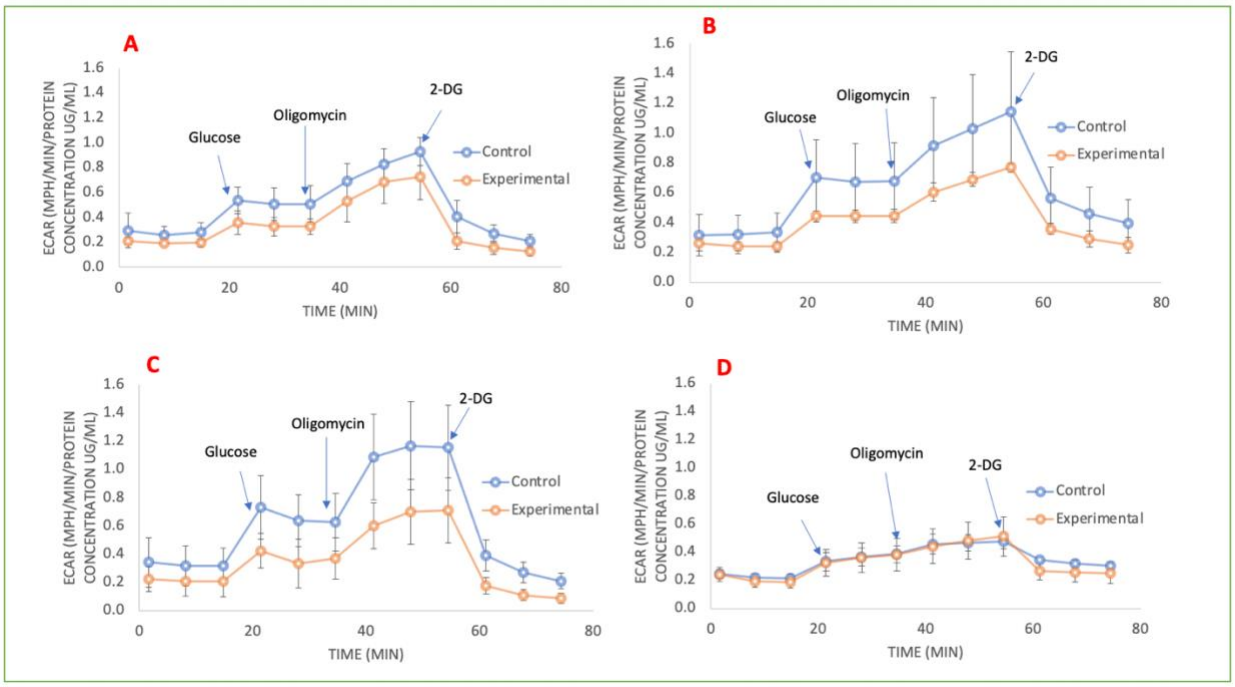

Figure 4. 8 The Glycolytic Function of Panc-1 and AsPC-1 Pancreatic Cancer Cell Lines After 2-Weeks and 6-Weeks of Metformin Treatment.
A Seahorse XFp Analyzer was used to run a Glyco Stress Test to measure the change Extracellular Acidification Rate (ECAR) in mpH/min vs. time in minutes for each cell line. Each panel of the figure illustrates the glycolytic function of the following: (A) AsPC-1 cell line after 2 weeks of metformin treatment, (B) Panc-1 cell line after 2 weeks of metformin treatment, (C) AsPC-1 cell line after 6 weeks of metformin treatment, and (D) Panc-1 cell line after 6 weeks of metformin treatment. The error bars represent the standard deviation of the ECAR measurements taken from each seahorse assay well. The points where each modulator, Glucose, Oligomycin, and 2-DG, were injected are labelled on the graphs. The data is normalized to the concentration of protein in µg/mL.

4.4.2 Change in Glycolysis, Glycolytic Capacity, and Glycolytic Reserve Averages

The results in Figure 4. 9 analyze the glycolysis, glycolytic capacity, and glycolytic reserve averages of both experimental and control Panc-1 and AsPC-1 cells. These parameters were calculated using the equations in Table 3. 14. The glycolysis parameter is determined by the injection of glucose, the glycolytic capacity parameter is determined by the injection of Oligomycin, and the glycolytic reserve is determined by the injection of 2-DG. The experimental AsPC-1 cells at both 2 weeks and 6 weeks of treatment in Figures 4.9A and 4.9C, respectively, have identical glycolysis and glycolytic capacities averages despite the difference in incubation lengths. Comparatively, the control AsPC-1 cells show a nominal increase in average glycolysis and glycolytic capacities from 2 weeks to 6 weeks of incubation. The control parameters are slightly larger than the experimental parameters. Like the AsPC-1 cells, the Panc-1 cells do not show prominent differences between the control and experimental. However, there is an overall decrease in parameter averages at 6 weeks of incubation seen in Figure 4.9D, compared to 2-weeks seen in Figure 4.9B. Additionally, the parameter averages at 6 weeks of incubation between the control and experimental are approximately equal. Lastly, the Panc-1 parameter averages at 6 weeks of incubation are smaller than their AsPC-1 counterpart, while the parameter values at 2 weeks of incubation between the two cell lines are similar.

Figure 4. 9 The Average Rate of Glycolysis, the Glycolytic Capacity, and the Glycolytic Reserve of Panc-1 and AsPC-1 Pancreatic Cancer Cell Lines After 2-Weeks and 6-Weeks of Metformin Treatment.

Glycolysis indicates the rate at which each cell line performs glycolysis which is measured as ECAR in mpH/min. Each panel of the figure illustrates the glycolytic rate, capacity, and reserve of the following: (A) AsPC-1 cell line after 2 weeks of metformin treatment, (B) Panc-1 cell line after 2 weeks of metformin treatment, (C) AsPC-1 cell line after 6 weeks of metformin treatment, and (D) Panc-1 cell line after 6 weeks of metformin treatment. The error bars represent the standard deviation of the calculations of glycolysis, glycolytic capacity, and glycolytic reserve, respectively, from each seahorse assay well. The data is normalized to the concentration of protein in µg/mL.

4.4.3 Change in Glycolytic Reserve Percentages

An analysis of Figure 4. 10, shows that overall, the experimental cells have slightly larger glycolytic reserves as a percentage compared to the control cells. The largest difference between control and experimental cells are observed in Figure 4.10A, which represent the AsPC-1 cells that were incubated for 2 weeks. The percentages are 257.2% and 344.5 %, respectively. In Figure 4.10C, which represent the AsPC-1 cells after 6 weeks of incubation, both the control and experimental cells show a decrease in glycolytic reserve with values of 206.4 % and 230.5 %, respectively. The Panc-1 cells that were incubated for 2 weeks and 6 weeks, as seen in Figures 4.10B and 4.10D, have slightly smaller glycolytic reserve percentages compared to their AsPC-1 counterparts. Additionally, the control and experimental Panc-1 groups experienced a decrease in glycolytic reserve after 6 weeks of incubation. The values decrease from 220.8 % to 155.69.8 % at 2 weeks to 268.83% to 170.5 % at 6 weeks.

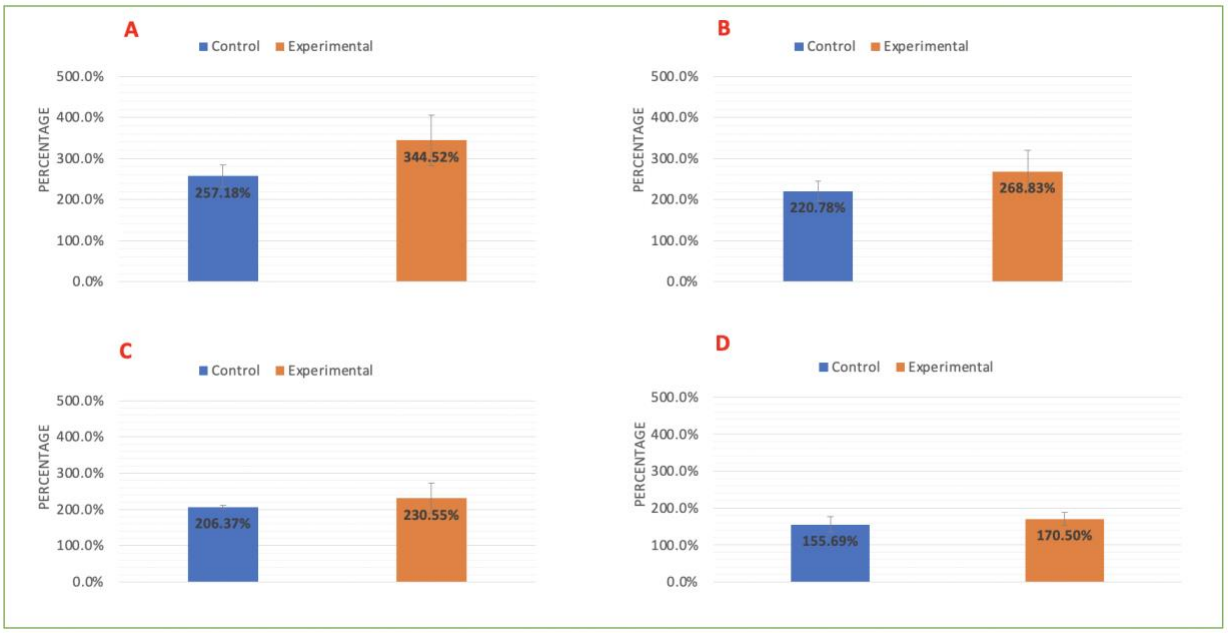

Figure 4. 10 The Glycolytic Reserve as a Percentage of Panc-1 and AsPC-1 Pancreatic Cancer Cell Lines After 2-Weeks and 6-Weeks of Metformin Treatment.
Each panel of the figure illustrates the glycolytic reserve percentage of the following: (A) AsPC-1 cell line after 2 weeks of metformin treatment, (B) Panc-1 cell line after 2 weeks of metformin treatment, (C) AsPC-1 cell line after 6 weeks of metformin treatment, and (D) Panc-1 cell line after 6 weeks of Metformin treatment. The error bars represent the standard deviation of the calculations of glycolytic reserve (%) from each seahorse assay well.

4.5 A Pretreatment of Metformin Combined with a 5-FU Chemotherapy Treatment Decreases the Size of AsPC-1 and Panc-1 Spheroids

To determine the effect a prolonged treatment with a clinical concentration of metformin has on chemotherapy efficacy, 3D spheroids of both cell lines were cultured. The spheroids were then exposed to clinically relevant concentrations of 5-FU, and the impact on spheroid growth was tracked by imaging the cells and measuring their diameters in µM. The changes in AsPC-1 spheroid growth in relation to 5-FU exposure are highlighted in Figure 4. 11. In general, the sizes of the metformin-treated spheroids are smaller than the spheroids that did not receive metformin. This is even more evident at 6 weeks of incubation in Figure 4.11B compared to 2 weeks of incubation, Figure 4.11A. It is also apparent that spheroid size increases from Day 0 to Day 4 to Day 5 in both the treated and non-treated cells at 0 µg/mL of 5-FU, which served as the control. This is true of both Figures 4.11A and 4.11B. However, treatment with chemotherapy hinders this increase, and the spheroids decrease in size with each passing day. However, increasing

concentrations of 5-FU does not appear to decrease the size of the spheroids. Interestingly, in Figures 4.11A and 4.11B, some spheroids grew larger despite the increasing concentrations of 5-FU. This is true of the spheroids that received and did not receive a pretreatment of metformin.

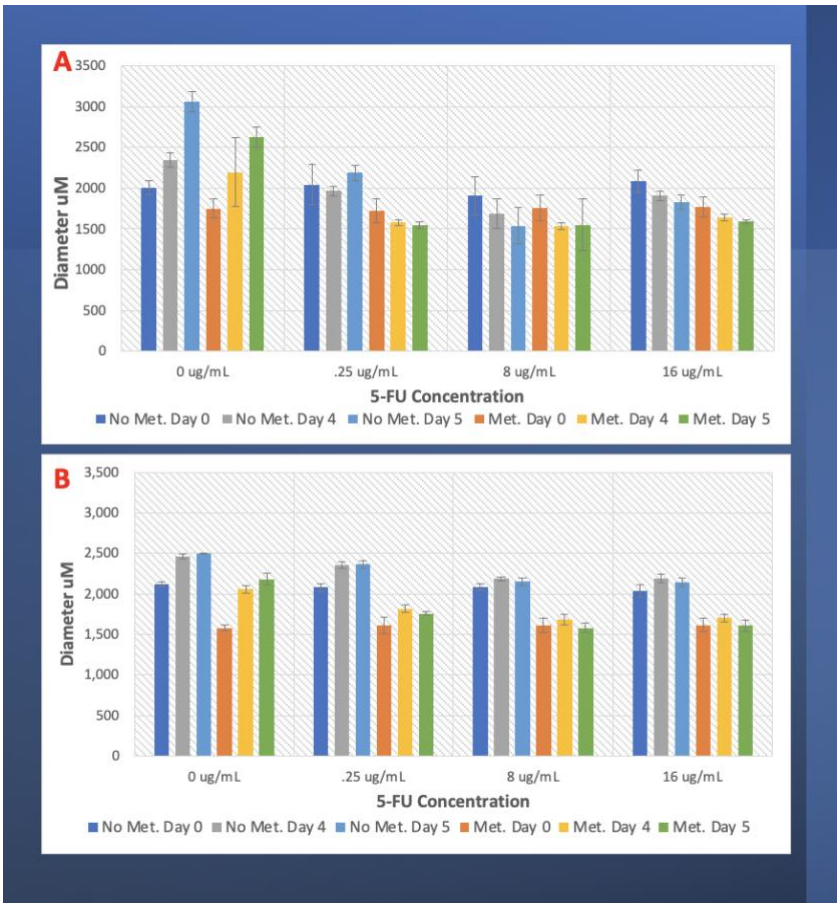

Figure 4. 11 The Spheroid Diameters in µM of AsPC-1 Cells After 2 Weeks and 6 Weeks of Metformin Treatment.
Spheroids were grown in low-attachment U-bottom wells and were exposed to 5-FU for 4 days before the effect on spheroid diameter were analyzed. Five spheroid replicates received 4 5-FU concentrations: 0 $\mu g/mL$, 0.25 $\mu g/mL$, 8 $\mu g/mL$, and 16 $\mu g/mL$. Each panel of the figure illustrates the average spheroid diameter in μM of the following: (A) Spheroids grown from AsPC-1 cells incubated in 11.6 μM metformin for 2 weeks, and (B) Spheroids grown from AsPC-1 cells incubated in 11.6 μM metformin for 6 weeks. Images were taken on Day 0 (before 5-FU exposure), Day 4 (after 4 days of 5-FU exposure), and Day 5 (one-day after a media exchange).

The same process was repeated for the Panc-1 cell line. The changes in spheroid size in response to 5-FU treatment is outlined in Figure 4. 12. Unlike the AsPC-1 cells, the cells treated in metformin for 2 weeks grew larger spheroids than those not treated in metformin, as shown in Figure 4.12A. Notably, the addition of 5-FU to the spheroids did not hinder their growth. The size of the spheroids remained largely the same at increasing concentrations of 5-FU. The

passing of days did not lead to any major changes in diameter either. However, the spheroids grown from cells incubated for 6 weeks were smaller than those incubated for 2 weeks as in Figures 4.12B. This decrease in spheroid diameter is even more pronounced among the metformin-treated cells. Again, exposure to 5-FU did not influence the size of the spheroids.

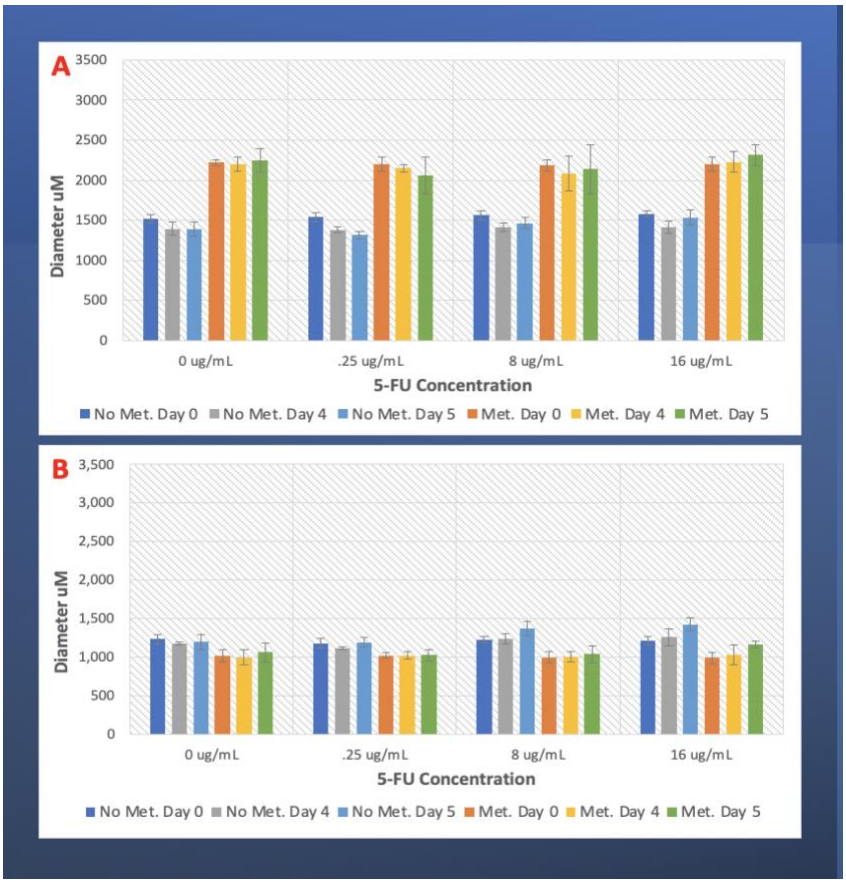

Figure 4. 12 The Spheroid Diameters µM of Panc-1 Cells After 2 Weeks and 6 Weeks of Metformin Treatment.
Spheroids were grown in low-attachment U-bottom wells and were exposed to 5-FU for 4 days before the effect on spheroid diameter was analyzed. Five spheroid replicates received 4 5-FU concentrations: 0 $\mu g/mL$, 0.25 $\mu g/mL$, 8 $\mu g/mL$, and 16 $\mu g/mL$. Each panel of the figure illustrates the average spheroid diameter in μM of the following: (A) Panc-1 cells exposed to 11.6 μM metformin for 2 weeks, and (B) Panc-1 cells exposed to 11.6 μM metformin for 6 weeks. Images were taken on Day 0 (before 5-FU exposure), Day 4 (after 4 days of 5-FU exposure), and Day 5 (one-day after a media exchange).

4.6 A Pretreatment of Metformin Combined with Various Chemotherapy Treatments Decreases the Volume of AsPC-1 and Panc-1 Spheroids over an 18-Day Period

4.6.1 Gemcitabine-Metformin Adjuvant Treatment

To continue the investigation of the impact a metformin-chemotherapy combination has on PDAC growth, other common chemotherapies used to treat PDAC were tested. Panc-1 and AsPC-1 cells were again incubated with a pretreatment of 11.6 μM of metformin for 2 weeks and 6 weeks in total. Varying clinically relevant concentrations of Gemcitabine, Oxaliplatin, and SN38 were added to the spheroids formed in U-bottom wells and were incubated for 18 days. The impact on spheroid size was determined by calculating the volume in uM^3 of the spheroids after brightfield images were collected using the Leica microscope. The impact of a combined of a metformin-chemotherapy treatment is illustrated in Figures 4.13-4.18. In Figure 4. 13, the pretreatment of 11.6 μM of metformin did not appear to have an impact on the growth of the Panc-1 spheroids without Gemcitabine (0 μM of gemcitabine). In Figures 4.13A and 4.13C, the volume of the spheroids treated in metformin for 2 weeks are on average larger than those that did not receive a pretreatment. In Figures 4.13B and 4.13D, the same disrupted pattern was demonstrated, where the spheroids that received a pretreatment of metformin for 6 weeks were either the same size or larger on average than the spheroids that received no pretreatment. Notably, an increase in concentration of Gemcitabine is not characterized by a decrease in spheroid volume. Instead, spheroids at the highest concentration of Gemcitabine, 500 μM, seem to be the same size or even slightly larger than those that received a smaller concentration. The Gemcitabine-treated media was exchanged on day 4, and every other day thereafter. The days that followed consequently showed an increase in spheroid size. However, the second dose of Gemcitabine was inoculated on day 14. It did not lead to a decrease in spheroid volume on days 16 and day 18, instead spheroid volume increased. On average the smallest spheroids are those that received no metformin pretreatment for 2 weeks of incubation and were inoculated with 25 μM of Gemcitabine, Figure 4.13A.

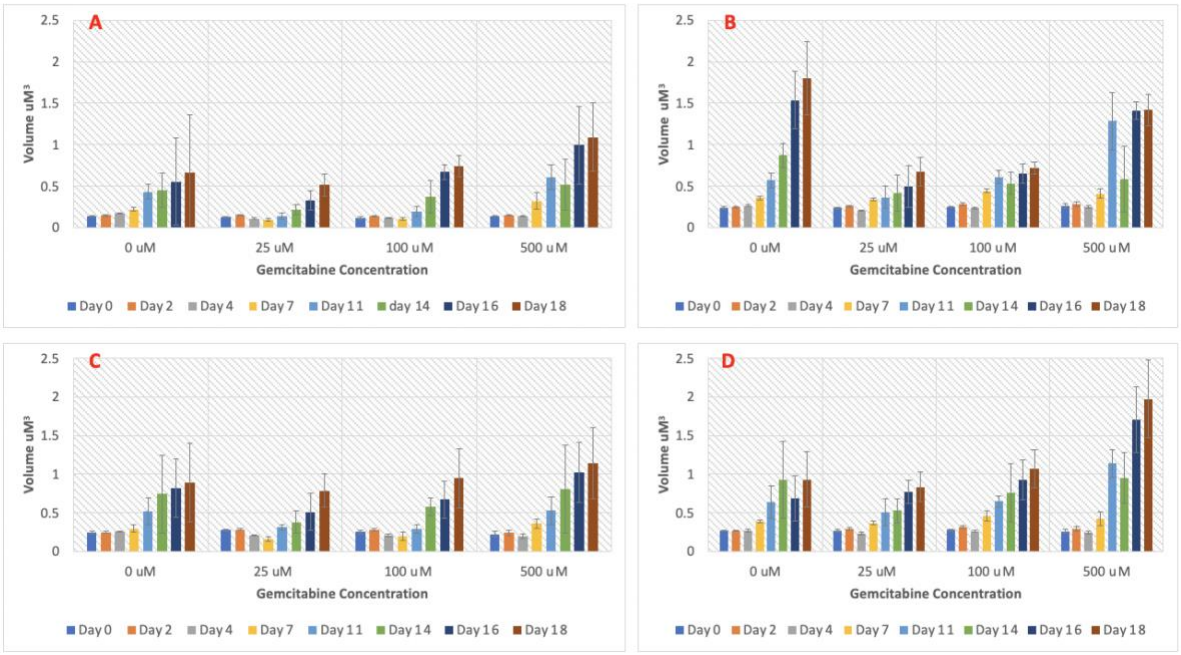

Figure 4. 13 The Change in Spheroid Volume in **µ**M^3 of Panc-1 Cells after a Gemcitabine Treatment of Varying Concentrations.
Spheroids were grown in a low-attachment U-bottom wells and were exposed to Gemcitabine for 18 days. The impact on spheroid growth was analyzed on day 0, 2, 4, 7, 11, 14, 16, and 18. Five spheroid replicates received 4 Gemcitabine concentrations: 0 µM, 25 µM, 100 µM, and 500 µM. Each panel of the figure illustrates the average spheroid volume in uM^3 of the following: (A) Panc-1 cells that did not receive a pretreatment of metformin for 2 weeks (B) Panc-1 cells that did not receive a pretreatment of metformin for 6 weeks (C) Panc-1 cells that were incubated in 11.6 µM of metformin for 2 weeks (D) Panc-1 cells that were incubated in 11.6 µM of metformin for 6 weeks.

In Figure 4. 14, the AsPC-1 cells were inoculated with Gemcitabine. The AsPC-1 cells that were pretreated with metformin for 2 weeks were on average smaller than those that did not receive a pretreatment, Figures 4.14C and 4.14A, respectively. However, the cells that were incubated in metformin for 6 weeks were similar sized as those that did not receive a metformin pretreatment, Figures 4.14D and 4.14B, respectively. In Figure 4.14A, the spheroids treated with Gemcitabine were dramatically smaller than those that received no chemo. However, an increase in Gemcitabine dose did not further impede the growth of the spheroids. In all other panels, the addition of Gemcitabine did not really impact spheroid growth. For example, in Figure 4.14D, the spheroid inoculated with 500 µM of Gemcitabine were larger than those that received no Gemcitabine.

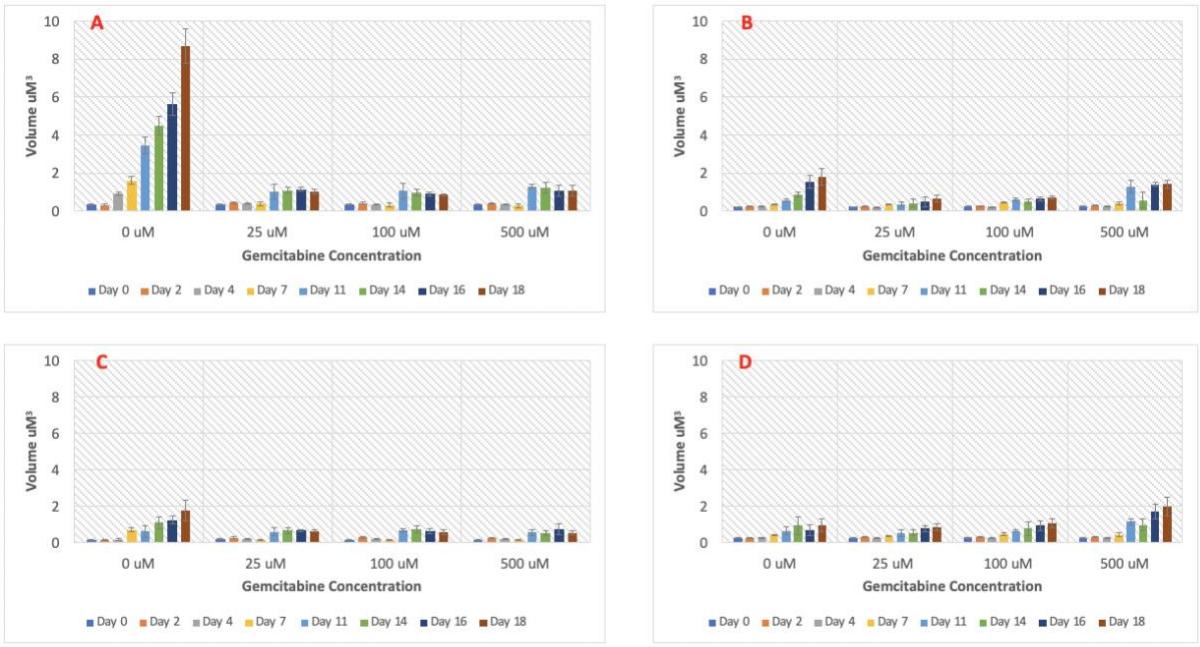

Figure 4. 14 The Change in Spheroid Volume in **µ**M^3 of AsPC-1 Cells after a Gemcitabine Treatment of Varying Concentrations.
Spheroids were grown in a low-attachment U-bottom wells and were exposed to Gemcitabine for 18 days. The impact on spheroid growth was analyzed on day 0, 2, 4, 7, 11, 14, 16, and 18. Five spheroid replicates received 4 Gemcitabine concentrations: 0 µM, 25 µM, 100 µM, and 500 µM. Each panel of the figure illustrates the average spheroid volume in µM^3 of the following: (A) AsPC-1 cells that did not receive a pretreatment of metformin for 2 weeks (B) AsPC-1 cells that did not receive a pretreatment of metformin for 6 weeks (C) AsPC-1 cells that were incubated in 11.6 µM of metformin for 2 weeks (D) AsPC-1 cells that were incubated in 11.6 µM of metformin for 6 weeks.

4.6.2 Oxaliplatin-Metformin Adjuvant Treatment

In Figure 4. 15, the Panc-1 spheroids treated with varying concentrations of Oxaliplatin revealed slightly different results than those treated with Gemcitabine. For instance, in Figures 4.15A and 4.15C, the Panc-1 cells that received a pretreatment of metformin had on average larger or similar sized spheroids compared to those that did not receive a pretreatment. Contrastingly, the cells that received a pretreatment of metformin for 6 weeks had on average smaller spheroids than their control counterpart, Figures 4.15D and 4.15B, respectively. The volume of the spheroids decreased in size with each dose increase of Oxaliplatin. The smallest spheroids overall, were those incubated in metformin for 6 weeks, Figure 4.15D. When the second dose of Oxaliplatin was added on day 14, the spheroids continued to grow larger.

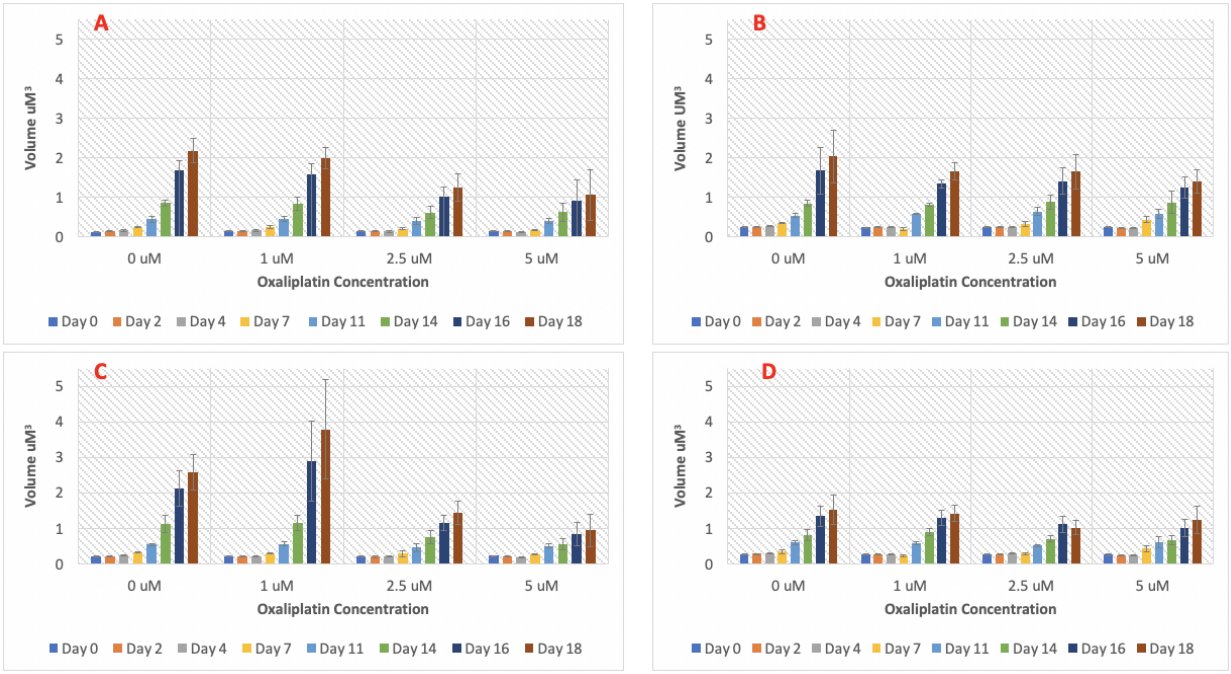

Figure 4. 15 The Change in Spheroid Volume in **µ**M^3 of Panc-1 Cells after an Oxaliplatin Treatment of Varying Concentrations.
Spheroids were grown in a low-attachment U-bottom wells and were exposed to Oxaliplatin for 18 days. The impact on spheroid growth was analyzed on day 0, 2, 4, 7, 11, 14, 16, and 18. Five spheroid replicates received 4 Oxaliplatin concentrations: 0 µM, 1 µM, 2.4 µM, and 5 µM. Each panel of the figure illustrates the average spheroid volume in uM^3 of the following: (A) Panc-1 cells that did not receive a pretreatment of metformin for 2 weeks (B) Panc-1 cells that did not receive a pretreatment of metformin for 6 weeks (C) Panc-1 cells that were incubated in 11.6 µM of metformin for 2 weeks (D) Panc-1 cells that were incubated in 11.6 µM of metformin for 6 weeks.

In Figure 4. 16, AsPC-1 cells were inoculated with Oxaliplatin. The AsPC-1 cells that were treated with metformin for 2 weeks were on average smaller than those that received no pretreatment, Figures 4.16C and 4.16A, respectively. Contrastingly, for the first 7 days of incubation, the spheroids that received a pretreatment of metformin for 6 weeks are smaller than those that received no treatment, Figures 4.16D and 4.16B, respectively. The size of the spheroids on the days that followed were comparable in size to those that did not receive a pretreatment of metformin. Interestingly, an increase in Oxaliplatin concentration led to a decrease in spheroid size in all panels. This size decrease was most dramatic in Figures 4.16A and 4.16C. The smallest spheroids were those that received a 2-week metformin pretreatment and were inoculated with 5 µM of Oxaliplatin as seen in Figure 4.16C. Additionally, when the second dose of Oxaliplatin was added on day 14, the spheroids on consecutive days continued to grow larger in Figures 4.16B and 4.16D.

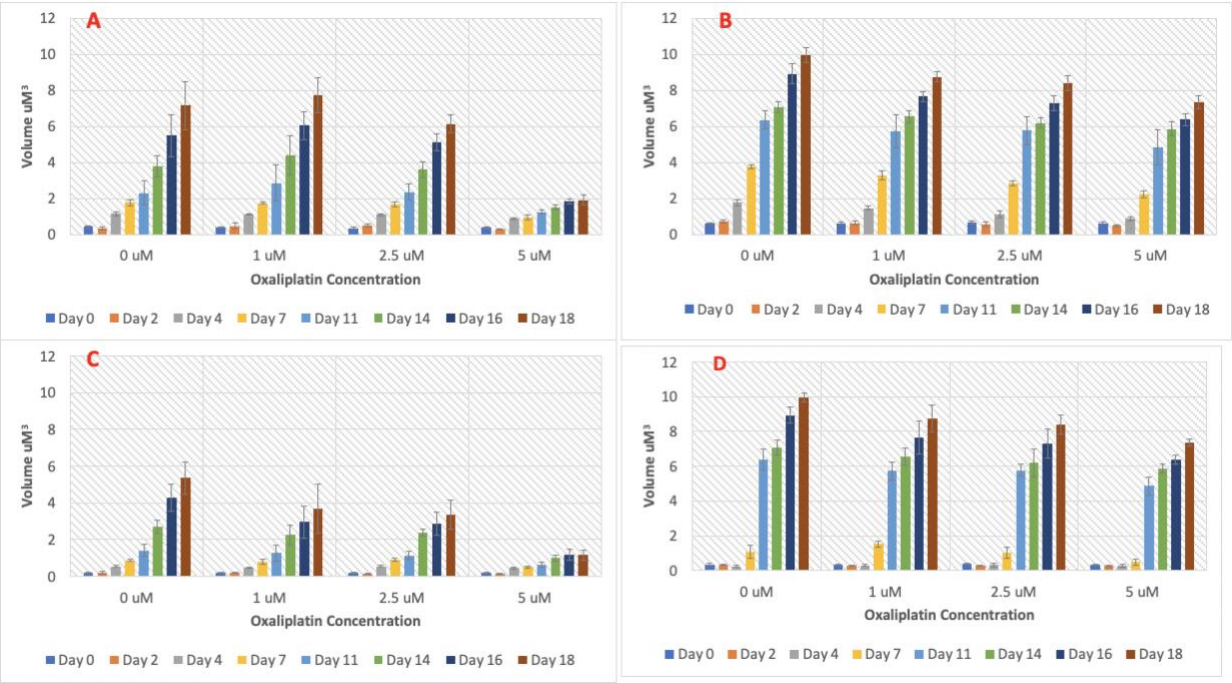

Figure 4. 16 The Change in Spheroid Volume in μM^3 of AsPC-1 Cells after an Oxaliplatin Treatment of Varying Concentrations.
Spheroids were grown in a low-attachment U-bottom wells and were exposed to Oxaliplatin for 18 days. The impact on spheroid growth was analyzed on day 0, 2, 4, 7, 11, 14, 16, and 18. Five spheroid replicates received 4 Oxaliplatin concentrations: 0 µM, 1 µM, 2.5 µM, and 5 µM. Each panel of the figure illustrates the average spheroid volume in μM^3 of the following: (A) AsPC-1 cells that did not receive a pretreatment of metformin for 2 weeks (B) AsPC-1 cells that did not receive a pretreatment of metformin for 6 weeks (C) AsPC-1 cells that were incubated in 11.6 µM of metformin for 2 weeks (D) AsPC-1 cells that were incubated in 11.6 µM of metformin for 6 weeks.

4.6.3 SN-38-Metformin Adjuvant Treatment

In Figure 4. 17, Panc-1 spheroids were inoculated with SN38. The cells that were treated with metformin for 2 weeks and received no SN38 (0 ng/mL) were on average larger than those that received no metformin pretreatment or SN38, Figures 4.17C and 4.17A, respectively. However, the Panc-1 cells that were treated with metformin for 6 weeks were slightly smaller or similar sized than those that received no pretreatment, Figures 4.17D and 4.17B, respectively. Although not drastic, an increase in SN38 concentration corresponded with a decrease in spheroid volume. The smallest group of spheroids on average are those that were treated with metformin for 6 weeks, Figure 4.17D. However, the smallest subgroup of spheroids is those that received no metformin pretreatment and were inoculated with 20 ng/mL SN38, the maximum concentration, Figure 4.17A. When the second dose of SN38 was added on day 14 it did hinder the growth of the spheroids on consecutive days, unlike the other chemotherapy treatments discussed.

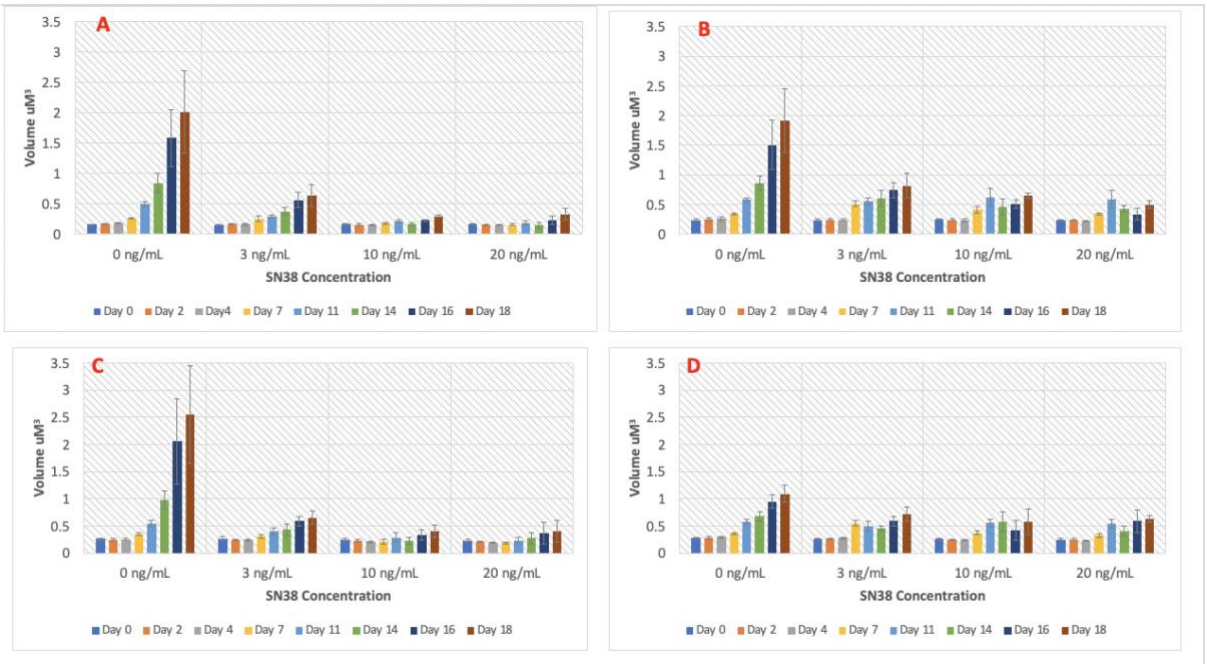

Figure 4. 17 The Change in Spheroid Volume in μM^3 of Panc-1 Cells after an SN-38 Treatment of Varying Concentrations.
Spheroids were grown in a low-attachment U-bottom wells and were exposed to SN38 for 18 days. The impact on spheroid growth was analyzed on day 0, 2, 4, 7, 11, 14, 16, and 18. Five spheroid replicates received 4 SN38 concentrations: 0 ng/mL, 3 ng/mL, 10 ng/mL, and 20 ng/mL. Each panel of the figure illustrates the average spheroid volume in uM^3 of the following: (A) Panc-1 cells that did not receive a pretreatment of metformin for 2 weeks (B) Panc-1 cells that did not receive a pretreatment of metformin for 6 weeks (C) Panc-1 cells that were incubated in 11.6 µM of metformin for 2 weeks (D) Panc-1 cells that were incubated in 11.6 µM of metformin for 6 weeks.

In Figure 4. 18, AsPC-1 spheroids were inoculated with SN38. The spheroids that received a pretreatment of metformin for 2 weeks were smaller on average than their no metformin counterparts, Figures 4.18C and 4.18A, respectively. The same is true for spheroids that received a pretreatment of metformin for 6 weeks, Figures 4.18D and 4.18B, respectively. The spheroids that were incubated for 6 weeks are larger than the spheroids that were incubated for 2 weeks. Furthermore, an increase in SN38 concentration consequently led to a decrease in spheroid volume. This decrease is most evident in Figures 4.18A and 4.18C. The smallest spheroids were incubated with metformin 2 weeks and inoculated with 20 ng/mL of SN38, Figure 4.18C. The largest spheroids were incubated for 6 weeks and received no chemotherapy treatment, Figure 4.18B.

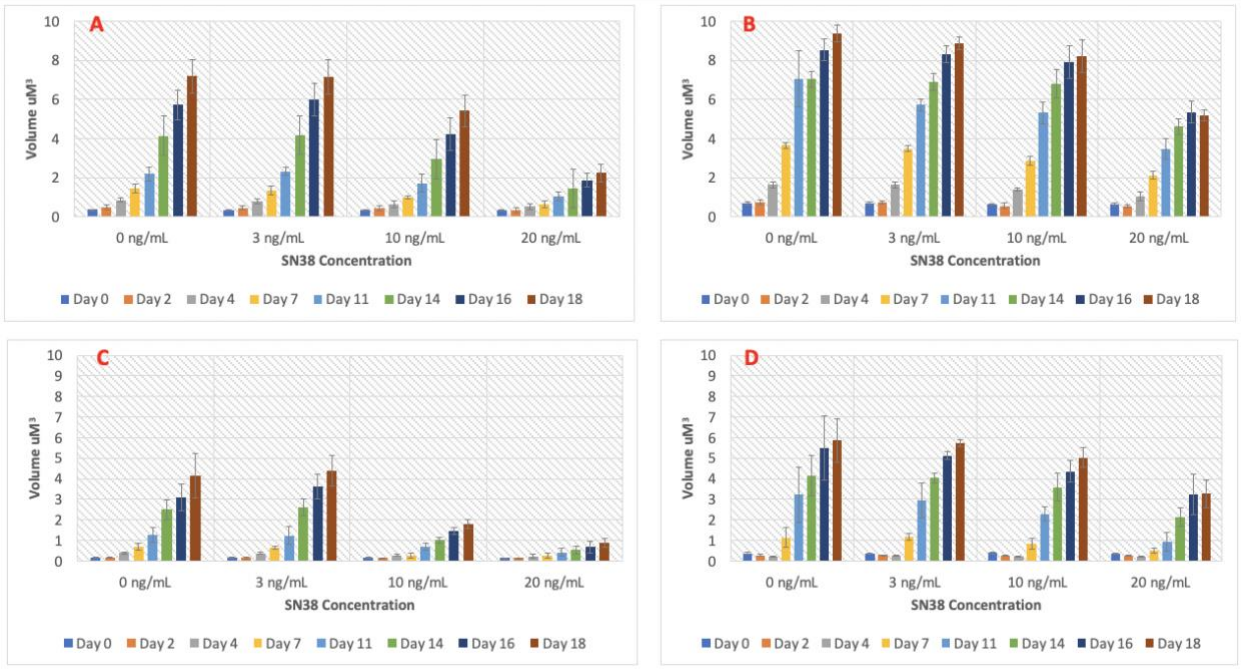

Figure 4. 18 The Change in Spheroid Volume in μM^3 of AsPC-1 Cells after an SN38 Treatment of Varying Concentrations.
Spheroids were grown in a low-attachment U-bottom wells and were exposed to SN38 for 18 days. The impact on spheroid growth was analyzed on day 0, 2, 4, 7, 11, 14, 16, and 18. Five spheroid replicates received 4 SN38 concentrations: 0 ng/mL, 3 ng/mL, 10 ng/mL, and 20 ng/mL. Each panel of the figure illustrates the average spheroid volume in μM^3 of the following: (A) AsPC-1 cells that did not receive a pretreatment of metformin for 2 weeks (B) AsPC-1 cells that did not receive a pretreatment of metformin for 6 weeks (C) Panc-1 cells that were incubated in 11.6 µM of metformin for 2 weeks (D) AsPC-1 cells that were incubated in 11.6 µM of metformin for 6 weeks.

4.7 An Analysis of Spheroid Viability after Chemotherapy Treatment

To assess how incubation time, metformin pretreatment, and chemotherapy exposure effects spheroid viability, spheroids were stained with Prodiudium Iodide and Calcein AM on day 17 of incubation for fluorescence analysis on day 18. PI stains dead cells, while Calcein stains live cells. The proportion of live to dead cells indicates how necrotic the spheroid is and how effective the combined treatment of metformin and chemotherapy was. The viability scores of the AsPC-1 and Panc-1 spheroids treated with Gemcitabine, SN-38, and Oxaliplatin are provided in Figure 4. 19, Figure 4. 20, and Figure 4. 21. The viability score constitutes the area of the spheroid stained with PI and Calcein in microns, which translates to the ratio of live cells to dead cells in the spheroid. The viability charts used to calculate these viability scores are included in Appendix H. The higher the size in microns of the area stained with PI, the more dead cells

encompass the spheroid, while the higher the size of the area stained with Calcein, the more live cells encompass the spheroid. In Figure 4. 19, the AsPC-1 spheroids previously incubated for 2 weeks reveal that the spheroid that received a metformin pretreatment and the highest Gemcitabine concentration of 500 μM (well 10) has the highest live cells to dead cells ratios, while the spheroid that received no metformin pretreatment and the highest Gemcitabine concentration (well 6) has the lowest live cells to dead cells ratio. Overall, the Panc-1 cells have larger areas of dead cells compared to AsPC-1 cells. In Figure 4.19B, the viability scores of the Panc-1 spheroids previously incubated for 2 weeks reveal that the spheroid that received no metformin pretreatment or Gemcitabine exposure (well 3) has the highest live cell to dead cell ratio, while the spheroid that received a metformin pretreatment and no Gemcitabine (well 7) has the lowest ratio. After 6 weeks of incubation, the results differ. In Figure 4.19C, the viability scores reveal that well 3 has the highest live cell to dead cells ratio, while well 6 has the lowest. In Figure 4.19D, the viability scores of the spheroids are similar, where well 6 has the highest ratio, and well 3 has the lowest.

The viability profiles of the spheroids treated with SN-38 are represented in Figure 4. 20. The results differ compared to the spheroids treated in Gemcitabine. In Figure 4.20A, the AsPC-1 spheroids previously incubated for 2 weeks reveal that the spheroid that received a metformin pretreatment and no SN-38 exposure (well 7) has the highest live cell to dead cell ratio, while the spheroid that received no metformin pretreatment and 5 ng/mL of SN-38 (well 6) has the lowest ratio. Again, the Panc-1 spheroids have larger dead areas compared to the AsPC-1 spheroids. In Figure 4.20B, well 6 has the highest live cell to dead cell ratio, while well 7 has the lowest. After 6 weeks of incubation, the areas of live and dead spheroids change. For the AsPC-1 cells in Figure 4.20C, well 6 has the highest ratio, while the spheroid that received a metformin pretreatment and 5 ng/mL of SN-38 (well 10) has the lowest ratio. Contrastingly, the Panc-1 cells in Figure 4.20D, reveals that well 6 has the highest live cells to dead cells ratio, while well 7 has the lowest ratio.

The viability profiles of the spheroids treated with Oxaliplatin are represented in Figure 4. 21. Out of the three chemotherapies tested, SN-38 and Oxaliplatin treated spheroids have the highest areas in microns of dead cells. Like all the chemotherapies tested, the Panc-1 cells in Figure 4. 21, have the highest areas of dead cells. For the AsPC-1 spheroids in Figures 4.21A and 4.21C, the spheroids that did not receive a metformin pretreatment and no Oxaliplatin

exposure (well 3), as well as the spheroids that received no metformin pretreatment and 5 μM of Oxaliplatin (well 6) have the highest ratios of live cells to dead cells. For the Panc-1 cells in Figures 4.12B and 4.12D, all the spheroids have low ratios of live cells to dead cells.

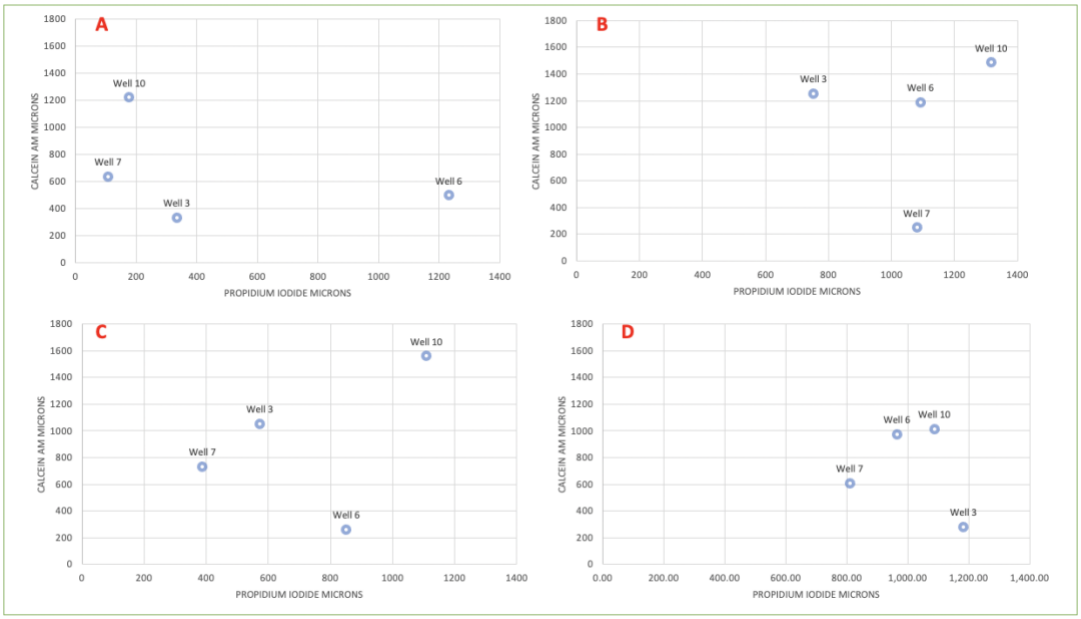

Figure 4. 19 Viability Score of AsPC-1 and Panc-1 Spheroids on Day 18 of Incubation of a Gemcitabine Treatment.

Spheroids were grown in a low-attachment U-bottom wells and were exposed to Gemcitabine for 18 days. The impact on spheroid viability was assessed with confocal microscopy on day 18 of incubation. One replicate from each treatment group was stained with Propidium Iodide and Calcein AM. The assessed spheroids are labeled Well 3, Well 6, Well 7, and Well 10 on the graph and the treatment groups they correlate with are as follows: No metformin pretreatment + No Gemcitabine exposure, No metformin +500 μM Gemcitabine, 11.6 μM metformin pretreatment + No Gemcitabine exposure, and 11.6 μM metformin pretreatment + 500 μM Gemcitabine, respectively. Each panel of the figure illustrates the viability profile of the following: (A) AsPC-1 cells incubated for 2 weeks (B) Panc-1 cells incubated for 2 weeks (C) AsPC-1 cells incubated for 6 weeks (D) Panc-1 cells incubated for 6 weeks.

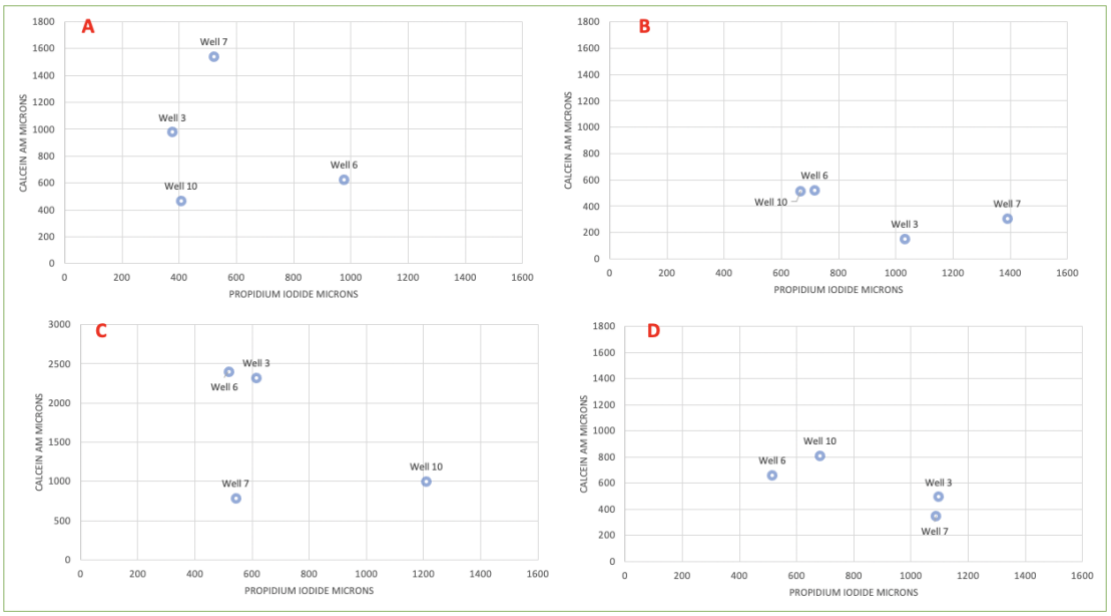

Figure 4. 20 Viability Score of AsPC-1 and Panc-1 Spheroids on Day 18 of Incubation of an SN-38 Treatment.

Spheroids were grown in a low-attachment U-bottom wells and were exposed to SN-38 for 18 days. The impact on spheroid viability was assessed with confocal microscopy on day 18 of incubation. One replicate from each treatment group was stained with Propidium Iodide and Calcein AM. The assessed spheroids are labeled Well 3, Well 6, Well 7, and Well 10 on the graph and the treatment groups they correlate with are as follows: No metformin pretreatment + No SN-38 exposure, No metformin +20 ng/mL SN-38, 11.6 μM metformin pretreatment + No SN-38 exposure, and 11.6 μM metformin pretreatment + 20 ng/mL SN-38, respectively. Each panel of the figure illustrates the viability profile of the following: (A) AsPC-1 cells incubated for 2 weeks (B) Panc-1 cells incubated for 2 weeks (C) AsPC-1 cells incubated for 6 weeks (D) Panc-1 cells incubated for 6 weeks.

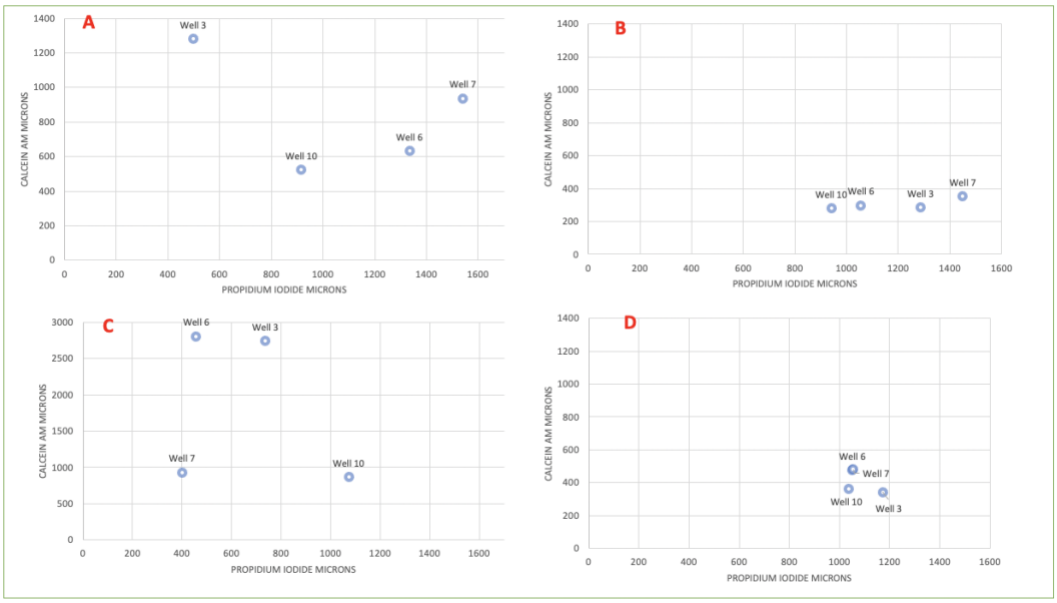

Figure 4. 21 Viability Score of AsPC-1 and Panc-1 Spheroids on Day 18 of Incubation of an Oxaliplatin Treatment.

Spheroids were grown in a low-attachment U-bottom wells and were exposed to Oxaliplatin for 18 days. The impact on spheroid viability was assessed with confocal microscopy on day 18 of incubation. One replicate from each treatment group was stained with Propidium Iodide and Calcein AM. The assessed spheroids are labeled Well 3, Well 6, Well 7, and Well 10 on the graph and the treatment groups they correlate with are as follows: No metformin pretreatment + No Oxaliplatin exposure, No metformin +5 μM Oxaliplatin, 11.6 μM metformin pretreatment + No Oxaliplatin exposure, and 11.6 μM metformin pretreatment + 5 μM Oxaliplatin, respectively. Each panel of the figure illustrates the viability profile of the following: (A) AsPC-1 cells incubated for 2 weeks (B) Panc-1 cells incubated for 2 weeks (C) AsPC-1 cells incubated for 6 weeks (D) Panc-1 cells incubated for 6 weeks.

4.8 Amplification Efficiencies of SYBR Green Primers

The primers used in this project are listed in Table 4. 2. They were designed according to the protocol outlined in section 3.2.11. The reference genes, ACTB and RRN-18S, were purchased as ready to use primers from QIAGEN. The QuantiTect Primer Assay guarantees an amplification efficiency of 100 $\pm$ 10 % for its primers. The efficiencies of all markers were tested to ensure the cDNA samples were doubled with each replication cycle, which would yield a 100% amplification efficiency. Therefore, efficiency values assess the performance of the qPCR assay. Optimal amplification efficiency values range from 90% to 110%. The amplification efficiencies for each primer, as well as the standard curve slopes from which they were generated from are listed in Table 4. 2. All the amplification efficiencies fall within the acceptable range except UPCP2, SLC22A1, ATP5F1A, and HK2 genes.

Table 4. 2 Amplification Efficiencies as a Percentage of SYBR Green Primers

Primer	Slope	R^2	E (%)
UPCP2	-2.5993	0.9996	142.50 %
LDHA	-3.5186	0.9990	92.40 %
SUCLA2	-3.5739	0.9990	90.50 %
SLC22A1	-2.3884	0.9945	162.23 %
SLC16A1	-3.3570	0.9943	98.56 %
PFKM	-3.5754	0.999	90.41 %
NDUFS1	-3.2808	0.9922	101.70 %
ATP5F1A	-2.7056	.9345	134.20 %
HK2	-.2.9395	0.9900	118.87 %
ACTB	-3.1830	0.9863	106 %
RRN-18S	-3.3945	0.9996	97.06 %

4.9 An Analysis of Relative Gene Expression Changes in Relation to Metformin Pretreatment

A SYBR Green primer assay was used to assess gene expression. Once the assay was run, relative gene expressions (RGE) were calculated using the Livak *el al.* method. The Cq values generated from each tested sample were used in the calculations. The result was a ratio of the target gene in the metformin treated group to the non-treated group, normalized to the reference gene with the most optimal Cq values. The relative gene expression values of AsPC-1 and Panc-1 cells that were pretreated (experimental) and not treated in metformin (control) are shown in Table 4. 3. Comparing the relative gene expression changes of common genes related to metabolism, reveals which genes are upregulated or downregulated upon a metformin pretreatment. Change in gene expression is correlated with color change in the table; red indicates downregulation, while green indicates upregulation. The genes associated with upregulated glycolysis are highlighted in orange, while the genes associated with upregulated OXPHOS are highlighted in blue. In Table 4. 3, the control AsPC-1 cells exhibit much higher relative gene expressions than the treated cells. In the table, the small RGE values associated with metformin treatment is represented by the color red. The only exception is the gene, SLC22A1, where the RGE of both the treated and untreated cells is approximately 0. The RGE values of the control cells are similar among all genes; they are all slightly above 1. Similarly, the gene expressions of the treated cells are also alike; they are all below 0.2. The genes with the highest expression among the control cells are HK2 and ATP5F1A, while the genes with the highest expression among the metformin treated cells are LDHA and PFKM. Therefore, the genes with the highest expression in the metformin treated cells are associated with glycolysis.

Unlike the AsPC-1 cells, the gene expression trends among the Panc-1 cells differ. Among the cells incubated for 2 weeks, RGE is generally higher in the metformin treated group compared with the control group. The greatest disparity in RGE between the treated and untreated cells is observed in the expressions of HK2 and NDUFS1. The only exception is the expression of SLC22A1, where the expression is above 25 for the untreated cells, and 0.041 in the treated cells. The two genes, UPCP2 and LDHA, show no difference in expression between the treated and untreated cells. At 6 weeks of incubation, the expression of SLC22A1 increases in the metformin treated cells and decreases dramatically in the untreated, compared to 2 weeks of incubation. Between the metformin treated and control group, the treated group exhibits larger

RGE expression values. The largest difference in RGE between the treated and untreated cells is observed in the expressions of SLC22A1 and SLC16A1. UPCP2 and ATP5F1A are the only genes with lower RGE in the metformin treated group compared to the control group.

Table 4. 3 The Relative Gene Expressions of Metabolic Genes Expressed in AsPC-1 and Panc-1 Cells Treated with 11.6 µM of Metformin.

	2 Weeks		6 Weeks		2 Weeks		6 Weeks	
	No Metformin				Metformin			
Gene	_	Panc-1	AsPC-1	Panc-1	_	Panc-1	AsPC-1	Panc-1
UPCP2 (Uncoupling Protein 2)		1.011	1.02	1.041		1.115	0.037	0
LDHA (Lactate Dehydrogenase A)		1.034	1.004	1		1.035	0.157	1.488
SUCLA2 (Succinate-CoA)		1.645	1.006	1		3.481	0.097	2.833
SLC22A1 (OCT1)		24.916	0	1.111		0.041	0	9.66
SLC16A1 (MCT1)		0.347	1.006	1.003		0.0004	0.054	6.258
PFKM (Phosphofructokinase PFK-1)		1.048	1.007	1		2.64	0.134	3.519
NDUFS1 (NADH: ubiquinone oxidoreductase core subunit S1)		1	1.014	1.002		6.046	0.038	1.779
ATP5F1A (ATP synthase F1 subunit alpha)		1	1.029	1.018		2.035	0.032	0.589
HK2 (hexokinase 2)		1	1.029	1.003		8.651	0.064	1.07

Lowest Expression

Highest Expression

Chapter 5 Discussion

5.1 The Effect of a Metformin Pretreatment on the Doubling Times of AsPC-1 and Panc-1 Cells

To determine whether a pretreatment of metformin impacts the proliferation rates of the treated AsPC-1 and Panc-1 cells, the doubling times were calculated by performing a Click-iT Edu Cell Proliferation assay. In Figure 4. 1, the Panc-1 cells show that the treated and control cells have overlapping fluorescent signal slopes and thus, the same growth rates and nearly the same doubling times, 155.82 hours, and 153.7 hours, respectively. Unlike the Panc-1 cells, the AsPC-1 cells in Figure 4. 2, which received a metformin pretreatment had a higher emitted fluorescence than the control cells. Additionally, the growth rate of the treated cells was less than that of the control cells and the doubling time of the treated cells was longer than the control, 77.41 and 25.34 hours, respectively. The results indicate that a pretreatment of 11.6 μM, had no effect on the proliferation rate of the Panc-1 cells. The metformin did not impede or promote a faster proliferation rate. In opposition, the AsPC-1 cells' proliferation rates are impacted by a pre-incubation of 11.6 μM metformin. The proliferation rate decreased in relation to metformin treatment. Therefore, the results might suggest that metformin impacts the proliferation rates of certain PDAC cell lines, but not others. Previous studies have provided supporting evidence that metformin decreases the proliferation rate, and therefore increases the doubling times of pancreatic cancer cells. Two studies found that metformin repressed the proliferation of Panc-1 and AsPC-1 pancreatic cancer cells in a concentration and time-dependent manner (60,61). Compared to the control group, the metformin-treated cells revealed that a higher proportion of cells were in the G_0/G_1 phases of growth than those in the S-phase (60,61). Moreover, the metformin treated cells were more apoptotic. The reason for this phenomenon is that metformin has been found to indirectly activate AMPK signaling and subsequently inhibit mTOR activity which results in reduced protein synthesis and cell proliferation (32). Furthermore, from a metabolic standpoint, metformin effectively eliminates pancreatic CSCs that exhibit an OXPHOS reliance by mitochondrial inhibition (63). Metformin thereby hinders cell proliferation by suppressing the synthesis of mitochondrial-dependent metabolic intermediates necessary for growth (87). Both metformin functions translate to a decreased proliferation rate among treated

AsPC-1 cells. However, the results cannot explain why the proliferation rate and doubling times of Panc-1 cells are unaffected.

There are several reasons why no decrease in growth rate or increase in doubling time was observed among the Panc-1 cells treated with metformin. Firstly, the Panc-1 cells in this study were treated with 11.6 μM of metformin, which is the maximum plasma concentration found in patients regularly using the drug (82). This concentration is significantly lower than the concentrations used in the in vitro studies described, which inoculated cells with both 20 and 40 mM of metformin. Perhaps 11.6 μM is too low of a dose to observe an effect on Panc-1 cells. Metformin enters the cell via OCT transporters, and thus larger concentrations of metformin are needed to observe an effect (59). Perhaps Panc-1 cells have an insufficient amount of OCT transporters to allow metformin to inhibit complex I of the mitochondria or activate AMPK signaling and instigate a decrease in proliferation. The analysis of metformin's impact on the mitochondrial and glycolytic rates in the following sections may clarify these results.

5.2 A Pretreatment of Metformin Alters the Metabolic Phenotype of Both Panc-1 and AsPC-1 Pancreatic Cancer Cell Lines

To examine how the cells' metabolisms are altered in response to a metformin pretreatment, the metabolic phenotypes of each cell line were determined. As seen in Figure 4. 3, the control AsPC-1 cells move from a slightly quiescent phenotype at baseline conditions to an energetic phenotype at stressed conditions. An energetic phenotype is characterized by high levels of both glycolysis and OXPHOS. At 2 weeks of metformin treatment, the AsPC-1 cells move from a quiescent phenotype at baseline conditions and remain in a quiescent state under stressed conditions, with slightly higher OCR and ECAR values. At 6 weeks of treatment, the cells remain in a highly quiescent state. Quiescence is defined as a state of reversible cell cycle arrest that allows the cells to protect themselves from environmental threats (88). It is often associated with low metabolic states that are characterized by a decrease in glucose uptake and glycolysis (88). Additionally, quiescent cells often inactivate TOR signaling to slow proliferation rates. Perhaps the environmental threat that promotes the quiescent metabolic state in AsPC-1 cells is metformin. This also explains the observed decrease in AsPC-1 proliferation rates in relation to metformin described in section 4.1. Metformin's inhibition of OXPHOS metabolically stresses the cells, which prompts them to enter a quiescent state to survive where the rate of glycolysis

and proliferation is slowed. Additionally, metformin indirectly inhibits mTOR activity by activating AMPK signaling, which promotes quiescence (32). Metformin's ability to shift metabolism to quiescence is supported by a study that found that metformin delayed satellite cell activation in muscle tissue and differentiation by favoring a quiescent, low metabolic state (89). This is attributed to metformin's inhibition of the ribosome protein RPS6, a downstream effector of the mTOR pathway (89). The control cells in this study, however, shift to an energetic state under stressed conditions to keep up with the energy demand. Contrastingly, the Panc-1 cells, at 2 weeks of incubation, appear to be slightly aerobic under baseline conditions with increased ECAR values under stressed conditions. This indicates that the Panc-1 cells perform OXPHOS at baseline conditions. Moreover, at 6 weeks of incubation, the metabolic phenotypes of the control and experimental overlap and shift from an aerobic-quiescent phenotype to a quiescent state with higher ECAR values. This may indicate that under stressed conditions, and in the presence of metformin, the cells enter a quiescent metabolic state with a slight upregulation of glycolysis. The shift from the aerobic phenotype to a slightly glycolytic phenotype observed among the Panc-1 cells supports the hypothesis that metformin inhibits complex I of the ETC thus hindering OXPHOS, which instigates the upregulation of glycolysis (45).

The metabolic potentials define the metabolic flexibility of the cells. In Figure 4. 4, the ECAR metabolic potentials are larger than the OCR potentials across both cell lines. The highest ECAR potentials are seen among the Panc-1 cells. Moreover, the control AsPC-1 cells observe larger metabolic potentials than the metformin treated. This indicates that the cells overall, especially the Panc-1 cells, prefer to increase the rate of glycolysis under stressed conditions compared to OXPHOS. Additionally, metformin decreases metabolic flexibility among AsPC-1 cells. Under stressed conditions such as hypoxia and high energy demand, glycolysis is upregulated to promote cell proliferation in PDAC (90). This explains why ECAR metabolic potentials are larger than OCR. Moreover, the metabolic phenotype of the Panc-1 cells exhibits a shift from OXPHOS to slightly glycolytic upon metformin treatment as described in section 4.2, which supports a higher ECAR metabolic potential compared to the AsPC-1 cells. The fact that the metabolic flexibilities of the AsPC-1 cells are negatively affected by metformin is supported by a study that revealed that metformin reduces metabolic flexibility by inhibiting OXPHOS and slowing glycolysis via mTOR inhibition (91). Metformin resistant cells remain metabolically flexible and able to switch fuel sources from OXPHOS to glycolysis upon

complex I inhibition (91). Perhaps the Panc-1 cells were metformin resistant and therefore, a metformin treatment did not hinder the metabolic flexibilities of the cells. However, as previously explained, the Panc-1 cells may lack the required OCT transporters to allow metformin into the cell and decrease metabolic flexibility.

5.3 A Pretreatment of Metformin Alters the Mitochondrial Metabolisms of both Panc-1 and AsPC-1 Cell Lines

5.3.1 Shift in OCR Values

To assess how a metformin pretreatment effects the rate of mitochondrial respiration, a Mito Stress Test was performed using the Seahorse XFp Analyzer for each cell line after both 2 weeks and 6 weeks of metformin treatment. In Figure 4. 5, the results show larger OCR values among the AsPC-1 cells that did not receive a metformin pretreatment (control), compared to those that did (experimental). Furthermore, the gap between the control and experimental group widens after 6 weeks of incubation in metformin due to a decrease in OCR values in the experimental group. The control group's OCR values, however, remain relatively the same from 2 weeks to 6 weeks of incubation. From these results it can be inferred that the mitochondrial respiration rates of the AsPC-1 cells are impacted by a pretreatment of 11.6 μM of metformin. This finding supports the overall hypothesis that metformin effects the metabolisms of PDAC cells by mitigating OXPHOS. It is speculated that metformin inhibits complex I or NADH dehydrogenase of the ETC, thereby hindering OXPHOS activity (45). Several studies show that metformin induces a decrease in oxygen consumption and ATP production by the mitochondria, which promotes glycolysis to compensate for the loss in energy production (45,92). Therefore, a pretreatment of metformin would initiate a decline in mitochondrial metabolism, OXPHOS, and an increase in aerobic glycolysis (63,92). However, instead of aerobic glycolysis upregulation, AsPC-1 enter a quiescent state upon metformin treatment. This is further supported by the stagnant OCR values in the control group at 2 weeks and 6 weeks of incubation. Because the control group did not receive a metformin pretreatment, the OCR values remain largely unaffected by the increase in incubation time.

The Panc-1 cells in Figure 4. 5 show contradicting results, where the OCR values of the control and experimental group overlap. At 2 weeks of incubation, the OCR values of the

experimental group are slightly smaller than the control group. At 6 weeks of incubation, that overlap is augmented. This finding does not correlate with the metabolic shift from OXPHOS to slightly glycolytic in response to metformin described in section 4.2. A possible explanation could be that the Panc-1 cells lack functional mitochondria. Tumor cells that lack functional mitochondria support lipid biosynthesis in the presence of metformin via glutamine-dependent reductive carboxylation and exhibit reduced sensitivity to metformin-induced proliferative decrease (87). If the Panc-1 cells have dysfunctional mitochondria, metformin will have little effect on their OCR values. This also provides evidence as to why metformin did not hinder the proliferation rates of the Panc-1 cells in section 4.1. However, another study revealed Panc-1 to be largely reliant on OXPHOS for ATP production (93). A MitoTracker staining procedure also revealed functional mitochondria (93). The study concluded that the lack of OCR decrease in relation to metformin was due to metformin's reliance on OCT transporters to enter the cell. Therefore, much higher concentrations of the drug are necessary to observe an effect. Perhaps, 11.6 μM of metformin was too low of a concentration to induce a result in Panc-1 cells, or there are not enough OCT transporters on the surface of Panc-1 cells to allow for metformin entry. The analysis of the mitochondrial parameters in the following sections will provide further clarity.

5.3.2 Change in Basal Respiration, Spare Respiratory Capacity, Proton Leak, and ATP Production Averages

When looking at the basal respiration averages of the cells in Figure 4. 6, it is evident that values of the cells that did not receive a metformin pretreatment (control) are larger, than those that did (experimental). The most prominent differences in basal respiration between the control and experimental group are seen among the AsPC-1 cells. At 6 weeks of incubation, the averages of the experimental group decreased from its average at 2 weeks of incubation. The basal respiration averages of the Panc-1 cells are larger than the AsPC-1 cells. Additionally, the difference in basal respiration rates between the control and experimental are minimal. These results indicate that metformin decreases the basal respirations of both AsPC-1 and Panc-1 cells, but metformin has a more prominent impact on AsPC-1 cells. Basal respiration is calculated by subtracting non-mitochondrial respiration from the last OCR value measured before the addition of modulators (72,74). Therefore, basal respiration is a measure of the initial rates of mitochondrial respiration and includes respiration used to drive ATP synthesis and proton leak

pathways (72). Because the basal respiration averages of the AsPC-1 control group are larger than the experimental, it can be deduced that a metformin pretreatment decreases the resting mitochondrial respiration rates used in relation to ATP synthesis by inhibiting complex I of the ETC (92). The inhibition of complex I leads to an overall decrease in NADH oxidation, proton pumping across the inner mitochondrial membrane, and oxygen consumption rate, resulting in a lower proton gradient and reduction in proton-driven ATP synthesis (94). Thus, AsPC-1's decrease in basal respiration in relation to metformin supports the hypothesis that metformin impacts PDAC metabolism by hindering OXPHOS (45). Among the Panc-1 cells, the nominal difference between the control and experimental group may be accredited to metformin's inability to traverse the cell membranes. As described previously, the Panc-1 cells show an OXPHOS phenotype at basal conditions, but the concentration of metformin used in this study may have been too low to inhibit complex I of the ETC. Moreover, if the Panc-1 cells are highly OXPHOS they are enriched in mitochondrial respiratory complex I at protein and mRNA levels, and thus, require more metformin to analyze a marked effect on OCR (47). Panc-1 cells may also lack enough OCT transporter to allow metformin into the cell.

In Figure 4. 6, the AsPC-1 control groups have larger spare respiratory capacities than the experimental groups. Furthermore, the spare respiratory capacities of the AsPC-1 cells treated with metformin show a further decrease from 2 weeks of treatment to 6 weeks. Additionally, the Panc-1 cells have spare respiratory values of 0 or values close to 0. The spare respiratory capacities of the cells are the calculated difference between the basal respiration and maximal respiration (72,74). Therefore, spare respiratory capacity measures the cell's ability to respond to an increased ATP demand and withstand metabolic stress beyond the basal level (95). The results indicate that a metformin pretreatment causes spare respiratory capacity to diminish, which lowers the cells' ability to respond to metabolic stress. Inadequate spare respiratory capacity values are correlated with mitochondrial dysfunction, which is exactly what is prompted by metformin's inhibition of complex I (95). This explains why AsPC-1 cells observe a decrease in spare respiratory capacity upon metformin treatment. Spare respiratory capacity depends on the integrity of the mitochondrial electron transport chain and of proton permeability of the inner mitochondrial membrane, which is hindered by metformin's inhibition of complex I (96). So far, it has been discussed that Panc-1 cells may exhibit a dysfunctional mitochondrion, which would account for their lack of spare respiratory capacity. However, the results in section 4.2, the Panc-

1 cells shift from OXPHOS to a slightly glycolytic phenotype in both the control and metformin-treated group. A minute spare respiratory capacity does not support this finding. Further investigations of the robustness of Panc-1 mitochondrion need to be conducted to assess whether they are functional or slightly dysfunctional, contributing to very small spare respiratory capacity values.

In Figure 4. 6, the AsPC-1 control groups have a higher average ATP production than the experimental groups. ATP production in the experimental group decreases further from 2 weeks to 6 weeks of treatment. On the contrary, the Panc-1 cells' ATP production averages are larger than that of AsPC-1, and differences between the experimental and control are minimal. ATP production is how much of the total mitochondrial respiration is attributed to ATP synthesis, which is determined by the injection of Oligomycin (72,74). Any OCR values that remain after the injection of Oligomycin are linked to proton leak, which occurs when OXPHOS is incompletely coupled to complex V (ATP synthase) (76). The protons leak back into the matrix of the mitochondria with the help of uncoupling proteins (UCPs) and oxygen consumption increases to produce energy in the form of heat, not ATP (97). Metformin inhibits complex I, which hinders the mitochondrial production of ATP, which is why the ATP production averages of the AsPC-1 experimental group are smaller than the control. This further supports the hypothesis that metformin hinders OXPHOS through the inhibition of complex I of the ETC (92). Metformin also instigates a quiescent state among AsPC-1 cells, which also contributes to the lower ATP production. The reason why the differences between Panc-1 control and experimental ATP production values are minimal could be due to Panc-1's lack of OCT transporters that allow metformin to enter the cells and initiate a response. A metformin treatment would have little effect on mitochondrial ATP production if too small a concentration was allowed into the cells. Moreover, because Panc-1 cells are phenotypically OXPHOS, they express more complex I protein, and would thus require more metformin to inhibit all the complexes (47). Additionally, because Panc-1 cells phenotypically OXPHOS, while AsPC-1 are slightly quiescent, the Panc-1 cells have larger ATP productions.

In Figure 4. 6, the Panc-1 proton leak OCR averages are also larger than that of AsPC-1, while the AsPC-1 cells show smaller proton leak values among the experimental group compared to the control. As discussed previously, proton leak is facilitated by UCP proteins. Recent literature suggests that cells may be turning off mitochondrial cellular respiration by

increasing the expression of UCP2, to mitigate the cytotoxic effects of ROS, thereby inducing the Warburg effect (78). Because increased proton leak prompted by increased UCP2 expression produces energy in the form of heat instead of ATP, the cells switch to glycolysis to compensate for the inefficient energy production. Additionally, another study confirmed that the proton leak pathway regulated ROS produced via the ETC (98). Because the Panc-1 cells are phenotypically OXPHOS, the cells engage in more proton leak pathways to regulate the ROS produced via the ETC. Moreover, the shift from OXPHOS to a slightly glycolytic phenotype upon metformin treatment would be in part caused by the upregulation of UCP2 and proton leak. The AsPC-1 cells have smaller proton leak averages because they are phenotypically quiescent and are therefore less metabolically active. Metformin induces a greater quiescent state among the AsPC-1 cells, which causes the further decrease in proton leak in the experimental group.

In Figure 4. 7, the AsPC-1 cells have larger coupling efficiencies than the Panc-1 cells. Additionally, the experimental groups have smaller coupling efficiencies compared to the control in AsPC-1 cells, but not Panc-1 cells. Coupling efficiency is the percentage of basal respiration that is coupled to ATP production (72). It therefore measures the efficiency of mitochondrial energy production. Because the coupling efficiencies of the AsPC-1 cells are larger than the Panc-1 cells, a larger percentage of basal respiration is attributed to ATP production among AsPC-1 cells. This is because the Panc-1 cells had a higher proton leak than the AsPC-1, and therefore, a larger portion of basal respiration among Panc-1 cells is attributed to proton leak compared ATP synthesis. The Panc-1 control group observed larger proton leak averages than the experimental group, and therefore observe smaller coupling efficiencies. Because, coupling efficiency of the experimental AsPC-1 group is smaller than the control group, it can be deduced that metformin targets complex I of the ETC to lower ATP production, thereby lowering the coupling efficiency.

5.4 A Pretreatment of Metformin Alters the Glycolytic Metabolisms of Both Panc-1 and AsPC-1 Pancreatic Cancer Cell Lines

5.4.1 Shift in ECAR Values

To assess the change in glycolytic function in response to a pretreatment of 11.6 μM metformin, a Glyco Stress Test was performed using a Seahorse XFp Analyzer for each cell line after 2

weeks and 6 weeks of a metformin pretreatment. In Figure 4. 8, the AsPC-1 control group has larger ECAR values than the experimental group. Furthermore, the Panc-1 cells in Figure 4. 8, also show that the experimental cells have smaller ECAR values at 2 weeks of incubation compared to the control. However, both the control and the experimental group experience a decrease in ECAR at 6 weeks of incubation. So far, it has been discussed that metformin inhibits complex I of the ETC, thereby promoting a shift of metabolism from OXPHOS to glycolysis (45,92). One study noted that an acute metformin treatment led to the decrease in OCR and increase in ECAR (87). However, whether the cells upregulate glycolysis upon metformin treatment depends on the metabolic flexibility of the cells (91). The AsPC-1 cells may lack the metabolic flexibility needed to switch to glycolysis thus, they enter a quiescent state to survive which promotes lower ECAR levels. Another study revealed that glucose concentration in cell growth media influences the metformin response (57). The cells in this study were cultured in low, fasting-level glucose concentrations. In the body, metformin reduces blood glucose levels by inhibiting gluconeogenesis and increasing the cellular uptake of glucose via GLUTs (99). The low amount of glucose in the media may not have been sufficient to support an increase in glycolysis rates among the cells treated in metformin. Therefore, the AsPC-1 and Panc-1 cells observed a decrease in ECAR. Finally, the decrease in Panc-1 ECAR levels of both the control and experimental group at 6 weeks of incubation could be attributed to experimental error. Because Panc-1 is characterized by a shift from OXPHOS to slightly glycolytic, metformin should increase ECAR (93). The Glyco Stress Test kit used contained old glucose, which may have been ineffective at increasing ECAR levels.

5.4.2 Change in Glycolysis, Glycolytic Capacity, and Glycolytic Reserve Averages

As seen in Figure 4. 9, the rate of glycolysis among the AsPC-1 cells shows a lower average among the experimental than the control group. Contrary to this, the glycolytic average of the Panc-1 cells between the control and experimental group both decrease to similar values at 6 weeks of incubation. The same patterns are observed for glycolytic capacity and glycolytic reserve. However, the AsPC-1 cells have slightly larger glycolytic capacities and reserves than the Panc-1 cells. The rate of glycolysis at basal conditions is determined by the injection of glucose. The spike in glucose causes an increase in glycolysis and a spike in the extrusion of lactate, and therefore, ECAR (77). Glycolytic capacity is determined by the injection of

Oligomycin, which shuts down mitochondrial respiration and shifts the entire energy production to glycolysis. The glycolytic reserve, or the cell's ability to handle metabolic stress by upregulating glycolysis, is determined by the injection of 2-DG, a glucose analog that inhibits glycolysis (77). The results denote that a metformin pretreatment negatively effects the rate of glycolysis, glycolytic capacity, and glycolytic reserve. It has already been discussed in section 5.4.1, that metformin may lower rate of glycolysis due to insufficient amount of glucose in the cell media. Moreover, the cells enter a quiescent state upon metformin treatment, which may be attributed to the lack of metabolic flexibility observed by AsPC-1 cells. The control AsPC-1 cells having slightly larger glycolytic capacities and reserves than the Panc-1 cells, which indicates that AsPC-1 cells respond better to metabolic stress by increasing the rate of glycolysis. This is supported by the control's shift from quiescence under basal conditions to an energetic phenotype under stressed conditions. An energetic phenotype is characterized by high amounts of OXPHOS and glycolysis. This also explains why the AsPC-1 control group in Figure 4. 10 has a higher glycolytic reserve percentages than the control group and the Panc-1 cells.

5.5 A Pretreatment of Metformin Combined with a 5-FU Chemotherapy Treatment Decreases the Size of AsPC-1 and Panc-1 Spheroids

To determine the effect a prolonged metformin treatment has on 5-FU efficacy, 3D spheroids were exposed to clinically relevant concentrations of 5-FU. In Figure 4. 11, the AsPC-1 spheroids that received a pretreatment of metformin, are smaller than the untreated spheroids. Moreover, the introduction of 5-FU did cause a slight decrease in spheroid diameter. However, the decrease is so slight that it may be considered negligible. Increasing concentrations of 5-FU did not mitigate spheroid growth. Therefore, it can be deduced that a metformin-5-FU treatment combination had little effect on the growth of AsPC-1 spheroids. The smaller spheroid sizes may be due to the metformin pretreatment alone. A possible reason why the AsPC-1 spheroids treated with metformin were smaller than those that were untreated is because metformin slows the proliferation rate of AsPC-1 cells by activating AMPK signaling as seen in Table 4. 1. A lot of variability exists in reported measured plasma concentration of 5-FU. Most studies have found the average steady state levels to range from 1-6 μg/mL or 0.3 to 60 μg/mL (100,101). Therefore, the clinically relevant concentrations of 5-FU chosen to inoculate the spheroids are 0.25, 8, and 26 μg/mL. However, perhaps these concentrations were too low to observe an effect

on spheroid diameter. Additionally, 5-FU is rarely used alone to treat pancreatic cancer. Instead, it is often paired in combination with folinic acid, irinotecan, and oxaliplatin (35). There is the possibility that 5-FU is largely ineffective at impacting spheroid growth when used alone. Its combination with other chemotherapies would need to be evaluated to support this claim. It has also been found that resistance to 5-FU among pancreatic cancer is growing in prevalence (102). Reasons for this include the upregulation of key enzymes in 5-FU metabolism (48,102). For example, PDAC patients with high levels of 5-FU catabolism enzymes, DPD and TS, were more resistant to 5-FU (48). Perhaps 5-FU resistance among PDAC cells is attributed to factors other than OXPHOS reliance. It has been theorized that a metformin-induced inhibition of OXPHOS may reverse chemoresistance. However, if 5-FU resistance has little to do OXPHOS reliance, a metformin-5-FU treatment combination would do little to impact spheroid size. It can be concluded therefore, that metformin does not sensitize the AsPC-1 cells to 5-FU treatment.

Much like the AsPC-1 cells, the Panc-1 spheroids in Figure 4. 12, experienced no change in growth in relation to increasing concentrations of 5-FU. However, unlike the AsPC-1 cells, the Panc-1 spheroids that have been treated with metformin for 2 weeks are larger than those not treated with metformin. Therefore, not only was metformin ineffective in its ability to alter Panc-1 OCR values, but the drug was also ineffective in decreasing the growth of spheroids, which can be attributed to metformin's inability to alter the proliferation rate of Panc-1 cells. Metformin also unsuccessfully decreased OCR values among Panc-1 cells. If metformin fails to inhibit OXPHOS, it cannot sensitize cells to chemotherapy treatments. Again, it can be concluded that metformin does not sensitize Panc-1 cells to 5-FU.

5.6 A Pretreatment of Metformin Combined with Various Chemotherapy Treatments Decreases the Volume of AsPC-1 and Panc-1 Spheroids over an 18-Day Period

5.6.1 Gemcitabine-Metformin Adjuvant Treatment

To further investigate the impact a chemotherapy-metformin treatment combination has on the growth of spheroids, other common chemotherapies were tested, Gemcitabine, Oxaliplatin, and SN-38. The spheroids were treated for a total of 18 days, where media was exchanged on day 4 of growth and every other day thereafter. A new round of treatment was introduced on day 14.

Spheroid growth was determined by measuring the volumes in μM^3. In Figure 4. 13, gemcitabine was tested against Panc-1 cells. In the absence of Gemcitabine, the spheroids that received a pretreatment of metformin are larger than those that did not, and therefore, the pretreatment of metformin did not impede the growth of the spheroids. Additionally, the addition of Gemcitabine did not decrease spheroid volume. Notably, an increase in gemcitabine concentration did not correlate with a decrease in spheroid volume. Similar results are seen among the AsPC-1 cells in Figure 4. 14. At 2 weeks of incubation, the AsPC-1 cells treated with metformin were on average smaller than those that were not treated. The addition of Gemcitabine did contribute to a decrease in size but increasing concentration of the drug had no effect. At 6 weeks of incubation, the addition of metformin and gemcitabine did not hinder spheroid growth. In general, a Gemcitabine-metformin treatment combination did not result in any pronounced decreased in spheroid volume compared to the controls. However, the treatment combination worked slightly better on the AsPC-1 cells. It can therefore be deduced that metformin does not sensitize cells to gemcitabine.

Mean gemcitabine peak plasma concentrations range from 24 μM at the lowest dose to 512 μM at the maximum dose, which is why it was decided to inoculate spheroids with 24, 100, and 500 μM of gemcitabine (85). However, other studies analyzing the impact of a gemcitabine treatment on the growth and viability of the same number of pancreatic cancer cells, have used significantly lower concentrations, 0.02 μM (103). Therefore, the concentrations used in this study were not too low to observe an effect, and the ineffectiveness of the Gemcitabine treatment are due to other factors. Gemcitabine is one of the first-line treatments for advanced pancreatic cancer disease, however it provides only marginal benefits to patients (104). Gemcitabine has therefore been used in combination with nab-paclitaxel to increase patient life expectancy(105). Gemcitabine may be ineffective at treating pancreatic cancer on its own due to well documented chemoresistance (40). If, however, the pancreatic cancer cells observed chemoresistance against Gemcitabine, a metformin pretreatment should have sensitized the cells as theorized. The inability of metformin to promote Gemcitabine effectiveness indicates chemoresistance may stem from factors not related to metabolism. One study found that Gemcitabine chemoresistance was mediated by IGF1R dependent upregulation of CD44 expression and isoform switching (49). If Gemcitabine resistance has little to do with metabolic phenotypes and flexibilities, a metformin pretreatment will do little to sensitize cells. Contrary to

this, another study demonstrated that targeting the mitochondria of PDAC cells with phenformin induced an energetic shift toward low OXPHOS, which enhanced the antitumoral effect of gemcitabine (93). However, they selected phenformin instead of metformin for their study because phenformin does not require OCT transporters to enter the cell and therefore, smaller concentrations of the drug yield a result (93). Perhaps the concentration of metformin used in this study was too low to observe a prominent effect. This is further supported by the lack of impact metformin treatment had on the OCR values of the Panc-1 cells in Figure 4. 5.

5.6.2 Oxaliplatin-Metformin Adjuvant Treatment

Unlike Gemcitabine, Oxaliplatin decreased spheroid volume in both Panc-1 and AsPC-1 cells. Additionally, increasing volumes of Oxaliplatin correlated with a further decrease in spheroid volume. In Figure 4. 15, the Panc-1 cells did not observe a marked difference in spheroid size between the cells that received and did not receive a metformin pretreatment. Similarly, in Figure 4. 16, the AsPC-1 spheroids that received a metformin pretreatment were slightly smaller than those that did not. Therefore, any impact Oxaliplatin had on the size of Panc-1 spheroids is due to Oxaliplatin's independent effectiveness at hindering spheroid growth. This may be due to the lack of OCT transporters on the surface of Panc-1 cells to allow for the transport of metformin into the cell as previously discussed. Oxaliplatin is one of the drugs used in FOLFIRINOX (35). Among folinic acid, 5-FU, irinotecan, perhaps Oxaliplatin is the most effective of the components in FOLFIRINOX, which may explain its success in decreasing the volume of spheroids. To confirm this, a study would have to test the effects of FOLFIRINOX compared to each individual component. Additionally, because Oxaliplatin is never used on its own to treat pancreatic cancer, the spheroids may have a higher sensitivity to the drug compared to a commonly used treatment like Gemcitabine. Nonetheless, metformin may have contributed to the sensitization of the AsPC-1 to the chemotherapy by inhibiting OXPHOS. One study confirmed that PDAC cells exhibit Oxaliplatin resistance (106). Therefore, perhaps metformin's effectiveness at lowering AsPC-1 OXPHOS activity, as supported by the decrease in OCR in Figure 4. 5, sensitizes the AsPC-1 spheroids to the Oxaliplatin treatment. Consequently, it can be concluded that metformin sensitizes AsPC-1 cells to Oxaliplatin, but not Panc-1 cells.

5.6.3 SN-38-Metformin Adjuvant Treatment

Like Oxaliplatin, the addition of SN-38, the metabolite to Irinotecan, also corresponded with a decrease in spheroid volume. In fact, SN-38 produced an even larger decrease in spheroid volume than Oxaliplatin did. Moreover, In Figure 4. 17, a metformin pretreatment in Panc-1 cells did not correlate with an additional decrease in spheroid size compared to those that did not receive a pretreatment. Oppositely, an AsPC-1 metformin pretreatment in Figure 4. 18 did correlate with smaller spheroid volumes. However, as described in section 5.5, that decrease may be due to metformin's impact on the proliferation rate of AsPC-1 cells. A smaller proliferation rate would result in smaller spheroid volumes. The metformin may have no effect on the performance or sensitivity of SN-38. On the other hand, metformin may sensitize AsPC-1 cells to the SN-38 by inhibiting OXPHOS. One study revealed that OXPHOS inhibition via phenformin treatment in non-small cell lung cancer did increase sensitivity to Irinotecan (47). This finding supports the theory that chemoresistance in cancer is partially due to the cells' ability to retain mitochondrial respiration. Because phenformin and metformin are both biguanide drugs that act on complex I of the ETC, the pretreatment of metformin may have sensitized the AsPC-1 cells to SN-38, allowing the chemotherapy to better mitigate spheroid growth. According to the National Cancer Institute, SN-38 is the biologically active metabolite of Irinotecan, a component of FOLFIRINOX. It is reported to exhibit up to 1000-fold more cytotoxic activity against various cancers than irinotecan (107). Perhaps SN-38's lethality is what accounts for its impressive impact on spheroid volume in Panc-1 spheroids, independent of metformin treatment. Again, it can be concluded that metformin sensitizes AsPC-1 cells to SN-38, but not Panc-1 cells. However, further molecular analysis needs to be performed to assess whether the metformin in AsPC-1 cells is what's creating the further decrease in spheroid size upon chemotherapy treatment.

5.7 An Analysis of Spheroid Viability after Chemotherapy Treatment

To assess spheroid viability on day 18 of chemotherapy treatment, the spheroids were stained with Prodiudium Iodide and Calcein AM the day before analysis. The number of live and dead cells based on the spheroid area in microns of PI and Calcein signal, reflects how necrotic the spheroid is and how effective the metformin-chemotherapy treatment combination was at decreasing spheroid size. Analyzing viability profiles of spheroids introduces another level of

complexity, the necrotic core (108). Typically, a spheroid has three zones associated with the availability of oxygen and nutrients: necrotic, hypoxic or quiescent, and proliferative (108). The lack of oxygen and nutrients accessing the spheroid cores leads to starvation induced cell death. Spheroid diameter is a critical parameter that affects the distribution of oxygen and nutrients. Thus, larger spheroids have larger necrotic cores and a greater percentage of dead cells (108). In Figure 4. 19, Figure 4. 20, and Figure 4. 21, each chemotherapy yielded different viability profiles. In Figure 4. 19, the metformin-Gemcitabine combination viability profiles appear to somewhat follow the spheroid size patterns observed in Figure 4. 14. For example, Figure 4.19A reveals that the spheroid treated with metformin and the highest Gemcitabine concentration of 500 μM (well 10) had the highest live cells to dead cells ratio, while the spheroid that received no metformin pretreatment and the highest Gemcitabine concentration (well 6) had the lowest live cells to dead cells ratio. The spheroid in well 10 was among the smallest, which may have attributed to a smaller necrotic core and a larger ratio of live cells to dead cells. However, the spheroid in well 6 was not among the largest and therefore should not observe the lowest live cell to dead cell ratio. Consequently, the size of a necrotic core can be attributed to factors other than spheroid size. For example, the high concentration of Gemcitabine may have killed some of the cells in the spheroid leading to a smaller percentage of live cells to dead cells. Additionally, a study discussed how metabolic stress induced by the lack of oxygen and nutrients triggers tumor necrosis (109). Metformin induces metabolic stress which may also contribute to a larger necrosis. It is therefore imperative to recognize the impact treatments have on viability along with the size of the spheroids. In section 5.6.1, it was noted that a metformin-Gemcitabine combination had little effect on the size of the spheroids, which may explain why no clear viability pattern is observed among the AsPC-1 or Panc-1 spheroids.

Unlike Gemcitabine, SN-38 and Oxaliplatin both contributed to a decrease in spheroid size as discussed in sections 5.6.2 and 5.6.3. Additionally, an increase in chemotherapy concentration further enhanced spheroid volume mitigation. Therefore, discounting the influence the treatments may have on necrosis, the spheroids that were pretreated in metformin and received the highest concentration of SN-38 and Oxaliplatin should have the highest live cells to dead cells ratio. However, the SN-38 and Oxaliplatin chemotherapies had smaller viability profiles than the gemcitabine treated spheroids. For example, in Figure 4. 20, the AsPC-1 spheroid that received no metformin pretreatment for 2 weeks and 5 ng/mL of SN-38 (well 6)

had the lowest ratio. The low viability profile may be due to SN-38's lethality, where the highest dose of SN-38 would kill many cells and thus contribute to a larger area of dead spheroid. Furthermore, at 6 weeks of incubation, the AsPC-1 spheroid that received a metformin pretreatment and 5 ng/mL of SN-38 (well 10) had the lowest ratio. This may be due to metformin's ability to metabolically stress AsPC-1 cells and contribute to their larger necrosis. In support of this claim, one study found that metformin's ability to induce cells cycle arrest, increases cell apoptosis and cell necrosis in MCF-7 breast cancer cells (110). Therefore, the size of the spheroid, metformin and chemotherapy all contribute to the size of necrosis, which accounts for the unclear patterns observed among the AsPC-1 and Panc-1 cells of the gemcitabine, SN-38, and Oxaliplatin treated spheroids.

5.8 Amplification Efficiencies of SYBR Green Primers

Amplification efficiency is defined as the fraction of target molecules, in the case of this project, cDNA samples, that are copied by a given primer in one PCR cycle (111). Therefore, a properly designed assay in the absence of contaminating material in the sample matrix should amplify the target with at least 90-110% efficiency (111). Amplification efficiencies of each primer was performed to determine the performance of the qPCR assay at varying dilutions of cDNA. The results in Table 4. 2, reveal that all target genes except for UPCP2, SLC22A1, ATP5F1A, and HK2 genes have amplification efficiencies that fall within the acceptable range. The poor amplification efficiencies are all above 100%. There are several reasons explaining why the amplification efficiencies exceed the appropriate range. The first may be poor primer design (111). Secondary structures and hairpin structures that manifest among the primers may lead to unwanted intramolecular interactions (111). During primer design, the existence of secondary structures among the primers may have been neglected. Another reason may have been the existence of inhibitor compounds or interfering substances in the sample matrix that contributed to poor amplification. For example, during sample preparation, contaminating DNA may have entered the cDNA samples. A third reason could be a result of suboptimal concentrations of qPCR reagents used (111). During assay design, it is vital to ensure assay components are used at an optimal concentration such as the amount and concertation of SYBR green, primers and cDNA sample. Because this project was restricted to a timeline, appropriate optimization procedures were not carried out. The final reason for poor amplification efficiency is competing

reactions, or more specifically, inhibition reactions which is the most likely cause of the high amplification efficiencies calculated for several genes in this study. Inhibiting agents may have been reagents used during RNA extraction or cDNA synthesis, or copurified components from the DNA sample such as bile salts, urea, or haeme (112). Inhibition is most often the cause of unrealistically high PCR efficiencies and is the most pronounced in the most concentrated cDNA sample (112). Because the amplification efficiencies of the genes, UPCP2, SLC22A1, ATP5F1A, and HK2 are abnormally high, analysis of relative gene expression changes for these genes may be inaccurate. Further qPCR assay quality assessments should be carried out to verify the reason for poor amplification efficiencies.

5.9 An Analysis of Relative Gene Expression Changes in Relation to Metformin Pretreatment

Relative gene expressions (RGE) of common metabolic genes associated with mitochondrial respiration and glycolysis were determined by performing a SYBR Green primer assay. The RGEs were calculated using the Livak *et al.* method. For the AsPC-1 cells in Table 4. 3, the cells that were not treated with metformin (control) have larger RGE values than the treated cells. The only exception is SLC22A1, where the RGE is approximately 0 for both groups. Additionally, the metformin treated cells have RGE values that are approximately 0.8 units smaller than the non-treated group. Finally, the genes with the highest expression among the no metformin cells are HK2 and ATP5F1A, while the genes with the highest expression among the metformin treated cells are LDHA and PFKM. Therefore, it can be deduced that a metformin pretreatment in AsPC-1 cells leads to the downregulation of UPCP2, LDHA, SUCLA2, SLC16A1, PFKM, NDUFS1, ATP5F1A, and HK2. In section 5.1, it was noted that metformin contributes to a decrease in proliferation among AsPC-1 cells, and in section 5.2, it was concluded that a metformin pretreatment led to the instigation of a quiescent state, while the cells that were not treated, exhibited an energetic phenotype under stressed conditions. This explains why metformin pretreated cells exhibit a downregulation in metabolic gene expression, while the RGEs of the control group are higher. If metformin successfully enters AsPC-1 cells via the OCT transporters and inhibits complex I of the ETC, NDUFS1 expression of complex I would plumet as a result. Additionally, the instigation of a quiescent state corresponds with decreased metabolism, and therefore a downregulation of metabolic associated genes, including both

glycolysis and mitochondrial respiration. This explains why the AsPC-1 metformin-treated cells experience a downregulation of metabolic associated genes. Moreover, the fact that the control AsPC-1 cells were metabolically energetic under stressed conditions (high levels of glycolysis and OXPHOS) explains why the RGEs of all metabolic genes are relatively the same. The slightly higher expression of LDHA and PFKM, or Lactate Dehydrogenase A and Phosphofructokinase, among the metformin-treated cells indicates that glycolysis is still moderately higher than OXPHOS even in a quiescent state, which reflects metformin's ability to inhibit OXPHOS (13,47). SLC22A1 expresses the protein OCT1, which is necessary for the transport of metformin into the cell. It, therefore, does not make sense that RGE levels are 0 considering AsPC-1 cells are impacted by metformin pretreatments. The specific gene tested in this study, SLC22A1, is mainly expressed in the liver not the pancreas, perhaps accounting for its low expression levels (113). Additionally, one study found that SLC22A1 was downregulated in pancreatic cancer compared to non-neoplastic pancreatic tissues (114). This supporting evidence may explain why SCL22A1 is downregulated in both treated and control AsPC-1 cells. The AsPC-1 RGE results are based on cells that were incubated in metformin for a total of 6 weeks. There are no 2-week incubation results since cDNA concentrations were too poor to work with. To further support the claims made so far, a comparison between the RGEs of AsPC-1 treated with metformin for 2 weeks and 6 weeks should be made.

In Table 4. 3, the Panc-1 cells appear to exhibit the total opposite effect of the AsPC-1 cells. Instead of the control group, the metformin treated cells display higher RGE values at both 2 weeks and 6 weeks of incubation. The genes that were upregulated the most after 2 weeks of treatment were HK2 and NDUFS1. However, the expression of UPCP2 and LDHA did not change between the control and treated group. Additionally, the expression of SLC22A1 and SLC16A1 (MCT1) were both downregulated in the treated group. At 6 weeks of incubation, SLC22A1 expression increased in the treated group, and decreased in the control group. Moreover, UPCP2 and ATP5F1A have lower RGEs in the metformin treated group compared to the control group, and NDUFS1 was downregulated at 6 weeks of treatment compared to 2 weeks. In section 5.1, the proliferation rate of the Panc-1 cells is not slowed by a pretreatment with metformin. Furthermore, the metabolic phenotype is OXPHOS at baseline conditions, but metformin contributed to no marked decrease in OCR or increase in ECAR (sections 5.3.1 and 5.4.1). Panc-1 spheroid size was also generally unaffected by a metformin

pretreatment. It has thus far been theorized that Panc-1 cells may have a low number of OCT transporters in their membrane and therefore, the metformin concentration used in this study was too low to exert influence on proliferation and metabolism. Metformin would, therefore, have little effect on the expression of metabolic genes. Whether the treated group has higher RGEs than the non-treated group has little to do with metformin. The speculation that Panc-1 cells have few OCT transporters is supported by the expression of SLC22A1 at 2 weeks of incubation, which is extremely low among the treated cells and extremely high in the non-treated group. The abnormally high RGE value in the non-treated group is attributed to the high Cq values generated from the qPCR assay. Therefore, both groups express SLC22A1 at a minute level. However, at 6 weeks, the expression is upregulated in the treated group. A study found that OCT1 is important for metformin therapeutic action and that any genetic variation in OCT1 may contribute to variation in drug response (114). Because OCT1 is so crucial to metformin transport, perhaps prolonged exposure to metformin induces an increase in SLC22A1 expression. To support this postulation, further studies investigating how metformin effects SLC22A1 expression would need to be conducted. Additionally, the downregulation of ATP5F1A and NDUFS1 at 6 weeks of metformin incubation compared to 2 weeks, may indicate that metformin has a slight ability to inhibit complex I and slow OXPHOS.

Chapter 6 Conclusion and Future Perspectives

6.1 Conclusion

Pancreatic cancer is a lethal malady that is virtually incurable due to the prevalence of chemoresistance. It has been found that mitochondrial respiration may have a major role in PDAC chemoresistance. It has therefore been theorized that OXPHOS inhibition may mitigate or reverse PDAC chemoresistance. Metformin has been found to inhibit complex I of the ETC, and therefore, hinders the cell's OXPHOS capabilities. Thus, metformin may be used as an adjuvant treatment in addition to chemotherapies traditionally used to treat PDAC. This study implemented clinically relevant concentrations and exposure times of metformin to test the hypothesis that metformin may reverse or mitigate chemoresistance by inhibiting OXPHPOS. The overall aim was to assess how metformin affects the metabolic profiles of treated PDAC cell lines, and to analyze how a combination of metformin and various chemotherapies impact the growth of PDAC cells grown in 3D. Several objectives were performed to support the aim and the following conclusions were drawn. Overall, the impact of metformin on PDAC cells depends strongly on the cell line tested. For example, a preincubation of 11.6 μM of metformin reduces the proliferation rates of AsPC-1, but not Panc-1 cells. However, the molecular mechanism that drives the metformin induced proliferation rate decrease among AsPC-1 cells remains inconclusive. It may be attributed to metformin's ability to activate AMPK and inhibit mTOR signaling, or its ability to inhibit complex I of the ETC. Furthermore, metformin's inability to slow Panc-1 proliferation may be attributed to the lack of OCT transporters on the cells' surfaces. Additionally, it was found that a preincubation of 11.6 μM of metformin reduces OXPHOS and glycolysis among AsPC-1 cells, but not Panc-1 cells. The decrease in mitochondrial respiration parameters among AsPC-1 cells may be attributed to metformin's ability to inhibit complex I of the ETC and therefore hinder OXPHOS. The decrease in glycolytic parameters among the AsPC-1 cells may be accredited to metformin's ability to instigate entry into a quiescent state. Again, metformin's inability to alter the metabolisms of the Panc-1 cells may be due to their lack of OCT transporters. To conclude, metformin alters the cellular energetics of certain cell lines, but not others. It was also found that metformin may sensitize AsPC-1 cells to Oxaliplatin and SN-38, but not 5-FU or Gemcitabine. Metformin does not sensitize Panc-1 to any of the chemotherapies. It can therefore be concluded that metformin

only sensitizes certain cell lines to chemotherapy perhaps based on their metabolic profiles and availability of OCT transporters, and not all chemotherapies benefit from an adjuvant treatment with metformin. It was also ascertained that spheroid size and treatment combinations influence the level of necrosis among both AsPC-1 and Panc-1 spheroids. Finally, it was discovered that metformin causes a downregulation of glycolytic and OXPHOS associated genes among AsPC-1 cells. Because metformin induces a quiescent state among AsPC-1 cells, a downregulation of metabolic genes retains consistency. Contrarily, metformin upregulates most metabolic genes among Panc-1 cells in no particular pattern. Because metabolic genes are influenced by a metformin pretreatment, they may be used as biomarkers to assess the effectiveness of a metformin-chemotherapy adjuvant treatment in clinical settings. In conclusion, metformin's effect on AsPC-1 supports the hypothesis that the drug may mitigate chemoresistance based on its ability to inhibit complex I of the ETC and hinder OXPHOS. However, because it was concluded that metformin is effective at altering the metabolisms of certain homogenous cell lines but not others, its effectiveness in treating PDAC among heterogenous tumors in vivo remain inconclusive.

6.2 Future Perspectives

As discussed previously, this study found that metformin affected the proliferation rates and metabolic profiles of AsPC-1 cells, but not Panc-1 cells. It was theorized that metformin's lack of effectiveness against Panc-1 was attributed to the lack of OCT transporters among the Panc-1 cells. The cell line would, therefore, require a higher concentration of metformin to observe an effect. To support this theory, it might be crucial to investigate how differing pretreatment concentrations of metformin impact the outcome of the various experiments. The pretreatment concentration used in this study, 11.6 μM, is in between the mean maximum plasma concentration range in vivo (82). To test whether higher concentrations of metformin are more effective against Panc-1, future studies could pretreat the cell lines in metformin concentrations of 11.6 μM, 20 μM, and 30 μM. However, higher concentrations fail to replicate in vivo conditions, and thus any effectiveness observed in vitro may not translate in vivo. Because PDAC tumors are heterogenous, it is important to test as many cell lines as possible under the objectives followed in this study. Testing two homogenous cell lines is not enough to successfully predict the outcome metformin would have in vivo. Future studies should therefore,

test other cell lines such as Capan-2, CFPAC-1, HPAF-II, SW 1990, and BxPC-3. Furthermore, other studies have found phenformin to be more effective at sensitizing Panc-1 cells to gemcitabine treatment due to its ability to freely traverse the cell membrane without the need for OCT transporters (93). It would therefore be interesting to analyze how a pretreatment with phenformin compares to a pretreatment with metformin in relation to its ability to inhibit OXPHOS. Future studies can incubate the PDAC cell lines in both metformin and phenformin before performing the experimental objectives executed in this study. Perhaps phenformin would have better outcomes in vitro and therefore, in vivo. Additionally, the cell lines in this study were only pretreated in metformin for a total of 6 weeks. In clinical cases, metformin is taken long-term (for years), it may therefore be worthwhile to test whether experimental outcomes change with longer metformin pretreatments. For example, future studies can test the effect of metformin on the cell lines throughout the course of a 6-month long pretreatment. Perhaps a longer pretreatment would correlate to better experimental outcomes, and a better representation of clinical outcomes. Lastly, it was discussed that chemoresistance in PDAC is complex and multifactorial (48). The impact of a metformin-chemotherapy adjuvant treatment, therefore, strongly depends on the root cause of chemoresistance. It is therefore crucial for future studies to investigate the primary molecular cause for PDAC resistance against common chemotherapies perhaps by performing a molecular analysis. This will elucidate which chemotherapies will work well in combination with metformin.

Chapter 7 References

1. Micheal J. Thun et al. The global burden of cancer: priorities for prevention. Carcinogenesis. 2009 Nov 24;31(1):100–10.

2. Li-Hui Wang, Chun-Fu Wu et al. Loss of Tumor Suppressor Gene Function in Human Cancer: An Overview. Cellular Physiology and Biochemistry. 2018 Dec 12;51:2647–93.

3. Ian A. Cree. Cancer Biology. Methods in Molecular Biology. 2011 Jan 1;731.

4. Amy Y. Chow. Cell Cycle Control by Oncogenes and Tumor Suppressors: Driving the Transformation of Normal Cells into Cancerous Cells. Nature Education. 2010;3(4).

5. Park JH, Pyun WY, Park HW. Cancer Metabolism: Phenotype, Signaling and Therapeutic Targets. Vol. 9, Cells. NLM (Medline); 2020.

6. Hanahan D. Hallmarks of Cancer: New Dimensions. Vol. 12, Cancer Discovery. American Association for Cancer Research Inc.; 2022. p. 31–46.

7. Hanahan D, Weinberg RA. Hallmarks of cancer: The next generation. Vol. 144, Cell. 2011. p. 646–74.

8. Kalyanaraman B. Teaching the basics of cancer metabolism: Developing antitumor strategies by exploiting the differences between normal and cancer cell metabolism. Vol. 12, Redox Biology. Elsevier B.V.; 2017. p. 833–42.

9. Ramsay EE, Hogg PJ, Dilda PJ. Mitochondrial metabolism inhibitors for cancer therapy. Vol. 28, Pharmaceutical Research. 2011. p. 2731–44.

10. Ahmad M, Wolberg A, Chadi, Kahwaji I. Biochemistry, Electron Transport Chain. 2022.

11. Akram M. Mini-review on glycolysis and cancer. Vol. 28, Journal of Cancer Education. 2013. p. 454–7.

12. Chaudhry R, Varacallo M. Biochemistry, Glycolysis. 2022.

13. Yan L, Raj P, Yao W, Ying H. Glucose Metabolism in Pancreatic Cancer. Cancers (Basel). 2019 Sep 29;11(10):1460.

14. Martínez-Reyes I, Chandel NS. Mitochondrial TCA cycle metabolites control physiology and disease. Vol. 11, Nature Communications. Nature Research; 2020.

15. Bandara AB, Drake JC, Brown DA. Complex II subunit SDHD is critical for cell growth and metabolism, which can be partially restored with a synthetic ubiquinone analog. BMC Mol Cell Biol. 2021 Dec 12;22(1):35.

16. Ristow M. Oxidative metabolism in cancer growth. Vol. 9, Current Opinion in Clinical Nutrition and Metabolic Care. 2006. p. 339–45.

17. Heiden MGV, Cantley LC, Thompson CB. Understanding the warburg effect: The metabolic requirements of cell proliferation. Vol. 324, Science. 2009. p. 1029–33.

18. Hoxhaj G, Manning BD. The PI3K–AKT network at the interface of oncogenic signalling and cancer metabolism. Vol. 20, Nature Reviews Cancer. Nature Research; 2020. p. 74–88.

19. Madden MZ, Rathmell JC. The complex integration of t-cell metabolism and immunotherapy. Vol. 11, Cancer Discovery. American Association for Cancer Research Inc.; 2021. p. 1636–43.

20. Martínez-Reyes I, Chandel NS. Cancer metabolism: looking forward. Nat Rev Cancer. 2021 Oct 16;21(10):669–80.

21. Yu L, Chen X, Sun X, Wang L, Chen S. The Glycolytic Switch in Tumors: How Many Players Are Involved? J Cancer. 2017;8(17):3430–40.

22. Ancey P, Contat C, Meylan E. Glucose transporters in cancer – from tumor cells to the tumor microenvironment. FEBS J. 2018 Aug 25;285(16):2926–43.

23. Eniafe J, Jiang S. The functional roles of TCA cycle metabolites in cancer. Oncogene. 2021 May 13;40(19):3351–63.

24. Nguyen TL, Durán R v. Glutamine metabolism in cancer therapy. Vol. 1, Cancer Drug Resistance. OAE Publishing Inc.; 2018. p. 126–38.

25. Zong WX, Rabinowitz JD, White E. Mitochondria and Cancer. Vol. 61, Molecular Cell. Cell Press; 2016. p. 667–76.

26. Anderson NM, Simon MC. The tumor microenvironment. Current Biology. 2020 Aug;30(16):R921–5.

27. Pavlova NN, Thompson CB. The Emerging Hallmarks of Cancer Metabolism. Vol. 23, Cell Metabolism. Cell Press; 2016. p. 27–47.

28. Florey O, Overholtzer M. Macropinocytosis and autophagy crosstalk in nutrient scavenging. Philosophical Transactions of the Royal Society B: Biological Sciences. 2019 Feb 4;374(1765):20180154.

29. Weinberg F, Hamanaka R, Wheaton WW, Weinberg S, Joseph J, Lopez M, et al. Mitochondrial metabolism and ROS generation are essential for Kras-mediated tumorigenicity. Proc Natl Acad Sci U S A. 2010 May 11;107(19):8788–93.

30. Sica V, Manuel J, Pedro BS, Stoll G, Kroemer G. Oxidative phosphorylation as a potential therapeutic targ for cancer therapy.

31. Mizrahi JD, Surana R, Valle JW, Shroff RT. Pancreatic cancer [Internet]. Vol. 395, www.thelancet.com. 2008. Available from: www.thelancet.com

32. Lonardo E, Cioffi M, Sancho P, Sanchez-Ripoll Y, Trabulo SM, Dorado J, et al. Metformin Targets the Metabolic Achilles Heel of Human Pancreatic Cancer Stem Cells. PLoS One. 2013 Oct 18;8(10):e76518.

33. Zeng S, Pöttler M, Lan B, Grützmann R, Pilarsky C, Yang H. Chemoresistance in pancreatic cancer. Vol. 20, International Journal of Molecular Sciences. MDPI AG; 2019.

34. Hu H feng, Ye Z, Qin Y, Xu X wu, Yu X jun, Zhuo Q feng, et al. Mutations in key driver genes of pancreatic cancer: molecularly targeted therapies and other clinical implications. Acta Pharmacol Sin. 2021 Nov 11;42(11):1725–41.

35. Hidalgo M, Cascinu S, Kleeff J, Labianca R, Löhr JM, Neoptolemos J, et al. Addressing the challenges of pancreatic cancer: Future directions for improving outcomes. Vol. 15, Pancreatology. Elsevier B.V.; 2015. p. 8–18.

36. Grant TJ, Hua K, Singh A. Molecular Pathogenesis of Pancreatic Cancer. In: Progress in Molecular Biology and Translational Science. Elsevier B.V.; 2016. p. 241–75.

37. Ware MJ, Keshishian V, Law JJ, Ho JC, Favela CA, Rees P, et al. Generation of an in vitro 3D PDAC stroma rich spheroid model. Biomaterials. 2016 Nov;108:129–42.

38. Li JT, Wang YP, Yin M, Lei QY. Metabolism remodeling in pancreatic ductal adenocarcinoma. Cell Stress. 2019 Dec 9;3(12):361–8.

39. Ho WJ, Jaffee EM, Zheng L. The tumour microenvironment in pancreatic cancer — clinical challenges and opportunities. Nat Rev Clin Oncol. 2020 Sep 12;17(9):527–40.

40. Qin C, Yang G, Yang J, Ren B, Wang H, Chen G, et al. Metabolism of pancreatic cancer: paving the way to better anticancer strategies. Mol Cancer. 2020 Dec 2;19(1):50.

41. Camelo F, Le A. The Intricate Metabolism of Pancreatic Cancers. In 2021. p. 77–88.

42. Vaziri-Gohar A, Zarei M, Brody JR, Winter JM. Metabolic Dependencies in Pancreatic Cancer. Front Oncol. 2018 Dec 12;8.

43. Son J, Lyssiotis CA, Ying H, Wang X, Hua S, Ligorio M, et al. Glutamine supports pancreatic cancer growth through a KRAS-regulated metabolic pathway. Nature. 2013 Apr 4;496(7443):101–5.

44. Bott AJ, Shen J, Tonelli C, Zhan L, Sivaram N, Jiang YP, et al. Glutamine Anabolism Plays a Critical Role in Pancreatic Cancer by Coupling Carbon and Nitrogen Metabolism. Cell Rep. 2019 Oct;29(5):1287-1298.e6.

45. Reyes-Castellanos G, Masoud R, Carrier A. Mitochondrial Metabolism in PDAC: From Better Knowledge to New Targeting Strategies. Biomedicines. 2020 Aug 3;8(8):270.

46. Valle S, Alcalá S, Martin-Hijano L, Cabezas-Sáinz P, Navarro D, Muñoz ER, et al. Exploiting oxidative phosphorylation to promote the stem and immunoevasive properties of pancreatic cancer stem cells. Nat Commun. 2020 Oct 16;11(1):5265.

47. Lee S, Lee JS, Seo J, Lee SH, Kang JH, Song J, et al. Targeting Mitochondrial Oxidative Phosphorylation Abrogated Irinotecan Resistance in NSCLC. Sci Rep. 2018 Oct 24;8(1):15707.

48. Grasso C, Jansen G, Giovannetti E. Drug resistance in pancreatic cancer: Impact of altered energy metabolism. Crit Rev Oncol Hematol. 2017 Jun;114:139–52.

49. Chen C, Zhao S, Zhao X, Cao L, Karnad A, Kumar AP, et al. Gemcitabine resistance of pancreatic cancer cells is mediated by IGF1R dependent upregulation of CD44 expression and isoform switching. Cell Death Dis. 2022 Aug 5;13(8):682.

50. Erkan M, Kleeff J, Esposito I, Giese T, Ketterer K, Büchler MW, et al. Loss of BNIP3 expression is a late event in pancreatic cancer contributing to chemoresistance and worsened prognosis. Oncogene. 2005 Jun 23;24(27):4421–32.

51. Zhao Z, Mei Y, Wang Z, He W. The Effect of Oxidative Phosphorylation on Cancer Drug Resistance. Cancers (Basel). 2022 Dec 22;15(1):62.

52. Subramaniam D, Kaushik G, Dandawate P, Anant S. Targeting Cancer Stem Cells for Chemoprevention of Pancreatic Cancer. Curr Med Chem. 2018 Jul 4;25(22):2585–94.

53. Mitchison TJ. The proliferation rate paradox in antimitotic chemotherapy. Mol Biol Cell. 2012 Jan;23(1):1–6.

54. Hu J, Fan HD, Gong JP, Mao QS. The relationship between the use of metformin and the risk of pancreatic cancer in patients with diabetes: a systematic review and meta-analysis. BMC Gastroenterol. 2023 Feb 24;23(1):50.

55. Li X, Li T, Liu Z, Gou S, Wang C. The effect of metformin on survival of patients with pancreatic cancer: a meta-analysis. Sci Rep. 2017 Jul 19;7(1):5825.

56. Gyawali M, Venkatesan N, Ogeyingbo OD, Bhandari R, Botleroo RA, Kareem R, et al. Magic of a Common Sugar Pill in Cancer: Can Metformin Raise Survival in Pancreatic Cancer Patients? Cureus. 2021 Aug 5;

57. Alhourani AH, Tidwell TR, Bokil AA, Røsland G V., Tronstad KJ, Søreide K, et al. Metformin treatment response is dependent on glucose growth conditions and metabolic phenotype in colorectal cancer cells. Sci Rep. 2021 May 18;11(1):10487.

58. Sutkowska E, Fortuna P, Wisniewski J, Sutkowska K, Hodurek P, Gamian A, et al. Low metformin dose and its therapeutic serum concentration in prediabetes. Sci Rep. 2021 Jun 3;11(1):11684.

59. Nasri H, Rafieian-Kopaei M. Metformin: Current knowledge. J Res Med Sci. 2014 Jul;19(7):658–64.

60. Wang LW, Li ZS, Zou DW, Jin ZD, Gao J, Xu GM. Metformin induces apoptosis of pancreatic cancer cells. World J Gastroenterol. 2008;14(47):7192.

61. H.-W. Zhao, N. Zhou, F. Jin RW. Metformin reduces pancreatic cancer cell proliferation and increases apoptosis through MTOR signaling pathway and its dose-effect relationship. Eur Rev Med Pharmacol Sci. 2020;24(10):5336–44.

62. Rozengurt E, Sinnett-Smith J, Kisfalvi K. Crosstalk between Insulin/Insulin-like Growth Factor-1 Receptors and G Protein-Coupled Receptor Signaling Systems: A Novel Target for the Antidiabetic Drug Metformin in Pancreatic Cancer. Clinical Cancer Research. 2010 May 1;16(9):2505–11.

63. Sancho P, Burgos-Ramos E, Tavera A, Bou Kheir T, Jagust P, Schoenhals M, et al. MYC/PGC-1α Balance Determines the Metabolic Phenotype and Plasticity of Pancreatic Cancer Stem Cells. Cell Metab. 2015 Oct;22(4):590–605.

64. Zhang HH, Guo XL. Combinational strategies of metformin and chemotherapy in cancers. Cancer Chemother Pharmacol. 2016 Jul 27;78(1):13–26.

65. Hirsch HA, Iliopoulos D, Tsichlis PN, Struhl K. Metformin Selectively Targets Cancer Stem Cells, and Acts Together with Chemotherapy to Block Tumor Growth and Prolong Remission. Cancer Res. 2009 Oct 1;69(19):7507–11.

66. Edmondson R, Broglie JJ, Adcock AF, Yang L. Three-Dimensional Cell Culture Systems and Their Applications in Drug Discovery and Cell-Based Biosensors. Assay Drug Dev Technol. 2014 May;12(4):207–18.

67. Kapałczyńska M, Kolenda T, Przybyła W, Zajączkowska M, Teresiak A, Filas V, et al. 2D and 3D cell cultures – a comparison of different types of cancer cell cultures. Archives of Medical Science. 2016;

68. Howes AL, Richardson RD, Finlay D, Vuori K. 3-Dimensional culture systems for anti-cancer compound profiling and high-Throughput screening reveal increases in EGFR inhibitor-mediated Cytotoxicity compared to monolayer culture systems. PLoS One. 2014 Sep 23;9(9).

69. Wen Z, Liao Q, Hu Y, You L, Zhou L, Zhao Y. A spheroid-based 3-D culture model for pancreatic cancer drug testing, using the acid phosphatase assay. Brazilian Journal of Medical and Biological Research. 2013 Jul;46(7):634–42.

70. Nunes AS, Barros AS, Costa EC, Moreira AF, Correia IJ. 3D tumor spheroids as in vitro models to mimic in vivo human solid tumors resistance to therapeutic drugs. Biotechnol Bioeng. 2019 Jan;116(1):206–26.

71. Bell EL, Chandel NS. Genetics of Mitochondrial Electron Transport Chain in Regulating Oxygen Sensing. 2007;447–61.

72. Divakaruni AS, Paradyse A, Ferrick DA, Murphy AN, Jastroch M. Analysis and Interpretation of Microplate-Based Oxygen Consumption and pH Data. In 2014. p. 309–54.

73. TeSlaa T, Teitell MA. Techniques to Monitor Glycolysis. In 2014. p. 91–114.

74. Technologies A. Agilent Technologies Agilent Seahorse XFp Cell Mito Stress Test Kit User Guide Kit 103010-100.

75. Underwood E, Redell JB, Zhao J, Moore AN, Dash PK. A method for assessing tissue respiration in anatomically defined brain regions. Sci Rep. 2020 Aug 6;10(1):13179.

76. Jastroch M, Divakaruni AS, Mookerjee S, Treberg JR, Brand MD. Mitochondrial proton and electron leaks. Essays Biochem. 2010 Jun 14;47:53–67.

77. Guide U. Agilent Technologies Agilent Seahorse XFp Glycolysis Stress Test Kit.

78. Vallejo FA, Vanni S, Graham RM. UCP2 as a Potential Biomarker for Adjunctive Metabolic Therapies in Tumor Management. Front Oncol. 2021 Mar 8;11.

79. ATCC. PANC-1 [Internet]. [cited 2022 Sep 27]. Available from: https://www.atcc.org/products/crl-1469

80. ATCC. AsPC-1 [Internet]. [cited 2022 Sep 27]. Available from: https://www.atcc.org/products/crl-1682

81. WHO. Mean fasting blood glucose [Internet]. World Health Organization; 2023 [cited 2023 Apr 16]. Available from: https://www.who.int/data/gho/indicator-metadata-registry/imr-details/2380

82. Li L, Guan Z, Li R, Zhao W, Hao G, Yan Y, et al. Population pharmacokinetics and dosing optimization of metformin in Chinese patients with type 2 diabetes mellitus. Medicine. 2020 Nov 13;99(46):e23212.

83. Terret C. Dose and time dependencies of 5-fluorouracil pharmacokinetics. Clin Pharmacol Ther. 2000 Sep;68(3):270–9.

84. Hahn RZ, Arnhold PC, Andriguetti NB, Schneider A, Klück HM, dos Reis SL, et al. Determination of irinotecan and its metabolite SN-38 in dried blood spots using high-performance liquid-chromatography with fluorescence detection. J Pharm Biomed Anal. 2018 Feb;150:51–8.

85. Ciccolini J, Serdjebi C, Peters GJ, Giovannetti E. Pharmacokinetics and pharmacogenetics of Gemcitabine as a mainstay in adult and pediatric oncology: an EORTC-PAMM perspective. Cancer Chemother Pharmacol. 2016 Jul 23;78(1):1–12.

86. Chen W, Wong C, Vosburgh E, Levine AJ, Foran DJ, Xu EY. High-throughput Image Analysis of Tumor Spheroids: A User-friendly Software Application to Measure the Size of Spheroids Automatically and Accurately. Journal of Visualized Experiments. 2014 Jul 8;(89).

87. Griss T, Vincent EE, Egnatchik R, Chen J, Ma EH, Faubert B, et al. Metformin Antagonizes Cancer Cell Proliferation by Suppressing Mitochondrial-Dependent Biosynthesis. PLoS Biol. 2015 Dec 1;13(12):e1002309.

88. Valcourt JR, Lemons JMS, Haley EM, Kojima M, Demuren OO, Coller HA. Staying alive. Cell Cycle. 2012 May 28;11(9):1680–96.

89. Pavlidou T, Marinkovic M, Rosina M, Fuoco C, Vumbaca S, Gargioli C, et al. Metformin Delays Satellite Cell Activation and Maintains Quiescence. Stem Cells Int. 2019 Apr 24;2019:1–19.

90. Derle A, De Santis MC, Gozzelino L, Ratto E, Martini M. The role of metabolic adaptation to nutrient stress in pancreatic cancer. Cell Stress. 2018 Dec 10;2(12):332–9.

91. Andrzejewski S, Siegel PM, St-Pierre J. Metabolic Profiles Associated With Metformin Efficacy in Cancer. Front Endocrinol (Lausanne). 2018 Aug 21;9.

92. Andrzejewski S, Gravel SP, Pollak M, St-Pierre J. Metformin directly acts on mitochondria to alter cellular bioenergetics. Cancer Metab. 2014 Dec 28;2(1):12.

93. Masoud R, Reyes-Castellanos G, Lac S, Garcia J, Dou S, Shintu L, et al. Targeting Mitochondrial Complex I Overcomes Chemoresistance in High OXPHOS Pancreatic Cancer. Cell Rep Med. 2020 Nov;1(8):100143.

94. Vial G, Detaille D, Guigas B. Role of Mitochondria in the Mechanism(s) of Action of Metformin. Front Endocrinol (Lausanne). 2019 May 7;10.

95. Marchetti P, Fovez Q, Germain N, Khamari R, Kluza J. Mitochondrial spare respiratory capacity: Mechanisms, regulation, and significance in non-transformed and cancer cells. The FASEB Journal. 2020 Oct 17;34(10):13106–24.

96. Marchetti P, Fovez Q, Germain N, Khamari R, Kluza J. Mitochondrial spare respiratory capacity: Mechanisms, regulation, and significance in non-transformed and cancer cells. The FASEB Journal. 2020 Oct 17;34(10):13106–24.

97. Cheng J, Nanayakkara G, Shao Y, Cueto R, Wang L, Yang WY, et al. Mitochondrial Proton Leak Plays a Critical Role in Pathogenesis of Cardiovascular Diseases. In 2017. p. 359–70.

98. Nanayakkara GK, Wang H, Yang X. Proton leak regulates mitochondrial reactive oxygen species generation in endothelial cell activation and inflammation - A novel concept. Arch Biochem Biophys. 2019 Feb;662:68–74.

99. Harada N. Effects of metformin on blood glucose levels and bodyweight mediated through intestinal effects. J Diabetes Investig. 2020 Nov 19;11(6):1420–1.

100. Terret C. Dose and time dependencies of 5-fluorouracil pharmacokinetics. Clin Pharmacol Ther. 2000 Sep;68(3):270–9.

101. CASALE F. Plasma concentrations of 5-fluorouracil and its metabolites in colon cancer patients. Pharmacol Res. 2004 Aug;50(2):173–9.

102. Wang WB. Recent studies of 5-fluorouracil resistance in pancreatic cancer. World J Gastroenterol. 2014;20(42):15682.

103. Patki M, Saraswat A, Bhutkar S, Dukhande V, Patel K. In vitro assessment of a synergistic combination of gemcitabine and zebularine in pancreatic cancer cells. Exp Cell Res. 2021 Aug;405(2):112660.

104. N'Guessan KF, Davis HW, Chu Z, Vallabhapurapu SD, Lewis CS, Franco RS, et al. Enhanced Efficacy of Combination of Gemcitabine and Phosphatidylserine-Targeted Nanovesicles against Pancreatic Cancer. Molecular Therapy. 2020 Aug;28(8):1876–86.

105. Fernández A, Salgado M, García A, Buxò E, Vera R, Adeva J, et al. Prognostic factors for survival with nab-paclitaxel plus gemcitabine in metastatic pancreatic cancer in real-life practice: the ANICE-PaC study. BMC Cancer. 2018 Dec 29;18(1):1185.

106. Xia R, Hu C, Ye Y, Zhang X, Li T, He R, et al. HNF1A regulates oxaliplatin resistance in pancreatic cancer by targeting 53BP1. Int J Oncol. 2023 Feb 22;62(4):45.

107. National Cancer Institute. liposomal SN-38. In: NCI Dictionaries [Internet]. [cited 2023 May 14]. Available from: https://www.cancer.gov/publications/dictionaries/cancer-drug/def/liposomal-sn-38

108. Barisam M, Saidi M, Kashaninejad N, Nguyen NT. Prediction of Necrotic Core and Hypoxic Zone of Multicellular Spheroids in a Microbioreactor with a U-Shaped Barrier. Micromachines (Basel). 2018 Feb 25;9(3):94.

109. Yee PP, Li W. Tumor necrosis: A synergistic consequence of metabolic stress and inflammation. BioEssays. 2021 Jul 16;43(7):2100029.

110. Queiroz EAIF, Puukila S, Eichler R, Sampaio SC, Forsyth HL, Lees SJ, et al. Metformin Induces Apoptosis and Cell Cycle Arrest Mediated by Oxidative Stress, AMPK and FOXO3a in MCF-7 Breast Cancer Cells. PLoS One. 2014 May 23;9(5):e98207.

111. Svec D, Tichopad A, Novosadova V, Pfaffl MW, Kubista M. How good is a PCR efficiency estimate: Recommendations for precise and robust qPCR efficiency assessments. Biomol Detect Quantif. 2015 Mar;3:9–16.

112. Nolan T, Hands RE, Ogunkolade W, Bustin SA. SPUD: A quantitative PCR assay for the detection of inhibitors in nucleic acid preparations. Anal Biochem. 2006 Apr;351(2):308–10.

113. NCBI. SLC22A1 solute carrier family 22 member 1 [Homo sapiens (human)]. In: National Center for Biotechnology Information (NCBI)[Internet]. 2023.

114. Mohelnikova-Duchonova B, Brynychova V, Hlavac V, Kocik M, Oliverius M, Hlavsa J, et al. The association between the expression of solute carrier transporters and the prognosis of pancreatic cancer. Cancer Chemother Pharmacol. 2013 Sep 11;72(3):669–82.

Chapter 8 Appendices

8.1 Appendix A

Table 8. 1 Cell lines

Name	Supplier	Product Code
AsPC-1	ATCC	ATCC® CRL-1469
Panc-1	ATCC	ATCC® CRL-1682

Table 8. 2 Reagents for Cell Culture

Chemicals	Supplier	Product Code
DMEM (Dulbecco's Modified Eagle's Media) without glucose, L-glutamine and sodium pyruvate	Corning	17-207-CV
Fetal Bovine Serum, heat inactivated, South America	Biowest	S181H
PenStrep solution 100 X	Biowest	L0022-020
100 X L-glutamine	Corning	25-005-Cl
45 % Glucose Solution	Corning	25-037-CI
Trypsin EDTA 1X	Corning	25-053-Cl
PBS tablets	ThermoFisher	189112-014
NaOH, 1M	Sigma-Aldrich	-
Seahorse Base Medium	-	-

Table 8. 3 Cell Culture Flasks and Microplates

Name	Supplier	Product Code
T-75 Ventilated Flasks	Falcon a Corning Brand	353136
T-25 Ventilated Flasks	Falcon a Corning Brand	353108
Microplate 96 Well, PS, U-Bottom, Clear CELLSTAR®	Greiner Bio-one	650970

Table 8. 4 Commercial Kits

Name	Supplier	Product Code
Muse® Count & Viability kit	Luminex	B86303
Pierce™ BCA Protein Assay Kit	Thermoscientific	23227
XFp Cell Mito Stress Test Kit	Agilent Technologies	103010

XFp Glycolysis Stress Test Kit	Agilent Technologies	103017
Quick-RNA™ MiniPrep	Zymo Research	R1055
QuantiTect® Reverse Transcription	Qiagen	205313
Click-iT™ EdU Proliferation Assay	Invitrogen	C10499
SsoAdvanced™ Universal SYBR Green Supermix	BioRad	172-5270

Table 8. 5 Equipment & Software

Name	Supplier
Muse™ Cell analyzer	Luminex
SpectraMax Paradigm Multi-Mode Microplate Reader	Molecular Devices
Seahorse XFp Extracellular Flux Analyzer	Agilent Technologies
Seahorse XFp FluxPak: Sensor Cartridges with utility Miniplates	Agilent Technologies
Seahorse XFp miniplate	Agilent Technologies
Wave Desktop	Agilent Technologies
Leica TCS SP8 CSU Confocal Microscope	Leica Microsystems
LAS X	Leica Microsystems
Image J	National Institutes of Health
Olympus CKX41 Light Microscope	Olympus
NanoDrop One	Thermo Scientific
Agilent 2100 Bioanalyzer	Agilent Technologies
CFX OPUS qPCR	BioRad

Table 8. 6 Drugs & Treatments

Name	Concentration	Supplier
Metformin Hydrochloride	11.6 µM	Sigma Aldrich
5-fluorouracil powder	0.25-16 µg/mL	EMD Millipore Corp.
Gemcitabine	25-500 µM	EMD Millipore Corp.
Oxaliplatin	1-5 µM	EMD Millipore Corp.
SN-38	2-20 ng/mL	EMD Millipore Corp.

8.2 Appendix B

Table 8. 7 RNA Extraction Concentrations in ng/uL and A260/A280 Results: AsPC-1 2 Weeks

AsPC-1 2 Weeks	ng/uL	A260/A280	A260/A230
Control 1	226.4	1.93	2.00

Control 2	216.8	1.95	2.08
Metformin 1	67.7	1.68	1.39
Metformin 2	85.7	1.90	2.14

Table 8. 8 RNA Extraction Concentrations in ng/uL and A260/A280 Results: Panc-1 2 Weeks

Panc-1 2 Weeks	ng/uL	A260/A280	A260/A230
Control 1	475.4	2.10	2.20
Control 2	638.8	2.08	2.24
Metformin 1	608.5	2.09	2.03
Metformin 2	719.9	2.09	2.24

Table 8. 9 RNA Extraction Concentrations in ng/uL and A260/A280 Results: AsPC-1 2 Weeks

AsPC-1 6 Weeks	ng/uL	A260/A280	A260/A230
Control 1	588.5	2.06	2.25
Control 2	584.7	2.09	2.22
Metformin 1	209.4	2.08	1.17
Metformin 2	190.3	2.06	2.17

Table 8. 10 RNA Extraction Concentrations in ng/uL and A260/A280 Results: Panc-1 6 Weeks

Panc-1 6 Weeks	ng/uL	A260/A280	A260/A230
Control 1	899.6	2.09	2.22
Control 2	469.5	2.10	2.21
Metformin 1	613	2.07	2.14
Metformin 2	401	2.08	2.18

8.3 Appendix C

Bioanalyzer RNA 6000 Nano Assay Results:

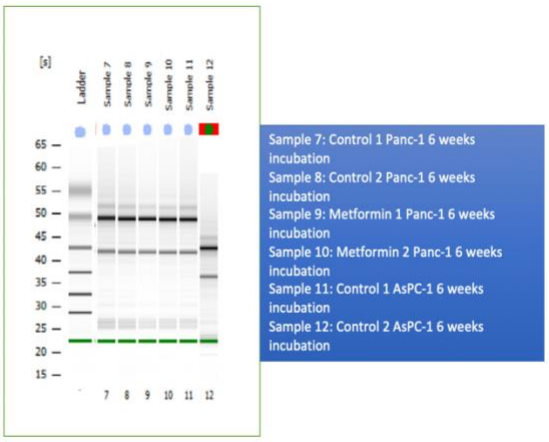
[s]
Ladder
Sample 7
Sample 8
Sample 9
Sample 10
Sample 11
Sample 12
65
60
55
50
45
40
35
30
25
20
15
7
8
9
10
11
12
Sample 7: Control 1 Panc-1 6 weeks incubation
Sample 8: Control 2 Panc-1 6 weeks incubation
Sample 9: Metformin 1 Panc-1 6 weeks incubation
Sample 10: Metformin 2 Panc-1 6 weeks incubation
Sample 11: Control 1 AsPC-1 6 weeks incubation
Sample 12: Control 2 AsPC-1 6 weeks incubation

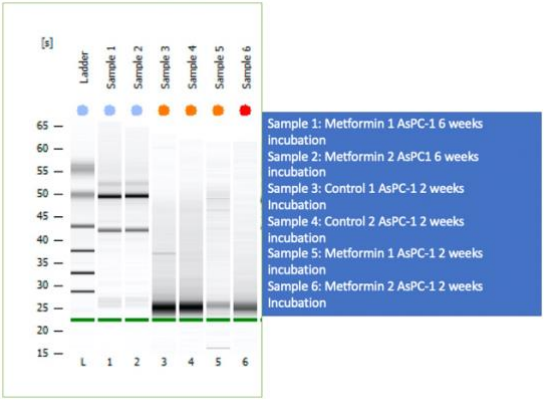
[s]
Ladder
Sample 1
Sample 2
Sample 3
Sample 4
Sample 5
Sample 6
65
60
55
50
45
40
35
30
25
20
15
L
1
2
3
4
5
6
Sample 1: Metformin 1 AsPC-1 6 weeks incubation
Sample 2: Metformin 2 AsPC1 6 weeks incubation
Sample 3: Control 1 AsPC-1 2 weeks Incubation
Sample 4: Control 2 AsPC-1 2 weeks incubation
Sample 5: Metformin 1 AsPC-1 2 weeks incubation
Sample 6: Metformin 2 AsPC-1 2 weeks Incubation

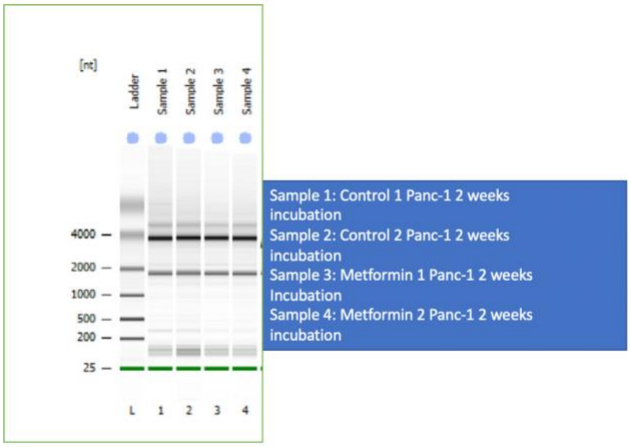
[nt]
Ladder
Sample 1
Sample 2
Sample 3
Sample 4
4000
2000
1000
500
200
25
L
1
2
3
4
Sample 1: Control 1 Panc-1 2 weeks incubation
Sample 2: Control 2 Panc-1 2 weeks incubation
Sample 3: Metformin 1 Panc-1 2 weeks Incubation
Sample 4: Metformin 2 Panc-1 2 weeks incubation

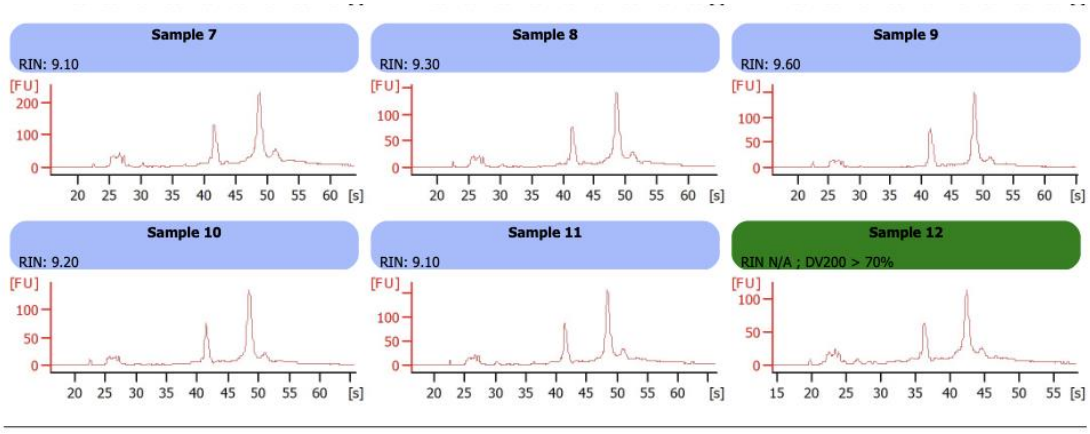
Sample 7
RIN: 9.10
Sample 8
RIN: 9.30
Sample 9
RIN: 9.60
Sample 10
RIN: 9.20
Sample 11
RIN: 9.10
Sample 12
RIN N/A ; DV200 > 70%
[FU]
[s]

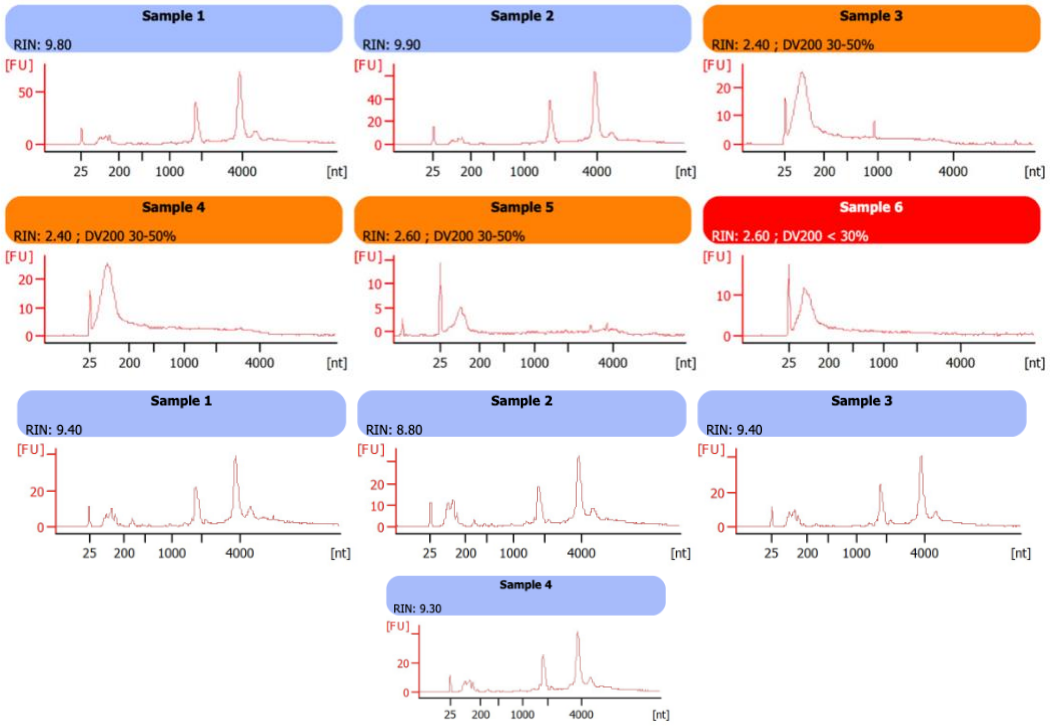

8.4 Appendix D

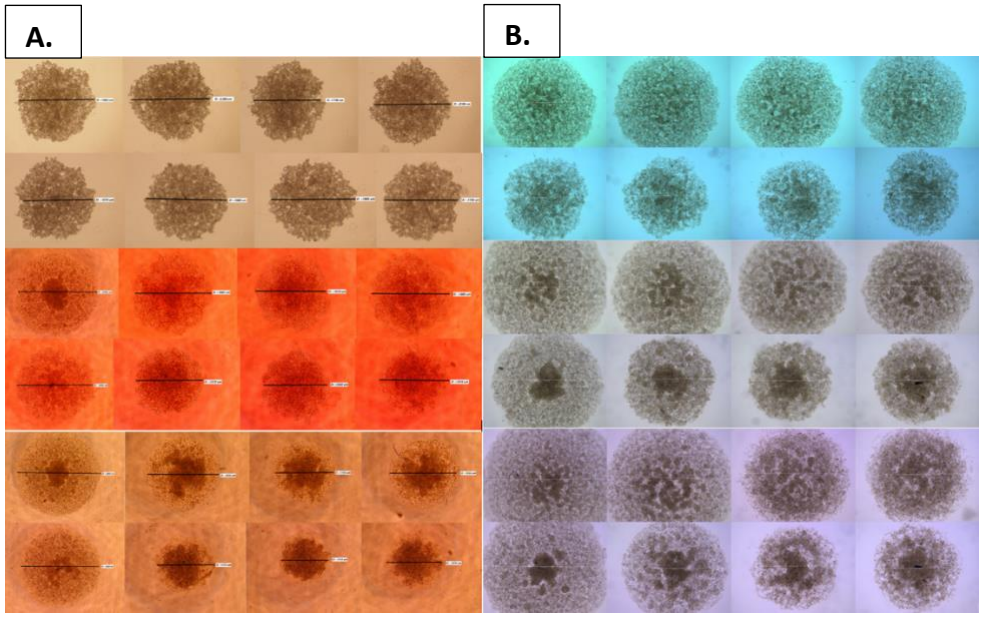

Figure 8. 1 Captured Images of Control and Metformin-treated AsPC-1 cells over the course of a 5-FU treatment.

Group A. indicates the AsPC-1 cells treated in Metformin for 2 weeks, while group B. indicates the cells treated in Metformin for 6 weeks. Each group contains three sets of images, where the top row of each set contains the control cells, and the bottom row contains the metformin-treated cells. The first set of images represents the cells at day 0, before the addition of chemo, the second set represents day 4, and the last

set represents day 5, one day after a media exchange. The images in group A. were captures with the Olympus CKX41 Light Microscope at a 4X objective, while group B. was captured with the Leica TCS SP8 CSU Confocal Microscope at a 5X objective.

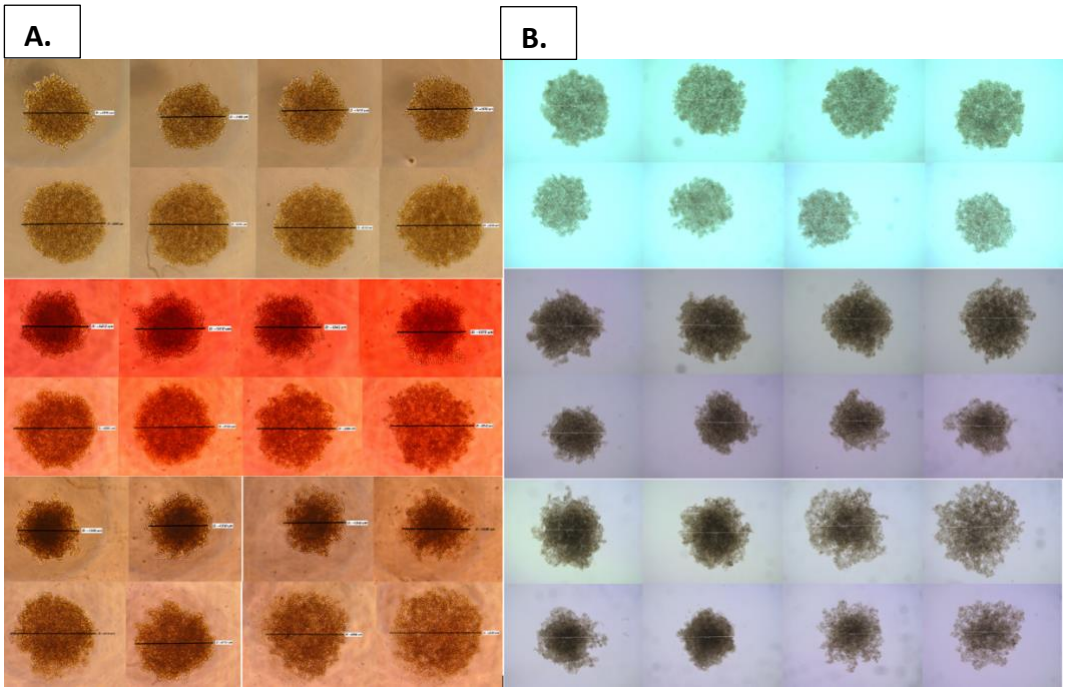

Figure 8. 2 Captured Images of Control and Metformin-treated Panc-1 cells over the course of a 5-FU treatment.
Group A. indicates the AsPC-1 cells treated in Metformin for 2 weeks, while group B. indicates the cells treated in Metformin for 6 weeks. Each group contains three sets of images, where the top row of each set contains the control cells, and the bottom row contains the metformin-treated cells. The first set of images represents the cells at day 0, before the addition of chemo, the second set represents day 4, and the last set represents day 5, one day after a media exchange. Both groups were captured with the Leica TCS SP8 CSU Confocal Microscope at a 5X objective.

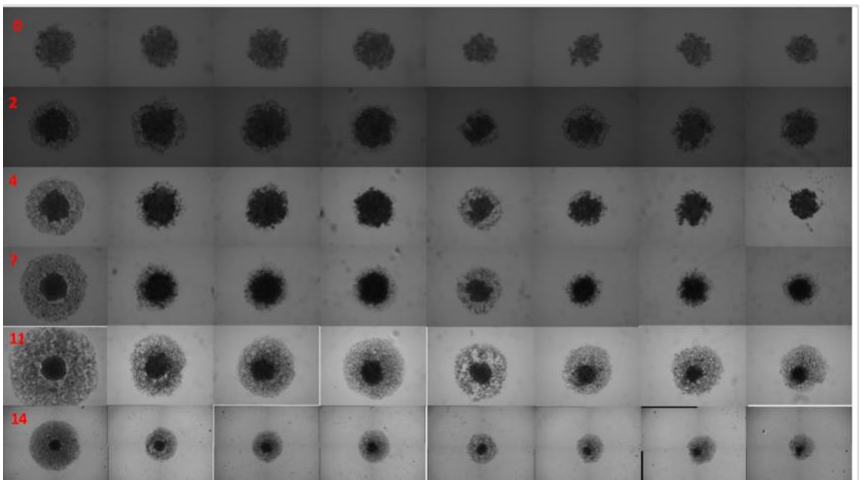

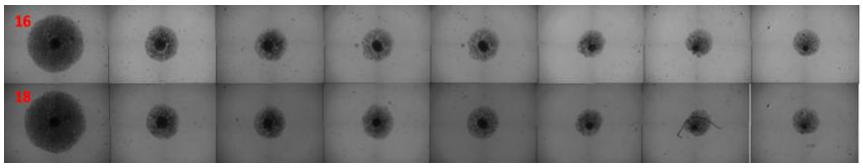

Figure 8. 3 Captured Images of Control and Metformin-treated (2 weeks) AsPC-1 cells over the course of an 18-day Gemcitabine Treatment.
Each row of the image is labeled with the day the image was captured. In each row, the various treatment groups are in order: No metformin, No metformin 25 μM of Gemcitabine, No metformin 100 μM of Gemcitabine, No metformin 500 μM of Gemcitabine, metformin, metformin 25 μM of Gemcitabine, metformin 100 μM of Gemcitabine, metformin 500 μM of Gemcitabine.

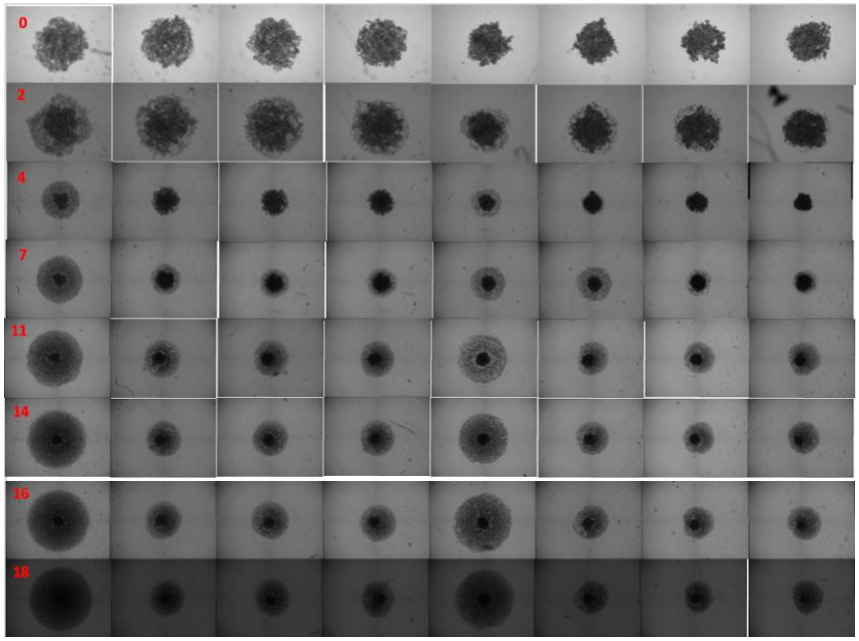

Figure 8. 4 Captured Images of Control and Metformin-treated (6 weeks) AsPC-1 cells over the course of an 18-day Gemcitabine Treatment.
Same explanation as above.

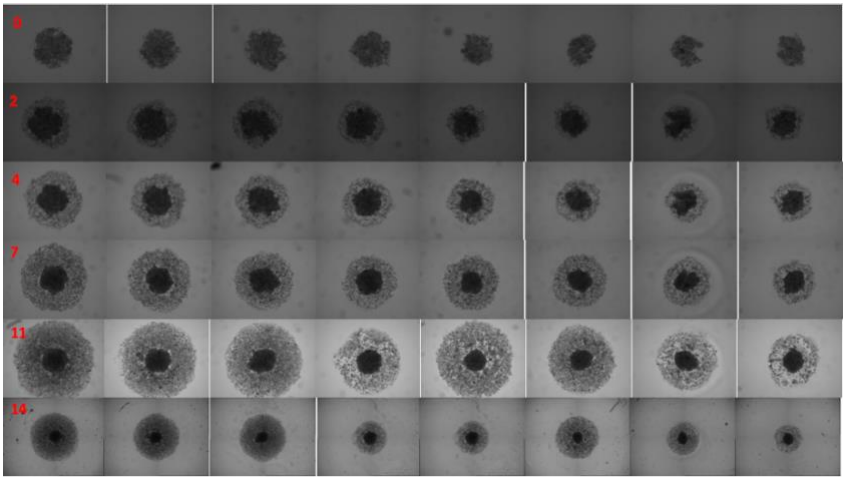

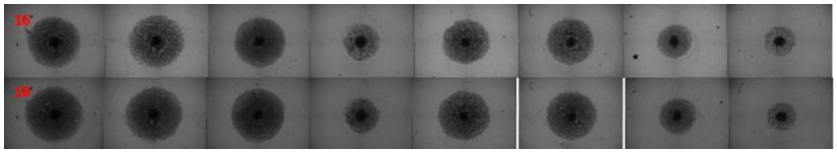

Figure 8. 5 Captured Images of Control and Metformin-treated (2 weeks) AsPC-1 cells over the course of an 18-day SN38 Treatment.
Each row of the image is labeled with the day the image was captured. In each row, the various treatment groups are in order: No metformin, No metformin 3 ng/mL of SN-38, No metformin 10 ng/mL of SN-38, No metformin 20 ng/mL of SN-38, metformin, metformin 3 ng/mL of SN-38, metformin 10 ng/mL of SN-38, metformin 20 ng/mL of SN-38.

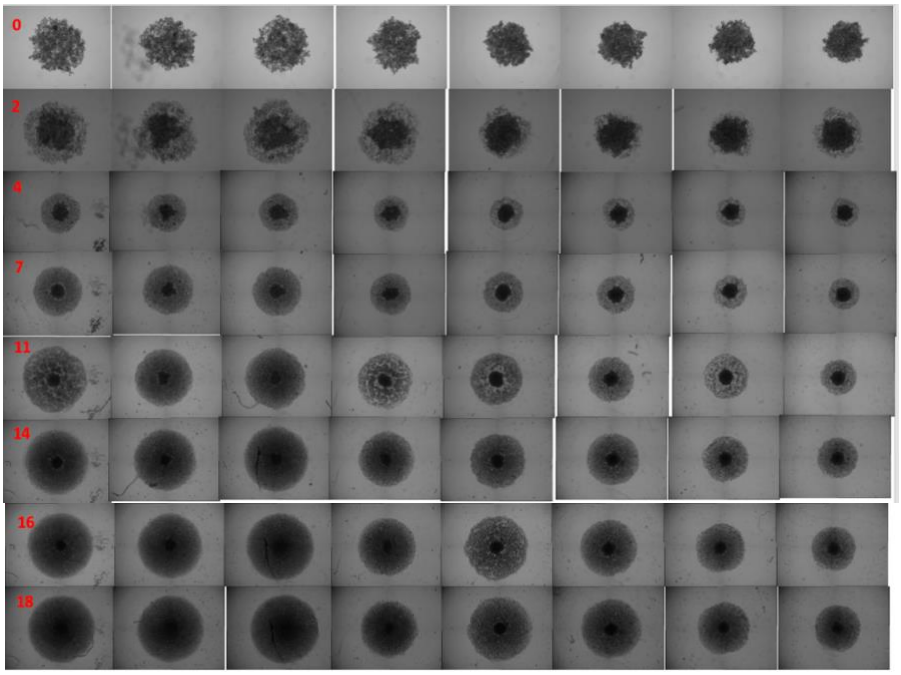

Figure 8. 6 Captured Images of Control and Metformin-treated (6 weeks) AsPC-1 cells over the course of an 18-day SN38 Treatment.
Same explanation as above.

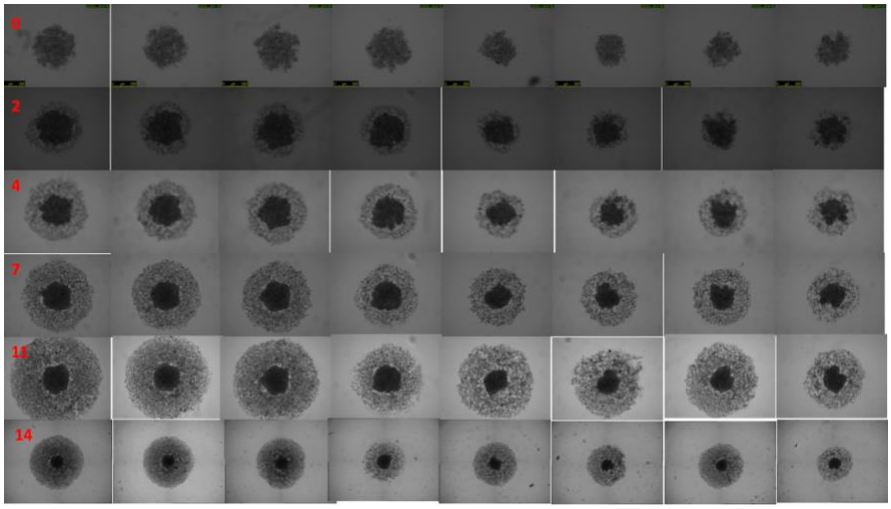

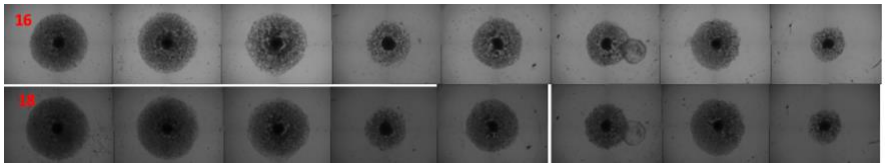

Figure 8. 7 Captured Images of Control and Metformin-treated (2 weeks) AsPC-1 cells over the course of an 18-day Oxaliplatin Treatment.
Each row of the image is labeled with the day the image was captured. In each row, the various treatment groups are in order: No metformin, No metformin 1 μM of Oxaliplatin, No metformin 2.5 μM of Oxaliplatin, No metformin 5 μM of Oxaliplatin, metformin, metformin 1 μM of Oxaliplatin, metformin 2.5 μM of Oxaliplatin, metformin 5 μM of Oxaliplatin.

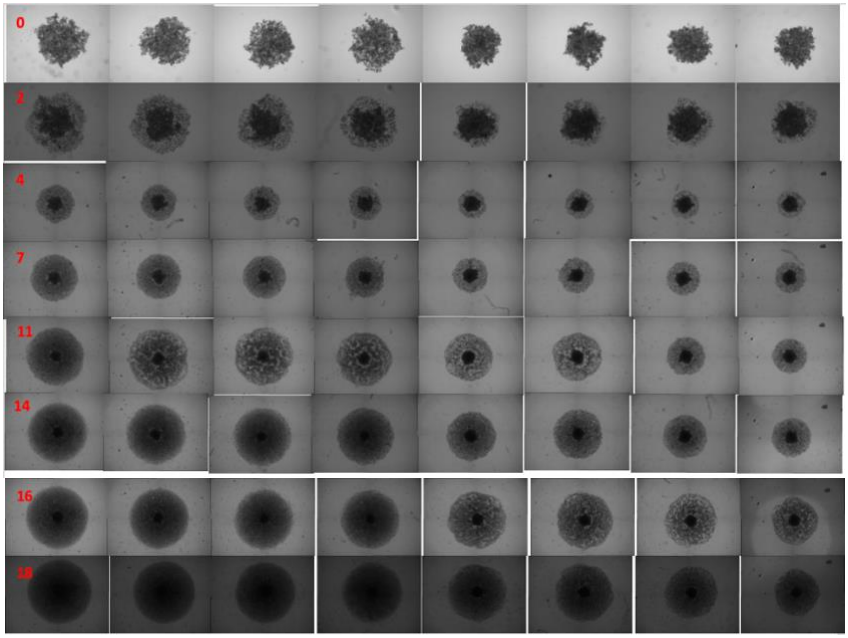

Figure 8. 8 Captured Images of Control and Metformin-treated (6 weeks) AsPC-1 cells over the course of an 18-day Oxaliplatin Treatment.
Same explanation as above.

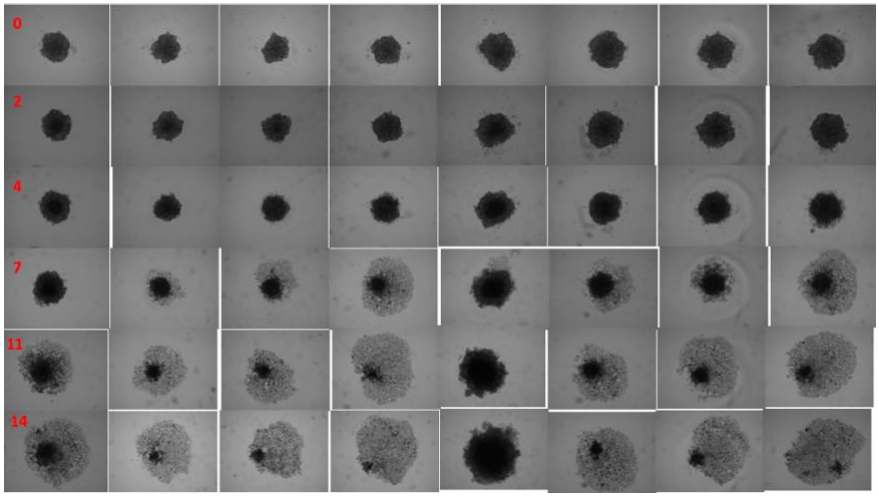

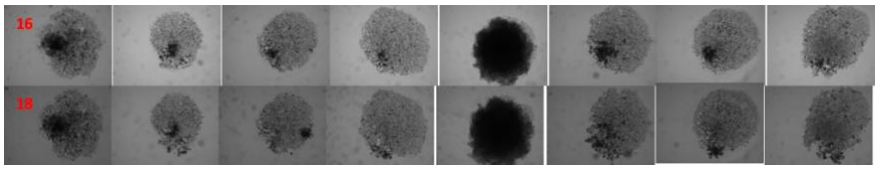

Figure 8. 9 Captured Images of Control and Metformin-treated (2 weeks) Panc-1 cells over the course of an 18-day Gemcitabine Treatment.
Each row of the image is labeled with the day the image was captured. In each row, the various treatment groups are in order: No metformin, No metformin 25 μM of Gemcitabine, No metformin 100 μM of Gemcitabine, No metformin 500 μM of Gemcitabine, metformin, metformin 25 μM of Gemcitabine, metformin 100 μM of Gemcitabine, metformin 500 μM of Gemcitabine.

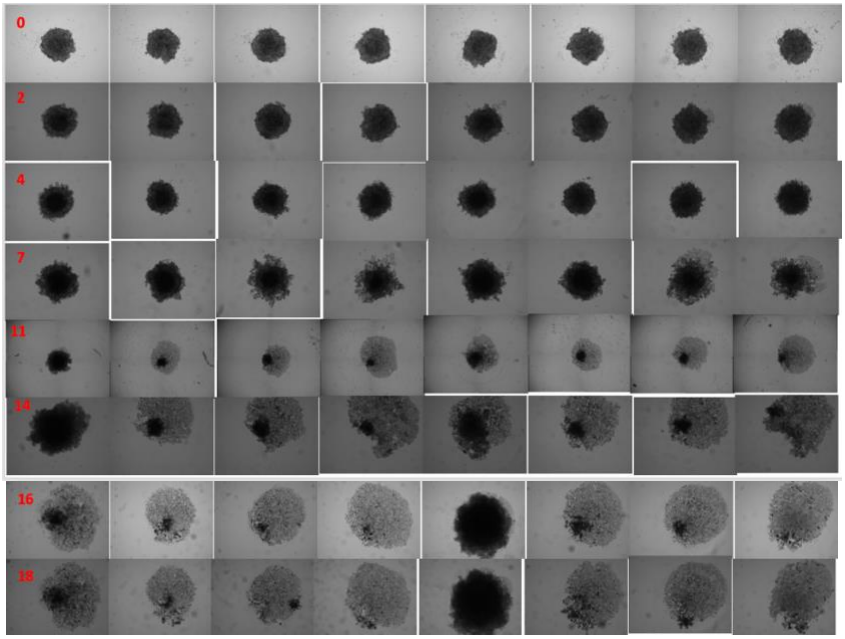

Figure 8. 10 Captured Images of Control and Metformin-treated (6 weeks) Panc-1 cells over the course of an 18-day Gemcitabine Treatment.
Same explanation as above.

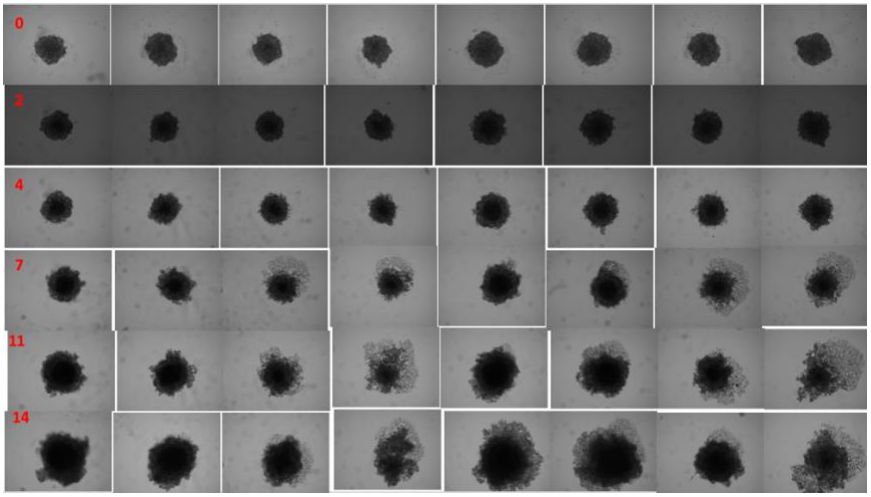

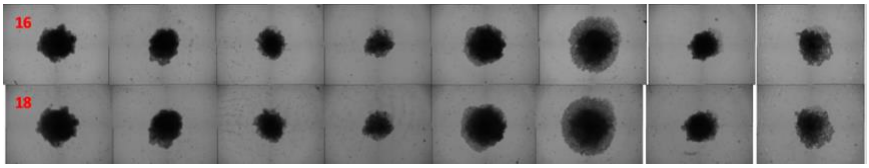

Figure 8. 11 Captured Images of Control and Metformin-treated (2 weeks) Panc-1 cells over the course of an 18-day Oxaliplatin Treatment.
Each row of the image is labeled with the day the image was captured. In each row, the various treatment groups are in order: No metformin, No metformin 1 μM of Oxaliplatin, No metformin 2.5 μM of Oxaliplatin, No metformin 5 μM of Oxaliplatin, metformin, metformin 1 μM of Oxaliplatin, metformin 2.5 μM of Oxaliplatin, metformin 5 μM of Oxaliplatin.

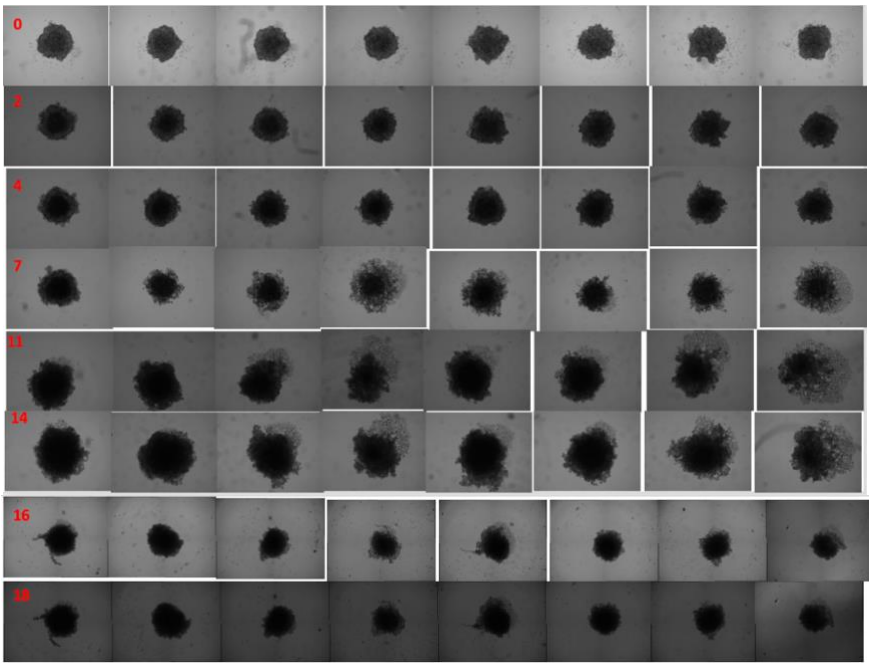

Figure 8. 12 Captured Images of Control and Metformin-treated (6 weeks) Panc-1 cells over the course of an 18-day Oxaliplatin Treatment.
Same explanation as above.

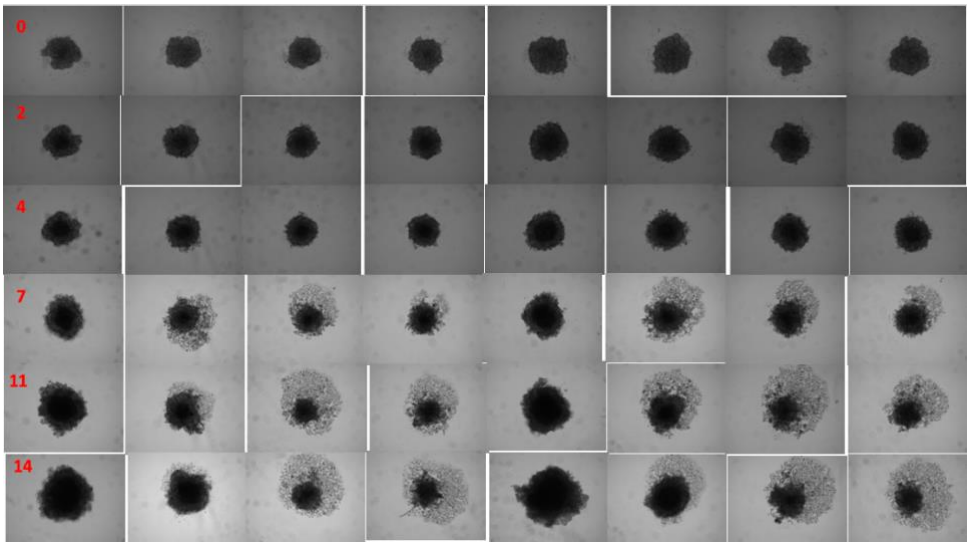

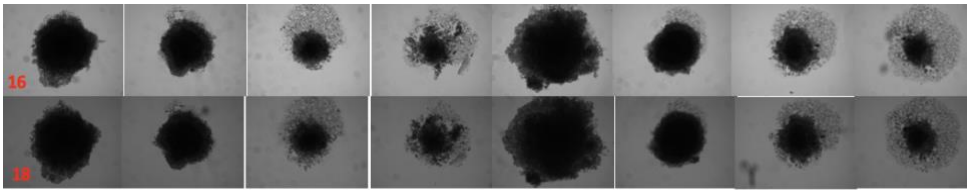

Figure 8. 13 Captured Images of Control and Metformin-treated (2 weeks) Panc-1 cells over the course of an 18-day SN38 Treatment.
Each row of the image is labeled with the day the image was captured. In each row, the various treatment groups are in order: No metformin, No metformin 3 ng/mL of SN-38, No metformin 10 ng/mL of SN-38, No metformin 20 ng/mL of SN-38, metformin, metformin 3 ng/mL of SN-38, metformin 10 ng/mL of SN-38, metformin 20 ng/mL of SN-38.

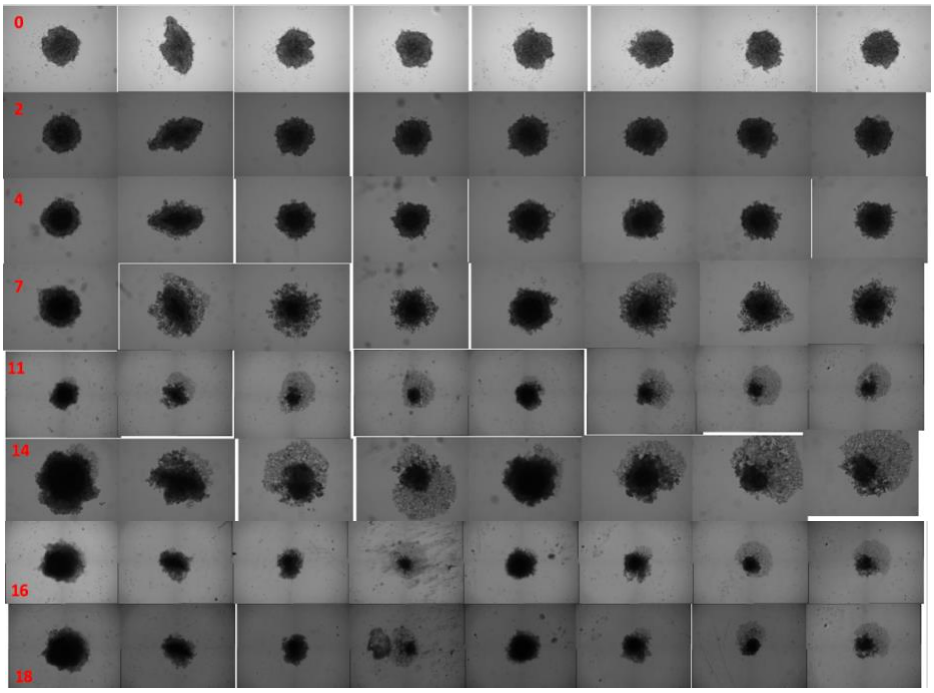

Figure 8. 14 Captured Images of Control and Metformin-treated (6 weeks) Panc-1 cells over the course of an 18-day SN38 Treatment.
Same explanation as above.

8.5 Appendix E

ANOVA: Two-factor with replication-AsPC-1 2 Weeks and 6 Weeks Metformin 5-FU, respectively

ANOVA- Day 0

Source of Variation	F	P-value	F crit	F	P-value	F crit
Sample	25.393082	1.77338E-05	4.149097446	497.144881	4.61218E-21	4.149097446
Columns	0.5765211	0.634644461	2.901119584	0.24594026	0.863598022	2.901119584
Interaction	0.578738	0.633224396	2.901119584	1.31793494	0.285646694	2.901119584

ANOVA-Day 4

Source of Variation	F	P-value	F crit	F	P-value	F crit
Sample	19.37957	0.000111776	4.149097446	1128.6387	1.58099E-26	4.149097446
Columns	28.023475	4.42678E-09	2.901119584	110.27004	5.93193E-17	2.901119584
Interaction	1.1400222	0.347774249	2.901119584	4.2307256	0.012563802	2.901119584

ANOVA- Day 5

Source of Variation	F	P-value	F crit	F	P-value	F crit
Sample	43.110014	2.13171E-07	4.149097446	984.690398	1.3179E-25	4.149097446
Columns	136.83042	2.49519E-18	2.901119584	189.323085	1.93036E-20	2.901119584
Interaction	7.9593475	0.000419409	2.901119584	16.7475302	1.0145E-06	2.901119584

ANOVA: Two-factor with replication-Panc-1 2 Weeks and 6 Weeks Metformin 5-FU, respectively

ANOVA- Day 0

Source of Variation	F	P-value	F crit	F	P-value	F crit
Sample	1033.90972	6.18116E-26	4.149097446	108.946609	7.8657E-12	4.149097446
Columns	0.26165284	0.85247291	2.901119584	0.29306378	0.83008796	2.901119584
Interaction	0.84138946	0.481322079	2.901119584	0.6357533	0.59746476	2.901119584

ANOVA-Day 4

Source of Variation	F	P-value	F crit	F	P-value	F crit
Sample	507.38237	3.39237E-21	4.149097446	51.5149111	3.7796E-08	4.149097446
Columns	0.82646057	0.489067677	2.901119584	1.64972664	0.19745499	2.901119584
Interaction	0.85708624	0.473292796	2.901119584	1.60815914	0.206813	2.901119584

ANOVA- Day 5

Source of Variation	F	P-value	F crit	F	P-value	F crit
Sample	227.334052	4.29968E-16	4.149097446	65.1914976	3.2134E-09	4.149097446
Columns	3.68828381	0.021827893	2.901119584	9.08375	0.00016958	2.901119584
Interaction	0.54916604	0.652344351	2.901119584	2.74291853	0.05928261	2.901119584

ANOVA: Two-factor with replication-2 Weeks and 6 Weeks Metformin Gemcitabine, respectively

ANOVA- Panc-1 Day 0

Source of Variation	SS	df	MS	F	P-value	F crit
Sample	0.14418	1	0.14418	415.1798	6.85E-20	4.149097
Columns	0.002321	3	0.000774	2.228239	0.103952	2.90112
Interaction	0.005042	3	0.001681	4.839676	0.006884	2.90112
Within	0.011113	32	0.000347			
Total	0.162656	39				

ANOVA- Panc1 Day 18

Source of Variation	SS	df	MS	F	P-value	F crit
Sample	0.352801	1	0.352801	2.084363	0.158534	4.149097
Columns	1.153556	3	0.384519	2.271751	0.099091	2.90112
Interaction	0.071623	3	0.023874	0.141051	0.93464	2.90112
Within	5.416347	32	0.169261			
Total	6.994327	39				

ANOVA- AsPC-1 Day 0

Source of Variation	SS	df	MS	F	P-value	F crit
Sample	0.3943004	1	0.3943004	1244.7438	3.435E-27	4.1490974
Columns	0.0007382	3	0.0002461	0.7768417	0.5155812	2.9011196
Interaction	0.0023711	3	0.0007904	2.4950966	0.0775846	2.9011196
Within	0.0101367	32	0.0003168			
Total	0.4075465	39				

ANOVA- AsPC-1 Day 18

Source of Variation	SS	df	MS	F	P-value	F crit
Sample	42.055961	1	42.055961	261.4265	5.914E-17	4.1490974
Columns	147.60882	3	49.20294	305.85325	1.258E-23	2.9011196
Interaction	79.825661	3	26.608554	165.40298	1.477E-19	2.9011196
Within	5.1478742	32	0.1608711			
Total	274.63831	39				

ANOVA- Panc-1 6 weeks Day 0

Source of Variation	SS	df	MS	F	P-value	F crit
Sample	0.00402	1	0.00402	16.493265	0.0002948	4.1490974
Columns	0.0012714	3	0.0004238	1.7387581	0.1788175	2.9011196
Interaction	0.0017734	3	0.0005911	2.4253277	0.0837294	2.9011196
Within	0.0077996	32	0.0002437			
Total	0.0148645	39				

ANOVA- Panc-1 6 weeks Day 18

Source of Variation	SS	df	MS	F	P-value	F crit
Sample	0.0255126	1	0.0255126	0.275177	0.6034953	4.1490974
Columns	5.6333584	3	1.8777861	20.25366	1.527E-07	2.9011196
Interaction	3.0128025	3	1.0042675	10.831954	4.546E-05	2.9011196
Within	2.9668295	32	0.0927134			
Total	11.638503	39				

ANOVA AsPC-1 6 weeks Day 0

Source of Variation	SS	df	MS	F	P-value	F crit
Sample	1.438988	1	1.438988	680.978	3.88E-23	4.149097
Columns	0.029907	3	0.009969	4.717591	0.007754	2.90112
Interaction	0.022026	3	0.007342	3.474421	0.027255	2.90112
Within	0.06762	32	0.002113			
Total	1.55854	39				

ANOVA AsPC-1 6 weeks Day 18

Source of Variation	SS	df	MS	F	P-value	F crit
Sample	15.2525	1	15.2525	79.47579	X	4.149097
Columns	279.6008	3	93.20027	485.6363	9.47E-27	2.90112
Interaction	29.21349	3	9.737829	50.74066	2.9E-12	2.90112
Within	6.14124	32	0.191914			
Total	330.208	39				

ANOVA: Two-factor with replication-2 Weeks and 6 Weeks Metformin Oxaliplatin, respectively

ANOVA- Panc-1 Day 0

Source of Variation	SS	df	MS	F	P-value	F crit
Sample	0.06728101	1	0.06728101	452.166796	1.916E-20	4.14909745
Columns	0.00045641	3	0.00015214	1.02245595	0.39565821	2.90111958
Interaction	0.00029686	3	9.8953E-05	0.66502013	0.57969477	2.90111958
Within	0.0047615	32	0.0001488			
Total	0.07279578	39				

ANOVA- Panc-1 Day 18

Source of Variation	SS	df	MS	F	P-value	F crit
Sample	3.23584634	1	3.23584634	8.03750589	0.00787571	4.14909745
Columns	23.2094508	3	7.73648359	19.2166209	2.613E-07	2.90111958
Interaction	5.40209014	3	1.80069671	4.47274343	0.00986884	2.90111958
Within	12.8829869	32	0.40259334			
Total	44.7303741	39				

ANOVA- AsPC-1 Day 0

Source of Variation	SS	df	MS	F	P-value	F crit
Sample	0.411481	1	0.411481	234.2642	2.81E-16	4.149097
Columns	0.00724	3	0.002413	1.373941	0.268419	2.90112
Interaction	0.011759	3	0.00392	2.231511	0.103578	2.90112
Within	0.056207	32	0.001756			
Total	0.486687	39				

ANOVA- AsPC-1 Day 18

Source of Variation	SS	df	MS	F	P-value	F crit
Sample	55.21537	1	55.21537	70.09822	1.45E-09	4.149097
Columns	133.8851	3	44.62836	56.65756	6.72E-13	2.90112
Interaction	14.58706	3	4.862352	6.17296	0.001969	2.90112
Within	25.20594	32	0.787686			
Total	228.8934	39				

ANOVA- Panc-1 6 weeks Day 0

Source of Variation	SS	df	MS	F	P-value	F crit
Sample	0.004219	1	0.004219	25.0213	1.97E-05	4.149097
Columns	0.001732	3	0.000577	3.42438	0.028718	2.90112
Interaction	0.000226	3	7.54E-05	0.447024	0.721093	2.90112
Within	0.005396	32	0.000169			
Total	0.011573	39				

ANOVA- Panc-1 6 weeks Day 18

Source of Variation	SS	df	MS	F	P-value	F crit
Sample	1.220175	1	1.220175	8.190753	0.007364	4.149097
Columns	1.016572	3	0.338857	2.274672	0.098774	2.90112
Interaction	0.312478	3	0.104159	0.699199	0.559458	2.90112
Within	4.767033	32	0.14897			
Total	7.316258	39				

ANOVA- AsPC-1 6 weeks Day 0

Source of Variation	SS	df	MS	F	P-value	F crit
Sample	0.793746	1	0.793746	344.5001	1.08E-18	4.149097
Columns	0.005892	3	0.001964	0.852341	0.475708	2.90112
Interaction	0.001042	3	0.000347	0.150722	0.928464	2.90112
Within	0.07373	32	0.002304			
Total	0.874409	39				

ANOVA- AsPC-1 6 weeks Day 18

Source of Variation	SS	df	MS	F	P-value	F crit
Sample	88.51309	1	88.51309	473.2693	9.67E-21	4.149097
Columns	38.27909	3	12.7597	68.22462	5.38E-14	2.90112
Interaction	2.413154	3	0.804385	4.300952	0.01171	2.90112
Within	5.984794	32	0.187025			
Total	135.1901	39				

ANOVA: Two-factor with replication-2 Weeks and 6 Weeks Metformin SN-38, respectively

ANOVA- Panc-1 Day 0

Source of Variation	SS	df	MS	F	P-value	F crit
Sample	0.072242	1	0.072242	195.8871	3.43E-15	4.1491
Columns	0.000998	3	0.000333	0.90248	0.450729	2.9011
Interaction	0.001601	3	0.000534	1.447205	0.247414	2.9011
Within	0.011801	32	0.000369			
Total	0.086642	39				

ANOVA- Panc-1 Day 18

Source of Variation	SS	df	MS	F	P-value	F crit
Sample	0.34188	1	0.34188	2.014735	0.165447	4.149097
Columns	25.48928	3	8.496428	50.07034	3.46E-12	2.90112
Interaction	0.432966	3	0.144322	0.850505	0.476645	2.90112
Within	5.430075	32	0.16969			
Total	31.69421	39				

ANOVA- Panc-1 Day 0

Source of Variation	SS	df	MS	F	P-value	F crit
Sample	0.072242	1	0.072242	195.8871	3.43E-15	4.1491
Columns	0.000998	3	0.000333	0.90248	0.450729	2.9011
Interaction	0.001601	3	0.000534	1.447205	0.247414	2.9011
Within	0.011801	32	0.000369			
Total	0.086642	39				

ANOVA- Panc-1 Day 18

Source of Variation	SS	df	MS	F	P-value	F crit
Sample	0.34188	1	0.34188	2.014735	0.165447	4.149097
Columns	25.48928	3	8.496428	50.07034	3.46E-12	2.90112
Interaction	0.432966	3	0.144322	0.850505	0.476645	2.90112
Within	5.430075	32	0.16969			
Total	31.69421	39				

ANOVA- Panc-1 6 weeks Day 0

Source of Variation	SS	df	MS	F	P-value	F crit
Sample	0.003897	1	0.003897	18.30789	0.000159	4.149097
Columns	0.001659	3	0.000553	2.597568	0.069393	2.90112
Interaction	0.000752	3	0.000251	1.177481	0.333703	2.90112
Within	0.006811	32	0.000213			
Total	0.013118	39				

ANOVA- Panc-1 6 weeks Day 18

Source of Variation	SS	df	MS	F	P-value	F crit
Sample	0.471758	1	0.471758	8.617096	0.00612	4.149097
Columns	5.706848	3	1.902283	34.74693	3.5E-10	2.90112
Interaction	1.309753	3	0.436584	7.97461	0.000414	2.90112
Within	1.751897	32	0.054747			
Total	9.240257	39				

ANOVA- AsPC-1 6 weeks Day 0

Source of Variation	SS	df	MS	F	P-value	F crit
Sample	0.8588709	1	0.8588709	291.55591	1.231E-17	4.149097446
Columns	0.005547	3	0.001849	0.6276689	0.6024443	2.901119584
Interaction	0.0110192	3	0.0036731	1.2468757	0.3090588	2.901119584
Within	0.0942662	32	0.0029458			
Total	0.9697034	39				

ANOVA- AsPC-1 6 weeks Day 18

Source of Variation	SS	df	MS	F	P-value	F crit
Sample	86.510398	1	86.510398	239.08687	2.11E-16	4.1490974
Columns	69.794494	3	23.264831	64.2965	1.214E-13	2.9011196
Interaction	3.659501	3	1.2198337	3.3712274	0.0303627	2.9011196
Within	11.578773	32	0.3618367			
Total	171.54317	39				

8.6 Appendix F

Table 8. 11 AsPC-1 2 Week BCA Assay

Seahorse Well	Protein Concentration **µg/mL** Mito stress Test	Protein Concentration **µg/mL** Glyco stress Test
A	**0**	**0**
B	**135**	**120.9**
C	**157.5**	**204.3**
D	**144.5**	**227.5**
E	**177.7**	**149**
F	**192.1**	**197.1**
G	**170.9**	**223**
H	**0**	**0**

Table 8. 12 Panc-1 2 Week BCA Assay

Seahorse Well	Protein Concentration **µg/mL** Mito stress Test	Protein Concentration **µg/mL** Glyco stress Test
A	**0**	**0**
B	**261.5**	**124.8**
C	**239.2**	**224.9**
D	**251.6**	**206.3**
E	**256.3**	**210.2**
F	**250.1**	**229.1**
G	**231.5**	**236.4**
H	**0**	**0**

Table 8. 13 AsPC-1 6 Weeks BCA Assay

Seahorse Well	Protein Concentration **µg/mL** Mito stress Test	Protein Concentration **µg/mL** Glyco stress Test
A	**0**	**0**
B	**144.6**	**160**
C	**149.5**	**241.2**
D	**117.3**	**184.9**
E	**154.7**	**231.5**
F	**190.6**	**132.6**
G	**213.2**	**167.3**
H	**0**	**0**

Table 8. 14 Panc-1 6 Weeks BCA Assay

Seahorse Well	Protein Concentration **µg/mL** Mito stress Test	Protein Concentration **µg/mL** Glyco stress Test
A	**0**	**0**
B	**255.9**	**267.4**
C	**236.7**	**314.8**
D	**222.3**	**271.4**
E	**222.3**	**325.2**
F	**266.8**	**194.9**
G	**263.8**	**189.8**

H	0	0

8.7 Appendix G

T Test paired two samples for means: AsPC-1 Mito Stress Test 2 Weeks and 6 Weeks

	Variable 1	*Variable 2*		*Variable 1*	*Variable 2*
Mean	1.080833641	0.580847962	Mean	0.9986	0.2416791
Variance	0.511146069	0.111456185	Variance	0.35986163	0.01216439
Observations	12	12	Observations	12	12
Pearson Correlation	0.996777116		Pearson Correlation	0.97729932	
Hypothesized Mean Difference	0		Hypothesized Mean Difference	0	
df	11		df	11	
t Stat	4.520927656		t Stat	5.32233434	
P(T<=t) one-tail	0.000435357		P(T<=t) one-tail	0.00012196	
t Critical one-tail	1.795884819		t Critical one-tail	1.79588482	
P(T<=t) two-tail	0.000870714		P(T<=t) two-tail	0.00024392	
t Critical two-tail	2.20098516		t Critical two-tail	2.20098516	

T Test paired two samples for means: AsPC-1 Glyco Stress Test 2 Weeks and 6 Weeks

	Variable 1	*Variable 2*		*Variable 1*	*Variable 2*
Mean	0.47710497	0.33849742	Mean	0.60485906	0.346651
Variance	0.05611465	0.04176266	Variance	0.12889631	0.04851978
Observations	12	12	Observations	12	12
Pearson Correlation	0.98402027		Pearson Correlation	0.98972713	
Hypothesized Mean Difference	0		Hypothesized Mean Difference	0	
df	11		df	11	
t Stat	9.40731016		t Stat	6.19063319	
P(T<=t) one-tail	6.783E-07		P(T<=t) one-tail	3.4026E-05	
t Critical one-tail	1.79588482		t Critical one-tail	1.79588482	
P(T<=t) two-tail	1.3566E-06		P(T<=t) two-tail	6.8053E-05	
t Critical two-tail	2.20098516		t Critical two-tail	2.20098516	

T Test paired two samples for means: Panc-1 Glyco 2 Weeks and 6 Weeks

	Variable 1	*Variable 2*		*Variable 1*	*Variable 2*
Mean	0.62719143	0.41968659	Mean	0.34500393	0.32525553
Variance	0.08032093	0.03399161	Variance	0.00846838	0.01220893
Observations	12	12	Observations	12	12
Pearson Correlation	0.99387124		Pearson Correlation	0.96642108	
Hypothesized Mean Difference	0		Hypothesized Mean Difference	0	
df	11		df	11	
t Stat	7.03181925		t Stat	2.13781188	
P(T<=t) one-tail	1.0887E-05		P(T<=t) one-tail	0.02790856	
t Critical one-tail	1.79588482		t Critical one-tail	1.79588482	
P(T<=t) two-tail	2.1774E-05		P(T<=t) two-tail	0.05581711	
t Critical two-tail	2.20098516		t Critical two-tail	2.20098516	

T Test paired two samples for means: Panc-1 Mito 2 Weeks and 6 Weeks

	Variable 1	*Variable 2*		*Variable 1*	*Variable 2*
Mean	1.11719241	0.98704371	Mean	0.96689461	0.900572338
Variance	0.31553439	0.22815237	Variance	0.23163193	0.215241147
Observations	12	12	Observations	12	12
Pearson Correlation	0.99082862		Pearson Correlation	0.99047469	
Hypothesized Mean Difference	0		Hypothesized Mean Difference	0	
df	11		df	11	
t Stat	4.11745627		t Stat	3.40433669	
P(T<=t) one-tail	0.00085402		P(T<=t) one-tail	0.00294192	
t Critical one-tail	1.79588482		t Critical one-tail	1.79588482	
P(T<=t) two-tail	0.00170805		P(T<=t) two-tail	0.00588383	
t Critical two-tail	2.20098516		t Critical two-tail	2.20098516	

8.8 Appendix H

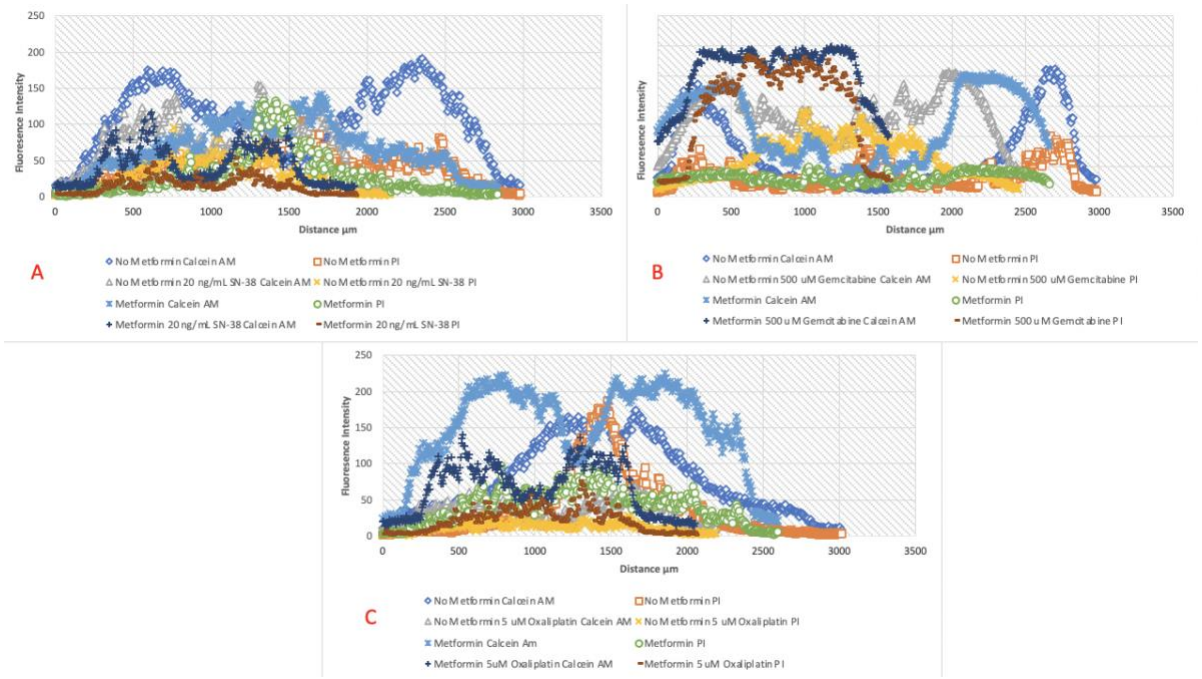

Figure 8. 15 Viability Plots of AsPC-1 Spheroids Treated in Metformin for 2 Weeks.

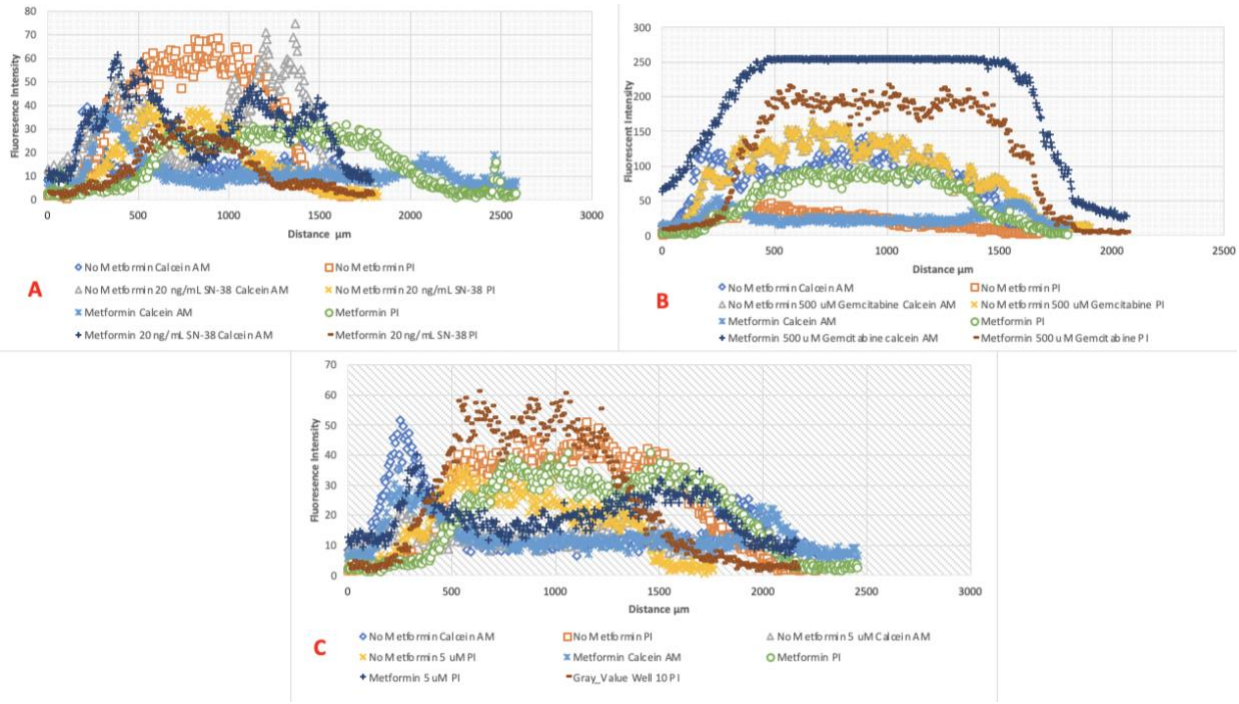

Figure 8. 16 Viability Plots of Panc-1 Spheroids Treated in Metformin for 2 Weeks.

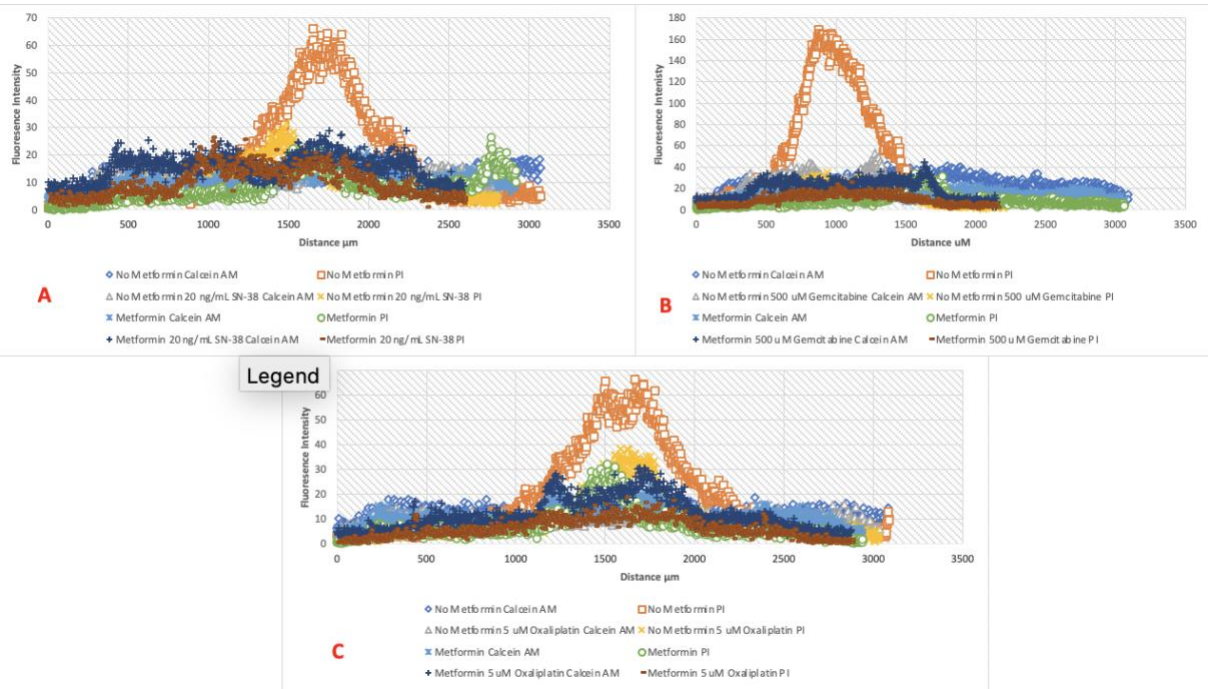

Figure 8. 17 Viability Plots of AsPC-1 Spheroids Treated in Metformin for 6 Weeks.

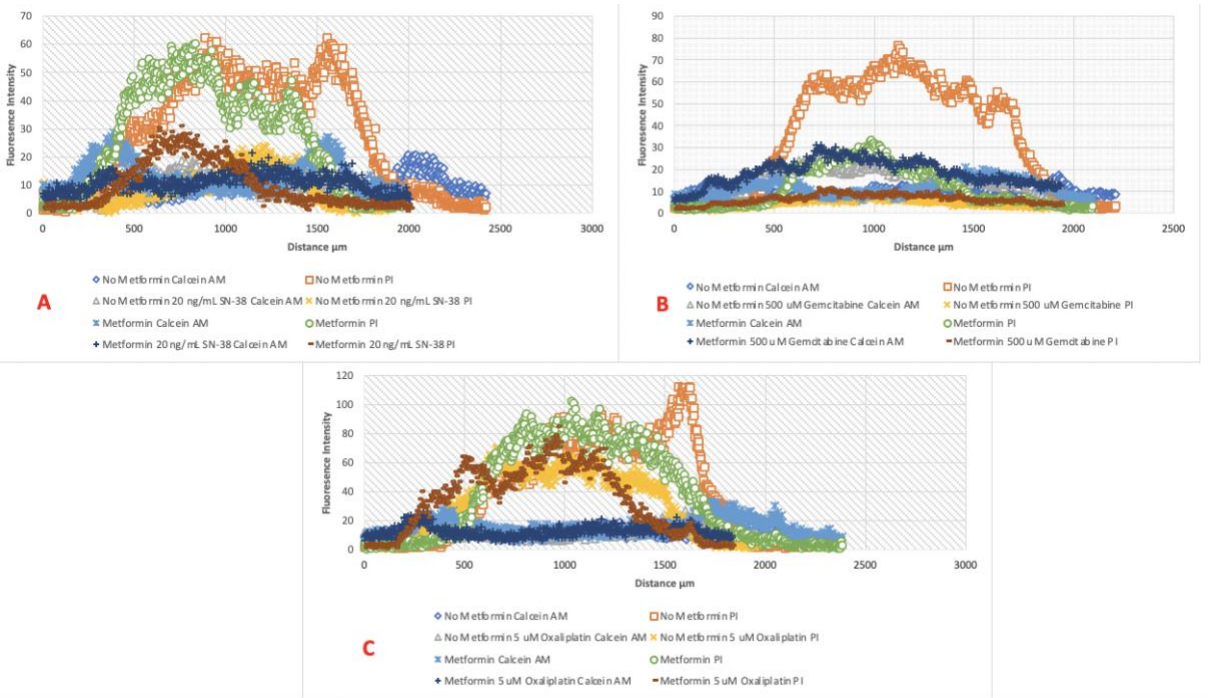

Figure 8. 18 Viability Plots of Panc-1 Spheroids Treated in Metformin for 6 Weeks.